ELSEVIER

One-dimensional wave turbulence

Vladimir Zakharov[a,b], Frédéric Dias[c,*], Andrei Pushkarev[d]

[a]*Landau Institute for Theoretical Physics, Moscow, Russia*
[b]*Department of Mathematics, University of Arizona, Tucson, AZ 85721, USA*
[c]*Centre de Mathématiques et de Leurs Applications, Ecole Normale Supérieure de Cachan,*
61 avenue du Président Wilson, 94235 Cachan cedex, France
[d]*Waves and Solitons LLC, 918 W. Windsong Dr., Phoenix, AZ 85045, USA*

Abstract

The problem of turbulence is one of the central problems in theoretical physics. While the theory of fully developed turbulence has been widely studied, the theory of wave turbulence has been less studied, partly because it developed later. Wave turbulence takes place in physical systems of nonlinear dispersive waves. In most applications nonlinearity is small and dispersive wave interactions are weak. The weak turbulence theory is a method for a statistical description of weakly nonlinear interacting waves with random phases. It is not surprising that the theory of weak wave turbulence began to develop in connection with some problems of plasma physics as well as of wind waves. The present review is restricted to one-dimensional wave turbulence, essentially because finer computational grids can be used in numerical computations.

Most of the review is devoted to wave turbulence in various wave equations, and in particular in a simple one-dimensional model of wave turbulence introduced by Majda, McLaughlin and Tabak in 1997. All the considered equations are model equations, but consequences on physical systems such as ocean waves are discussed as well. The main conclusion is that the range in which the theory of pure weak turbulence is valid is narrow. In general, wave turbulence is not completely weak. Together with the weak turbulence component, it can include coherent structures, such as solitons, quasisolitons, collapses or broad collapses. As a result, weak and strong turbulence coexist. In situations where coherent structures cannot develop, weak turbulence dominates.

Even though this is primarily a review paper, new results are presented as well, especially on self-organized criticality and on quasisolitonic turbulence.

----
*Corresponding author.
E-mail address: dias@cmla.ens-cachan.fr (F. Dias).

Contents

1. Introduction

The problem of turbulence is one of the main problems in theoretical physics. While the theory of fully developed turbulence has been widely studied (see the pioneer work of Kolmogorov [54] and the book [34] for a review on fully developed turbulence), the theory of wave turbulence has been less studied, partly because it developed later. Wave turbulence takes place in physical systems of nonlinear dispersive waves. The energy transfer between waves occurs mostly among resonant sets of waves. Wave turbulence is a very common natural phenomenon. Here is a partial list of physical situations where wave turbulence is realized: capillary waves [79,42,87,14–17], plasmas with or without magnetic field [52,64,63], magnetohydrodynamics [78,35–37],[1] superfluid helium and processes of Bose–Einstein condensation [53,59,65], nonlinear optics [26], acoustic waves (compressible fluid for which the flow is potential and constitutes a set of interacting sound waves) [100]. Wave turbulence plays an important role in physical oceanography and in the physics of the atmosphere [2–4], where waves of different types and different scales are excited. These are capillary and gravity waves on the ocean surface, internal waves inside the ocean, Rossby and inertial gravity waves in the ocean and in the atmosphere.

In most of these examples, nonlinearity is small and wave interactions are weak. Then wave interactions can be described by one or several kinetic equations for averaged squared wave amplitudes. The initial work on wave turbulence was done by Hasselmann [39], who developed four-wave equations for water waves. The three-wave equations appeared at the same time in plasma physics. Soon after that, the four-wave equations also appeared in plasma physics. These early achievements of plasma physicists are summarized in the monograph by Kadomtsev [49,50]. Later Benney and

---

[1] Strictly speaking, Alfvén waves from incompressible magnetohydrodynamics are nondispersive waves, but this does not prevent a weak turbulence theory to be developed.

Saffman [8] as well as Benney and Newell [9] also introduced the statistical closures based on the resonant wave interactions. The resulting kinetic equations have families of exact Kolmogorov type solutions. These solutions were found by one of the authors of this article (V.E. Zakharov) in the mid 1960s, first in the context of weak turbulence in plasmas [88], then in the context of surface waves [94,95]. Following Balk [1], we will call them Kolmogorov–Zakharov spectra (KZ spectra). KZ spectra describe the transport of integrals of motion (energy, wave action, momentum) to the regions of small or large scales. In our opinion KZ spectra play a central role in wave turbulence. There is strong experimental evidence in support of this point of view. KZ spectra for capillary wave turbulence were observed independently in three laboratories (at the Physics Department of the University of California, Los Angeles [87], at the Niels Bohr Institute, Denmark [79,42] and at the Institute of Solid State Physics, Russia [14–17]). High-frequency tails of wind-driven gravity waves are perfectly described by the spectrum $\mathbf{E}(\omega) \approx \omega^{-4}$ [94], which is a KZ solution to the kinetic equation with constant energy flux [43,44,71,82,51]. Here, ω denotes the frequency while $\mathbf{E}$ denotes the spectral density (in frequency space) of the free-surface elevation. Recently, comparisons were performed between the universally observed Garrett–Munk spectrum of internal waves and the corresponding KZ spectrum [58]: both spectra look quite similar.

KZ spectra have been obtained in several numerical simulations of the time-dependent behavior of solutions to the kinetic equations [76]. Moreover, the theory of KZ spectra looks elegant and self-contained. Therefore this theory should not be left aside. But further developments and justification are needed to strengthen it. In fact the validity of the kinetic wave equation, even in the limit of small nonlinearity, should be investigated more carefully. The derivation of the kinetic equation is based on the assumption of phase randomness, which means that the statistics of a wave ensemble is as close to Gaussian as possible. This is a very strong assumption which needs stronger foundations. Doubts in the universal applicability of the weak turbulence (WT) scenario of wave turbulence appeared with the results of Majda, McLaughlin and Tabak (MMT) [61], who performed massive numerical computations on a one-dimensional model of wave interactions (MMT model) and found in some cases spectra which were different from the KZ spectra of weak turbulence (see also the additional numerical computations in [18–20], as well as the computations on a Benney–Luke-type equation in [10]). The introduction of the MMT model was a crucial step in understanding wave turbulence.

In our opinion, the results of the MMT group can be explained by the interference of coherent nonlinear structures. In general, wave turbulence is not completely weak. Together with the weak turbulence component, it can include coherent structures. Inside such structures, the phase correlation is very strong. The presence of the coherent component violates to some extent the assumption of phase randomness and can lead to deviations of spectra from the KZ form. The dynamic breakdown of the weak turbulence approximation by intermittent events associated with nonlinear coherent structures was recently addressed in [11,12].

The theory of possible coherent structures is far from being complete. So far only three types of coherent structures have been studied properly—solitons, quasisolitons and collapses [96,97]. In this report we display one more type of coherent structure, the so-called 'broad collapse', which was observed in numerical solutions to the 'negative' (focusing) MMT model.

The coherent structures that have received the most attention are the stable solitons. In a few integrable models, such as the nonlinear Schrödinger (NLS) equation or the sine-Gordon equation, they interact elastically and their amplitudes do not change after collision. In general solitons interact

inelastically, thus showing a tendency to merge and form a rare gas of solitons of high amplitude. This gas can be called 'solitonic turbulence'. In reality solitonic turbulence is always mixed with weak turbulence, which carries away what is left after soliton collisions.

Wave collapses are nonstationary localized coherent structures, which lead to the formation of point singularities. Often (but not always) collapses appear as a result of the instability of solitons. Both the merging of solitons and the formation of singularities are mechanisms of energy transport to large wave numbers, which compete with the weakly turbulent Kolmogorov cascade of energy.

Quasisolitons are in fact 'envelope solitons', which can exist when 'true' solitons cannot be formed. They live only for a finite time and can be compared with unstable particles in nuclear physics. We believe that they play an important role in wave turbulence. Quasisolitons collide, elastically or not, merge and create 'quasisolitonic turbulence'. Quasisolitons of high amplitude can be unstable and lead to singularity formation. Again, the collision, merging and collapse of quasisolitons provide a mechanism of direct cascade of energy, which is quite different from the weakly turbulent Kolmogorov cascade.

In our opinion, the results of the MMT numerical experiments might be explained by the formation of quasisolitonic turbulence. One of the remarkable aspects of the MMT paper [61] is that it attracted attention to the numerical simulation of wave turbulence in one-dimensional models. The idea that the basic conclusions of weak turbulence theory should be examined by direct numerical simulations of the primitive equations is not new. Massive numerical simulations of the two-dimensional nonlinear Schrödinger equation were done in 1992 [26]. Four years later, direct numerical simulations of capillary wave turbulence were successfully performed [75] (see also [77,27] for more recent computations). Successful numerical experiments on two-dimensional gravity waves were also performed [68,28,29,80] (see also [33] for computations on a modified nonlinear Schrödinger equation and [47] for computations on the Zakharov equations). All these experiments support weak-turbulence theory in two dimensions.

Nevertheless, numerical simulations of wave turbulence in one-dimensional (1D) primitive equations are very important. In 1D computations, one can use much more modes than in two dimensions. Typically two-dimensional experiments are performed on a mesh with 256×256 modes. In 1D, 10^4 is typical for the number of modes in the computational grid. It is possible to have a much wider inertial range (two decades for example) and to perform a careful measurement of the basic statistical features of a wave field, including frequency spreading of spectra, cumulants and higher-order moments. In addition, in the 1D case, coherent structures play a more important role than in higher dimensions. The study of solitonic or quasisolitonic turbulence as well as the study of the turbulence created by wave collapses are interesting problems. One should not think that 1D wave turbulence is a subject of pure academic interest. In many real situations the turbulence is almost one dimensional. This is especially true for wind-driven gravity waves. Their energy spectra are usually pretty narrow. One can say that they are 'quasi-one-dimensional'.

Coherent structures lead to some effects that are important from a practical point of view. In the ocean, the formation of 'freak' or 'rogue' waves of very large amplitude and steepness can apparently be explained by the existence of coherent structures [67]. Real freak waves are not one-dimensional but a careful study of the one-dimensional limit is essential.

In this report we gather the main results obtained in direct numerical simulations of one-dimensional wave turbulence. An essential part of the results is new and has not been published before. Hence this paper is a combination of original and review material.

A large part of the report is devoted to various versions of the MMT model and some of its generalizations. However, consequences on physical systems such as ocean waves are discussed as well.

The report is organized as follows. Section 2 provides an overview of the weak turbulence theory in the framework of the MMT model. In Section 3, the difference between solitons and quasisolitons is explained. Section 4 gives a description of coherent structures—solitons and collapses—in the 'negative' (self-focusing) MMT model. In Section 5, we describe quasisolitons in the 'positive' (defocusing) MMT model. In Section 6, the tools used for the numerical integration of the model and its generalizations are briefly described. Section 7 presents numerical simulations in the framework of the focusing MMT model. We observe wave collapses on the weakly turbulent background and discuss their role in energy transport. Section 8 provides again a discussion on the focusing MMT model when the background state is unstable. In this case, the development of wave turbulence leads to 'self-organized criticality', that is relaxation oscillations of wave energy. The numerical simulations of wave turbulence in the defocusing MMT model are discussed in Section 9. The spectrum of wave turbulence is well described by the MMT spectrum, first introduced in [61] and revisited in [96]. Section 10 is devoted to the description of quasisolitonic turbulence in the defocusing MMT model. With some caution, one may believe that in this case the MMT model can be used for the study of one-dimensional gravity wave turbulence. In Sections 11 and 12, generalizations of the MMT model are studied. First (Section 11), we study a defocusing model including two types of waves, in the case where both quasisolitons and solitons are forbidden. Then (Section 12), we discuss a generalized MMT model including not only $2 \rightarrow 2$ interacting waves, but also $1 \rightarrow 3$ interacting waves. The notation $m \rightarrow n$ is used to describe the scattering process of m waves into n waves. In these two cases, the applicability of the theory of weak turbulence and the formation as well as the universality of the KZ spectra are demonstrated. Section 13 is devoted to one-dimensional wave turbulence on the surface of a deep fluid layer. The relevance of the MMT model for the description of water waves is discussed. In Section 14, we go beyond the scope of the report by presenting some ideas on what is beyond weak turbulence. Section 15 provides a conclusion. Details on water waves (governing equations, Hamiltonian formulation, spectra) are summarized in Appendix B.

2. Weak turbulence in the Majda–McLaughlin–Tabak (MMT) model equation

Most of the results presented in this review paper are based on the family of dynamical equations

$$\mathrm{i}\frac{\partial \psi}{\partial t} = \left|\frac{\partial}{\partial x}\right|^{\alpha}\psi + \lambda\left|\frac{\partial}{\partial x}\right|^{\beta/4}\left(\left|\left|\frac{\partial}{\partial x}\right|^{\beta/4}\psi\right|^{2}\left|\frac{\partial}{\partial x}\right|^{\beta/4}\psi\right), \quad \lambda = \pm 1 , \qquad (2.1)$$

where $\psi(x,t)$ denotes a complex wave field. The real parameter α controls dispersion while the real parameter β controls nonlinearity. The fractional derivative $|\partial/\partial x|^{\alpha}$ is formally defined in Appendix A. Its interpretation in Fourier space is clear: the Fourier transform of $|\partial/\partial x|^{\alpha}\psi$ simply is $|k|^{\alpha}\hat{\psi}_k$, where $\hat{\psi}_k$ denotes the Fourier transform of ψ. The nonlinear Schrödinger equation is a special case of Eq. (2.1) with $\alpha = 2$, $\beta = 0$, if one recognizes that $|\partial/\partial x|^{2} = -\partial^{2}/\partial x^{2}$. The two-parameter family of dispersive wave equations (2.1) was first introduced in [61] with $\lambda = 1$ (defocusing model). This

one-dimensional model has resonant quartets for $\alpha < 1$, and an exactly solvable weak turbulence theory with explicit dependence of the predicted wave number spectra on the parameters α and β.

Our parameter β is the opposite of the parameter β in the original paper by MMT. The extension $\lambda = \pm 1$ in Eq. (2.1) was first treated independently in [18] and [38]. This extension is nontrivial because the balance between nonlinear and dispersive effects may change according to the sign of λ.

System (2.1) is a Hamiltonian system with Hamiltonian

$$H = E + H_{\mathrm{NL}} = \int \left| \left| \frac{\partial}{\partial x} \right|^{\alpha/2} \psi \right|^2 \mathrm{d}x + \frac{1}{2} \lambda \int \left| \left| \frac{\partial}{\partial x} \right|^{\beta/4} \psi \right|^4 \mathrm{d}x , \tag{2.2}$$

where E is the part of the Hamiltonian corresponding to the linearization of Eq. (2.1). The level of nonlinearity ϵ, defined as the ratio of the nonlinear part H_{NL} to the linear part E of the Hamiltonian, i.e.

$$\epsilon = \frac{H_{\mathrm{NL}}}{E} , \tag{2.3}$$

will be useful later on to monitor the level of turbulence. Besides the Hamiltonian, system (2.1) preserves two other integrals of motion: wave action and momentum, respectively

$$N = \int |\psi|^2 \, \mathrm{d}x \quad \text{and} \quad M = \frac{1}{2} \mathrm{i} \int \left(\psi \frac{\partial \psi^*}{\partial x} - \frac{\partial \psi}{\partial x} \psi^* \right) \mathrm{d}x , \tag{2.4}$$

where $(*)$ stands for complex conjugation. In Fourier space, Eq. (2.1) becomes

$$\mathrm{i} \frac{\partial \hat{\psi}_k}{\partial t} = \omega(k)\hat{\psi}_k + \lambda \int T_{123k} \hat{\psi}_1 \hat{\psi}_2 \hat{\psi}_3^* \delta(k_1 + k_2 - k_3 - k) \, \mathrm{d}k_1 \, \mathrm{d}k_2 \, \mathrm{d}k_3 , \tag{2.5}$$

where

$$\hat{\psi}_k(t) = \frac{1}{2\pi} \int_{-\infty}^{\infty} \psi(x,t) \mathrm{e}^{-\mathrm{i}kx} \, \mathrm{d}x, \quad k \in \mathbb{R} .$$

The inverse Fourier transform gives

$$\psi(x,t) = \int_{-\infty}^{\infty} \hat{\psi}_k(t) \mathrm{e}^{\mathrm{i}kx} \, \mathrm{d}k, \quad x \in \mathbb{R} .$$

In the form (2.5), the MMT model looks like the one-dimensional Zakharov's equation determined by the linear dispersion relation

$$\omega(k) = |k|^{\alpha}, \quad \alpha > 0 , \tag{2.6}$$

and the simple interaction coefficient

$$T_{123k} = T(k_1, k_2, k_3, k) = |k_1 k_2 k_3 k|^{\beta/4} . \tag{2.7}$$

In Fourier space, the Hamiltonian reads

$$H = \int \omega(k) |\hat{\psi}_k|^2 \, \mathrm{d}k + \frac{1}{2} \lambda \int T_{123k} \hat{\psi}_1 \hat{\psi}_2 \hat{\psi}_3^* \hat{\psi}_k^* \, \delta(k_1 + k_2 - k_3 - k) \, \mathrm{d}k_1 \, \mathrm{d}k_2 \, \mathrm{d}k_3 \, \mathrm{d}k , \tag{2.8}$$

and Eq. (2.5) can be rewritten as

$$\mathrm{i} \frac{\partial \hat{\psi}_k}{\partial t} = \frac{\delta H}{\delta \hat{\psi}_k^*} . \tag{2.9}$$

Table 1
Various shorthand notations for the interaction coefficient $T(k_1, k_2, k_3, k)$

Notation	T_{123k}	T_{0k}	T_0	R_{kk_0}
Meaning	$T(k_1, k_2, k_3, k)$	$T(k_0, k, k_0, k)$	$T(k_0, k_0, k_0, k_0)$	$T(k, 2k_0 - k, k_0, k_0)$

The integrals of motion N (wave action) and M (momentum) become

$$N = \int |\hat{\psi}_k|^2 \, \mathrm{d}k \quad \text{and} \quad M = \int k |\hat{\psi}_k|^2 \, \mathrm{d}k \ . \tag{2.10}$$

One easily sees that the kernel T_{123k} possesses the symmetry associated with the fact that Eq. (2.1) is Hamiltonian:

$$T_{123k} = T_{213k} = T_{12k3} = T_{3k12} \ . \tag{2.11}$$

The last equality comes from the fact that the Hamiltonian is real. Moreover, the absolute values in Eqs. (2.6) and (2.7) ensure the basic assumptions of isotropy and scale invariance. In other words, $\omega(k)$ and T_{123k} are invariant with respect to the symmetry $k \to -k$ (which is equivalent to rotation invariance in higher dimensions) and they are homogeneous functions of their arguments with degrees α and β respectively, i.e.

$$\omega(\xi k) = \xi^\alpha \omega(k), \quad T(\xi k_1, \xi k_2, \xi k_3, \xi k) = \xi^\beta T(k_1, k_2, k_3, k), \quad \xi > 0 \ . \tag{2.12}$$

When some of the wave numbers appearing in the interaction coefficient $T(k_1, k_2, k_3, k)$ are equal, a shorthand notation is introduced and summarized in Table 1.

Following MMT, we fix $\alpha = \frac{1}{2}$ by analogy with deep-water gravity waves whose dispersion relation is $\omega(k) = (g|k|)^{1/2}$, g being the acceleration due to gravity. Appendix B provides some essential results on gravity waves. The power β takes the value 3 if the analogy between water waves and the MMT model is extended to the nonlinear term. Most of the new results presented in this paper are for the case $\beta = 3$. In order to make the comparison with hydrodynamics more visible, we introduce the variable [2]

$$\eta(x, t) = \int_{-\infty}^{\infty} \mathrm{e}^{\mathrm{i}kx} \sqrt{\frac{\omega_k}{2}} (\hat{\psi}_k + \hat{\psi}_{-k}^*) \, \mathrm{d}k \ . \tag{2.13}$$

In the theory of surface waves, formula (2.13) gives a connection between the complex normal amplitude $\hat{\psi}_k$ and the shape of the free surface $\eta(x, t)$. Another useful variable is $|\psi(x, t)|^2$. Note that Willemsen [85,86] introduced an alternative toy model to mimic water waves in deep water.

Eq. (2.5) describes four-wave interaction processes obeying the resonant conditions

$$k_1 + k_2 = k_3 + k \ , \tag{2.14}$$

$$\omega_1 + \omega_2 = \omega_3 + \omega \ . \tag{2.15}$$

---

[2] In order to make $\eta(x, t)$ the real shape of the free surface in the water-wave problem, Eq. (2.13) should read $\eta(x, t) = \int_{-\infty}^{\infty} \mathrm{e}^{\mathrm{i}kx} \sqrt{(\omega_k/2g)} (\hat{\psi}_k + \hat{\psi}_{-k}^*) \, \mathrm{d}k$. For simplicity, we keep (2.13) for the definition of η. It is important to use the proper definition of η only when comparing with experiments.
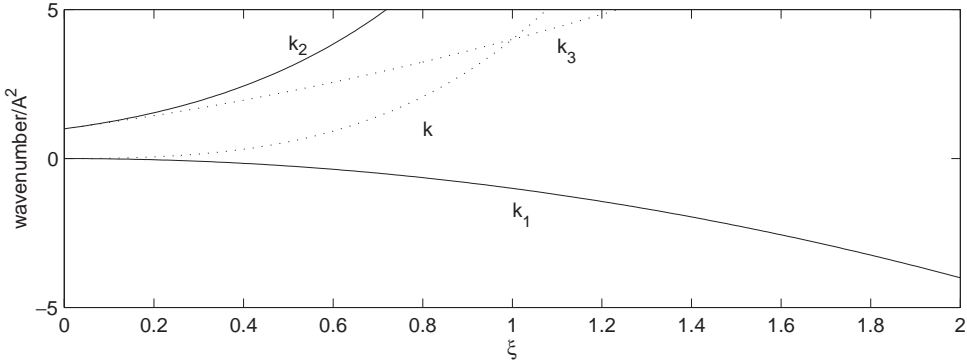
Fig. 1. Nontrivial solutions (2.16) to the four-wave resonance condition, $k_1 + k_2 = k_3 + k$, $\omega_1 + \omega_2 = \omega_3 + \omega$, for the dispersion relation $\omega(k) = |k|^{1/2}$.

When three-wave decay processes are not allowed, the terminology *nondecay case* is sometimes used. The four-wave interaction described by (2.14) and (2.15) is called $2 \to 2$ interacting waves. In Section 12, we discuss an extension including also $1 \to 3$ interacting waves. For $\alpha > 1$, Eqs. (2.14) and (2.15) only have the trivial solution $k_3 = k_1$, $k = k_2$ or $k_3 = k_2$, $k = k_1$. For $\alpha < 1$ there are also nontrivial solutions. In this case the signs of the wave numbers cannot be all the same. For instance, $k_1 < 0$ and $k_2, k_3, k > 0$. If $\alpha = \frac{1}{2}$, nontrivial solutions to Eqs. (2.14) and (2.15) can be parametrized by two parameters A and $\xi > 0$:

$$k_1 = -A^2\xi^2, \quad k_2 = A^2(1 + \xi + \xi^2)^2, \quad k_3 = A^2(1 + \xi)^2, \quad k = A^2\xi^2(1 + \xi)^2. \tag{2.16}$$

Plots of k/A^2, k_i/A^2, $i = 1, 2, 3$, versus ξ are shown in Fig. 1.

The dynamic equation (2.5) describes the time evolution of $\hat{\psi}_k(t) = |\hat{\psi}_k(t)|e^{i\varphi(k,t)}$, i.e. of the wave amplitude $|\hat{\psi}_k(t)|$ and its phase $\varphi(k,t)$. For weak nonlinearities and a large number of excited waves, such a description is in general highly redundant: it includes the slow evolution of amplitudes (constant in the linear approximation) and the fast but uninteresting phase dynamics $\varphi(k,t) \approx -\omega(k)t$ which leaves the amplitude evolution virtually unaffected. This redundancy is eliminated by the transition from the dynamic description of a wave system of $|\hat{\psi}_k(t)|$ and $\varphi(k,t)$ to the statistical one in terms of the correlation functions of the field $\hat{\psi}_k(t)$. The two-point correlation function is defined by

$$\langle \hat{\psi}_k(t)\hat{\psi}_{k'}^*(t)\rangle = n(k,t)\delta(k - k') \; ,$$

where brackets denote ensemble averaging. The function $n(k,t)$ can be interpreted as the spectral density (in k-space) of the wave field ψ:

$$\int |\psi(x,t)|^2 \, \mathrm{d}x = \int n(k,t) \, \mathrm{d}k = N \; . \tag{2.17}$$

Recall that the definition of N was given in (2.4). Below, we will also use the function $e(k,t) = \omega(k)n(k,t)$, which can be interpreted as the spectral density (in k-space) of the free-surface elevation:

$$\int |\eta(x,t)|^2 \, \mathrm{d}x = \int e(k,t) \, \mathrm{d}k = E \; . \tag{2.18}$$

These two equations can be interpreted in frequency space. Let

$$\mathbf{N}(\omega, t) = n(k(\omega), t)\frac{\mathrm{d}k}{\mathrm{d}\omega} \quad \text{and} \quad \mathbf{E}(\omega, t) = \omega\mathbf{N}(\omega, t) \ .$$

Then

$$N = \int \mathbf{N}(\omega)\,\mathrm{d}\omega \quad \text{and} \quad E = \int \mathbf{E}(\omega)\,\mathrm{d}\omega \ .$$

We also introduce the four-wave correlation function

$$\langle \hat{\psi}_{k_1}(t)\hat{\psi}_{k_2}(t)\hat{\psi}_{k_3}^*(t)\hat{\psi}_k^*(t)\rangle = J_{123k}\delta(k_1 + k_2 - k_3 - k) \ . \tag{2.19}$$

On this basis, WT theory leads to the kinetic equation for $n(k, t)$ and provides tools for finding stationary power-law solutions. The main steps of the procedure applied to model (2.1) are reviewed below. As said in the introduction, the derivation of the kinetic equation is based on the assumption of phase randomness.

The starting point is the original equation for $n(k, t)$. The notation $n_k(t) = n(k, t)$ is introduced. From Eq. (2.5), we have

$$\frac{\partial n_k}{\partial t} = 2\lambda \int \mathrm{Im}\, J_{123k}T_{123k}\delta(k_1 + k_2 - k_3 - k)\,\mathrm{d}k_1\,\mathrm{d}k_2\,\mathrm{d}k_3 \ . \tag{2.20}$$

Due to the quasi-Gaussian random phase approximation

$$\mathrm{Re}\, J_{123k} \approx n_1 n_2[\delta(k_1 - k_3) + \delta(k_1 - k)] \ . \tag{2.21}$$

The imaginary part of J_{123k} can be found through an approximate solution to the equation imposed on this correlator. The result is (see for example [98])

$$\mathrm{Im}\, J_{123k} \approx 2\pi\lambda T_{123k}\delta(\omega_1 + \omega_2 - \omega_3 - \omega)(n_1 n_2 n_3 + n_1 n_2 n_k - n_1 n_3 n_k - n_2 n_3 n_k) \ . \tag{2.22}$$

This gives the kinetic wave equation

$$\frac{\partial n_k}{\partial t} = 4\pi \int T_{123k}^2(n_1 n_2 n_3 + n_1 n_2 n_k - n_1 n_3 n_k - n_2 n_3 n_k)$$

$$\times \delta(\omega_1 + \omega_2 - \omega_3 - \omega)\,\delta(k_1 + k_2 - k_3 - k)\,\mathrm{d}k_1\,\mathrm{d}k_2\,\mathrm{d}k_3 \ . \tag{2.23}$$

An analogy with the quantum kinetic equation is given in [98], Section 2.1.6.[3]

It is clear that the WT approach is independent on λ. It should be pointed out that in Eq. (3.9) of [61], which is the equivalent of Eq. (2.23), the 12π factor should read 4π and that the negative sign in the right hand side of Eq. (2.23) should be a positive sign. This sign is particularly important when determining the fluxes of wave action and energy.

---

[3] The kinetic wave equation is sometimes called Boltzmann's equation. This terminology is, in fact, misleading because the kinetic wave equation and Boltzmann's equation are the opposite limiting cases of a more general kinetic equation for particles which obey Bose–Einstein statistics like photons in stellar atmospheres or phonons in liquid helium. It was first derived by Nordheim in 1928 [66] in the context of a Bose gas (see [48] for a review) and by Peierls in 1929 [70] in the context of thermal conduction in crystals. In spite of the fact that the kinetic wave equation and Boltzmann's equation can both be derived from the quantum kinetic equation, the kinetic wave equation was derived independently and almost simultaneously in plasma physics and for surface waves on deep water. This was done in the early 1960s while Boltzmann's equation was derived in the 19th century! The derivation for surface waves is due to Hasselmann [39–41].

The next step consists in averaging over the sign of the wave numbers (this is the one-dimensional equivalent of angle averaging in higher dimensions). One gets

$$\frac{\partial \mathbf{N}(\omega)}{\partial t} = \frac{4\pi}{\alpha^4} \int (\omega_1 \omega_2 \omega_3 \omega)^{\frac{\beta/2 - \alpha + 1}{\alpha}} (n_1 n_2 n_3 + n_1 n_2 n_\omega - n_1 n_3 n_\omega - n_2 n_3 n_\omega)$$

$$\times \delta(\omega_1 + \omega_2 - \omega_3 - \omega) \left[\delta(\omega_1^{1/\alpha} + \omega_2^{1/\alpha} - \omega_3^{1/\alpha} + \omega^{1/\alpha}) \right.$$

$$+ \delta(\omega_1^{1/\alpha} + \omega_2^{1/\alpha} + \omega_3^{1/\alpha} - \omega^{1/\alpha}) + \delta(\omega_1^{1/\alpha} - \omega_2^{1/\alpha} - \omega_3^{1/\alpha} - \omega^{1/\alpha})$$

$$\left. + \delta(-\omega_1^{1/\alpha} + \omega_2^{1/\alpha} - \omega_3^{1/\alpha} - \omega^{1/\alpha}) \right] \mathrm{d}\omega_1 \, \mathrm{d}\omega_2 \, \mathrm{d}\omega_3, \quad \omega_i > 0 , \tag{2.24}$$

where n_ω stands for $n(k(\omega))$.

The next step consists in inserting the power-law ansatz

$$n(\omega) \approx \omega^{-\gamma} , \tag{2.25}$$

and then performing the Zakharov's conformal transformations [61,26,98]. Finally, the kinetic equation becomes

$$\frac{\partial \mathbf{N}(\omega)}{\partial t} \approx \omega^{-y-1} I(\alpha, \beta, \gamma) , \tag{2.26}$$

where

$$I(\alpha, \beta, \gamma) = \frac{4\pi}{\alpha^4} \int_\Delta (\xi_1 \xi_2 \xi_3)^{\beta/2\alpha + 1/\alpha - 1 - \gamma} (1 + \xi_3^\gamma - \xi_1^\gamma - \xi_2^\gamma) \delta(1 + \xi_3 - \xi_1 - \xi_2)$$

$$\times \delta(\xi_1^{1/\alpha} + \xi_2^{1/\alpha} + \xi_3^{1/\alpha} - 1)(1 + \xi_3^y - \xi_1^y - \xi_2^y) \, \mathrm{d}\xi_1 \, \mathrm{d}\xi_2 \, \mathrm{d}\xi_3 \tag{2.27}$$

with

$$\Delta = \{0 < \xi_1 < 1, 0 < \xi_2 < 1, \xi_1 + \xi_2 > 1\} \quad \text{and} \quad y = 3\gamma + 1 - \frac{2\beta + 3}{\alpha}.$$

The dimensionless integral $I(\alpha, \beta, \gamma)$ is obtained by using the change of variables $\omega_j \rightarrow \omega \xi_j$ ($j = 1, 2, 3$).

Ansatz (2.25) makes sense if the integral in (2.24) converges. It could diverge both at low and high frequencies. The condition of convergence at low frequencies coincides with the condition of convergence of the integral in (2.27) and can be easily found. It reads

$$2\gamma < -1 + \frac{\beta + 4}{\alpha} . \tag{2.28}$$

The condition of convergence at high frequencies can be found after substituting (2.25) into (2.24). Omitting the details, we get the result

$$\gamma > \frac{\beta + \alpha - 1}{\alpha} . \tag{2.29}$$

The combination of both conditions implies that β must be less than $3(2 - \alpha)$. In all the cases discussed in this article, both conditions (2.28) and (2.29) are satisfied. Recall that it is assumed that $\alpha < 1$, otherwise the kinetic equation (2.24) does not hold and should be replaced by the

six-wave kinetic equation. The nonlinear Schrödinger equation ($\beta = 0, \alpha = 2$) is an integrable system, and the theory of weak turbulence is not applicable in this case to any order of nonlinearity.

For the case $\alpha = \frac{1}{2}$, one can transform Eq. (2.24) into the form

$$\frac{\partial \mathbf{N}(\omega)}{\partial t} = 64\pi\omega^{4(\beta+1)}(S_1 + S_2 + S_3 + S_4) . \tag{2.30}$$

The four integrals S_1, S_2, S_3 and S_4 are given below, with the use of the shorthand notation

$$u_0 = \frac{1+u}{1+u+u^2}, \quad u_1 = \frac{u}{1+u+u^2}, \quad u_2 = \frac{u(1+u)}{1+u+u^2} ,$$

$$S_1 = 2\int_0^1 u_0^{\beta+2} u_1^{\beta+3} u_2^{\beta-1} \left[n(u_0\omega)n(u_1\omega)n(u_2\omega) + n(\omega)n(u_0\omega)n(u_2\omega) \right.$$
$$\left. - n(\omega)n(u_0\omega)n(u_1\omega) - n(\omega)n(u_1\omega)n(u_2\omega) \right] \mathrm{d}u ,$$

$$S_2 = \int_0^1 u_0^{\beta+2} u_1^{-3\beta-2} u_2^{\beta-1} \left[n(u_1^{-1}\omega)n(u_1^{-1}u_2\omega)n(u_0 u_1^{-1}\omega) + n(\omega)n(u_1^{-1}u_2\omega)n(u_0 u_1^{-1}\omega) \right.$$
$$\left. - n(\omega)n(u_1^{-1}\omega)n(u_0 u_1^{-1}\omega) - n(\omega)n(u_1^{-1}\omega)n(u_1^{-1}u_2\omega) \right] \mathrm{d}u ,$$

$$S_3 = \int_0^1 u_0^{-3\beta-3} u_1^{\beta+2} u_2^{\beta} \left[n(u\omega)n(u_0^{-1}\omega)n(u_0^{-1}u_1\omega) + n(\omega)n(u_0^{-1}\omega)n(u_0^{-1}u_1\omega) \right.$$
$$\left. - n(\omega)n(u\omega)n(u_0^{-1}\omega) - n(\omega)n(u\omega)n(u_0^{-1}u_1\omega) \right] \mathrm{d}u ,$$

$$S_4 = \int_0^1 u_0^{\beta+2} u_1^{\beta+1} u_2^{-3\beta-4} \left[n(u^{-1}\omega)n(u_2^{-1}\omega)n(u_1 u_2^{-1}\omega) + n(\omega)n(u_2^{-1}\omega)n(u_1 u_2^{-1}\omega) \right.$$
$$\left. - n(\omega)n(u^{-1}\omega)n(u_1 u_2^{-1}\omega) - n(\omega)n(u^{-1}\omega)n(u_2^{-1}\omega) \right] \mathrm{d}u .$$

Note that there are some typos in the expression of S_4 in [96]. Eq. (2.30) can be used for the numerical simulation of weak turbulence.

Next, one looks for stationary solutions to the kinetic equation. From Eqs. (2.26) and (2.27) one easily finds that the stationarity condition

$$\frac{\partial \mathbf{N}(\omega)}{\partial t} = 0 \iff I(\alpha, \beta, \gamma) = 0 \tag{2.31}$$

is satisfied only for $\gamma = 0, 1$ and $y = 0, 1$.

The case $\gamma = 0$ represents the thermodynamic equilibrium solution

$$n(\omega) = c , \tag{2.32}$$

where c is an arbitrary constant, while the case $\gamma = 1$ represents the equilibrium solution

$$n(\omega) \approx \omega^{-1} = |k|^{-\alpha} , \tag{2.33}$$

which stems from the more general Rayleigh–Jeans distribution

$$n_{\text{RJ}}(\omega) = \frac{c_1}{c_2 + \omega} \ . \tag{2.34}$$

Solutions (2.32) and (2.33) correspond, respectively, to the equipartition of wave action N and quadratic energy E,

$$N = \int n(k)\,\mathrm{d}k = \int \mathbf{N}(\omega)\,\mathrm{d}\omega \ , \tag{2.35}$$

$$E = \int \omega(k)n(k)\,\mathrm{d}k = \int \omega\,\mathbf{N}(\omega)\,\mathrm{d}\omega \ . \tag{2.36}$$

In particle physics, the quantity which plays the role of wave action is the number of particles. These equilibrium solutions are not what we are looking for, since we are interested in open systems, where energy is pumped into the system and then dissipated, through viscous damping or wave breaking. What we are looking for are stationary nonequilibrium distributions. The cases $y = 0, 1$ give the nonequilibrium Kolmogorov-type solutions, respectively

$$n(\omega) \approx \omega^{-2\beta/3\alpha - 1/\alpha + 1/3} = |k|^{-2\beta/3 - 1 + \alpha/3} \tag{2.37}$$

and

$$n(\omega) \approx \omega^{-2\beta/3\alpha - 1/\alpha} = |k|^{-2\beta/3 - 1} \ , \tag{2.38}$$

which exhibit dependence on the parameter β of the interaction coefficient. Realistic sea spectra are of Kolmogorov type by analogy [43,44,71,82,51].

For the case $\alpha = \frac{1}{2}$ and $\beta = 0$, the Kolmogorov-type solutions are

$$n(\omega) \approx \omega^{-5/3} = |k|^{-5/6} \ , \tag{2.39}$$

$$n(\omega) \approx \omega^{-2} = |k|^{-1} \ . \tag{2.40}$$

Both exponents satisfy the conditions of locality (2.28)–(2.29).

The stationary nonequilibrium states are related to fluxes of integrals of motion, namely the quantities N (2.17) and E (2.18). The fluxes of wave action and quadratic energy are defined as

$$Q(\omega) = -\int_0^\omega \frac{\partial \mathbf{N}(\omega')}{\partial t}\,\mathrm{d}\omega' \ , \tag{2.41}$$

$$P(\omega) = -\int_0^\omega \omega' \frac{\partial \mathbf{N}(\omega')}{\partial t}\,\mathrm{d}\omega' \ . \tag{2.42}$$

In fact, flux (2.42) is not an 'exact' flux of energy. Eq. (2.42) is valid only in the case of weak nonlinearity. The more general case will be discussed later on. Solution (2.37), resp. (2.38), is associated with a constant mean flux Q_0, resp. P_0, of wave action, resp. quadratic energy. Let us now mention a physical argument which plays a crucial role in deciding the realizability of Kolmogorov-type spectra (a more detailed justification is provided at the end of the section—see also [61,98]). Suppose that pumping is performed at some frequencies around $\omega = \omega_f$ and damping at ω near zero and $\omega \gg \omega_f$. The weak turbulence theory states that the energy is expected to flow from ω_f to higher frequencies (direct cascade with $P_0 > 0$) while the wave action mainly flows to lower frequencies (inverse cascade with $Q_0 < 0$). Accordingly, we need to evaluate the fluxes

Table 2
Signs of the fluxes of wave action and quadratic energy for the Kolmogorov-type solutions to the model system (2.1) with dispersion relation $\omega = |k|^{1/2}$

β	-1	$-\frac{3}{4}$	$-\frac{1}{2}$	$-\frac{1}{4}$	0	3
γ_Q	$\frac{1}{3}$	$\frac{2}{3}$	1	$\frac{4}{3}$	$\frac{5}{3}$	$\frac{17}{3}$
Sign of Q_0	$+$	$+$	0	$-$	$-$	$-$
γ_P	$\frac{2}{3}$	1	$\frac{4}{3}$	$\frac{5}{3}$	2	6
Sign of P_0	$-$	0	$+$	$+$	$+$	$+$

in order to select, among the rich family of power laws (2.37) and (2.38), those that are likely to result from numerical simulations of Eq. (2.1) with damping and forcing.

By inserting Eq. (2.26) into Eqs. (2.41) and (2.42), we obtain

$$Q_0 \propto \lim_{y \to 0} \frac{\omega^{-y}}{y} I, \quad P_0 \propto \lim_{y \to 1} \frac{\omega^{-y+1}}{y-1} I , \tag{2.43}$$

which become

$$Q_0 \propto \left. \frac{\partial I}{\partial y} \right|_{y=0}, \quad P_0 \propto \left. \frac{\partial I}{\partial y} \right|_{y=1} . \tag{2.44}$$

Using Eq. (2.27), the derivatives in Eq. (2.44) can be expressed as

$$-\left. \frac{\partial I}{\partial y} \right|_{y=0} = \int_\Delta S(\xi_1, \xi_2, \xi_3)(1 + \xi_3^\gamma - \xi_1^\gamma - \xi_2^\gamma)\delta(1 + \xi_3 - \xi_1 - \xi_2)$$

$$\times \ln \left(\frac{\xi_1 \xi_2}{\xi_3} \right) \delta(\xi_1^{1/\alpha} + \xi_2^{1/\alpha} + \xi_3^{1/\alpha} - 1)\,d\xi_1\,d\xi_2\,d\xi_3 ,$$

$$\left. \frac{\partial I}{\partial y} \right|_{y=1} = \int_\Delta S(\xi_1, \xi_2, \xi_3)(1 + \xi_3^\gamma - \xi_1^\gamma - \xi_2^\gamma)\delta(1 + \xi_3 - \xi_1 - \xi_2)$$

$$\times (\xi_3 \ln \xi_3 - \xi_2 \ln \xi_2 - \xi_1 \ln \xi_1)\delta(\xi_1^{1/\alpha} + \xi_2^{1/\alpha} + \xi_3^{1/\alpha} - 1)\,d\xi_1\,d\xi_2\,d\xi_3$$

with

$$S(\xi_1, \xi_2, \xi_3) = \frac{4\pi}{\alpha^4}(\xi_1 \xi_2 \xi_3)^{\beta/2\alpha + 1/\alpha - 1 - \gamma} .$$

The sign of each integral above is determined by the factor (see [26])

$$f(\gamma) = 1 + \xi_3^\gamma - \xi_1^\gamma - \xi_2^\gamma .$$

It is found that $f(\gamma)$ is positive when

$$\gamma < 0 \quad \text{or} \quad \gamma > 1 . \tag{2.45}$$

For the same values of β as those considered by MMT and the additional value $\beta = 3$, Table 2 displays the corresponding frequency slopes from Eqs. (2.37), (2.38) and the signs of Q_0, P_0 according to criterion (2.45).

Our calculations show that the WT theory should work most successfully for $\beta = 0$ (instead of $\beta = -1$ in [61]). They yield both $Q_0 < 0$ and $P_0 > 0$. Incidentally, MMT reported the smallest

difference between numerics and theory for $\beta = 0$. The cases with spectral slopes smaller than the Rayleigh–Jeans distribution (i.e. $\gamma < 1$) are nonphysical. At best, a thermodynamic equilibrium is expected in the conservative regime. Hence, we cannot strictly rely on the Kolmogorov-type exponents for $\beta = -1, -\frac{3}{4}$ to compare with the numerical results in forced regimes. The case $\beta = -\frac{1}{2}$ is a critical case. There is a 'regular' WT theory only for $\beta > -\frac{1}{2}$. At $\beta = -\frac{1}{2}$, although we find $P_0 > 0$, a pure thermodynamic equilibrium state (i.e. $\gamma = 1$) is predicted instead of the inverse cascade. This is however not valid because of the necessity for a finite flux of wave action towards $\omega = 0$. The direct cascade may then be influenced one way or another, and the theory may not be applicable to the whole spectrum. Using condition (2.45), we deduce that the fluxes of wave action and energy simultaneously have the correct signs in the region of parameter

$$\beta < -\frac{3}{2} \quad \text{and} \quad \beta > 2\alpha - \frac{3}{2} , \tag{2.46}$$

or

$$\beta < -\frac{3}{2} \quad \text{and} \quad \beta > -\frac{1}{2} \quad \text{if } \alpha = \frac{1}{2} . \tag{2.47}$$

Since the strength of the nonlinearity increases with β, the case $\beta < -\frac{3}{2}$, which is close to a linear problem, is not interesting from a general point of view and may raise some difficulties in numerical studies.

Restricting again to $\alpha = \frac{1}{2}$ and $\beta = 0$, one has for the spectrum

$$n(\omega) = a P^{1/3} \omega^{-2} , \tag{2.48}$$

where P is the flux of energy towards high frequencies, and

$$a = \left(\left. \frac{\partial I}{\partial y} \right|_{y=1} \right)^{-1/3} \tag{2.49}$$

is the Kolmogorov constant. Numerical calculations give

$$a = 0.376 . \tag{2.50}$$

It is interesting that in this case the link between the spectral density $n(k)$ of the wave field and the spectral density $\mathbf{E}(\omega)$ of the free-surface elevation,

$$\mathbf{E}(\omega)\,\mathrm{d}\omega = \omega_k n(k)\,\mathrm{d}k ,$$

leads to $\mathbf{E} \approx$ constant. This is not the equipartition. In comparison, one has for the Rayleigh–Jeans spectrum $n(k) \approx 1/\omega$, or $\mathbf{E} \approx \omega$. This is the real equipartition.

The general turbulent solution to the kinetic equation (2.24) has the form

$$n_k = \frac{P^{1/3}}{\omega^{2\beta/3-1}} F\left(\frac{Q_\omega}{P} \right) .$$

Here F is some function of one variable, P is the energy flux (2.42) and Q the flux of wave action (2.41). The meaning of this solution is that there is a source of energy of intensity P at $\omega = 0$ and a source of wave action of intensity $-Q$ at $\omega \to \infty$. The fluxes P and Q flow in opposite directions ($P > 0$ and $Q < 0$). If the intensity of one of the sources is zero, one gets one of the two nonequilibrium KZ solutions.

In a real situation, the existence of a stationary distribution requires the presence of damping regions both at large and small ω, even if there is only one source. In the presence of damping and linear instability, Eq. (2.9) can be written in the form

$$\mathrm{i}\frac{\partial\hat{\psi}_k}{\partial t} = \frac{\delta H}{\delta\hat{\psi}_k^*} + \mathrm{i}D(k)\hat{\psi}_k \ , \tag{2.51}$$

where $D(k)$ is the damping ($D(k) < 0$) or the growth rate of instability ($D(k) > 0$).

Recall that the wave action N is equal to $\int |\hat{\psi}_k|^2 \, \mathrm{d}k$. From (2.51), one obtains the exact equation for the wave action balance

$$Q = \frac{\mathrm{d}N}{\mathrm{d}t} = 2\int D(k)|\hat{\psi}_k|^2 \, \mathrm{d}k \ . \tag{2.52}$$

After averaging, one has

$$\langle Q\rangle = \frac{\mathrm{d}\langle N\rangle}{\mathrm{d}t} = 2\int D(k)n_k \, \mathrm{d}k. \tag{2.53}$$

The total mean flux of wave action $\langle Q\rangle$ is a linear functional of n_k at any level of nonlinearity.

For the total flux of energy, one has the exact identity

$$\frac{\mathrm{d}H}{\mathrm{d}t} = 2\int \omega(k)D(k)|\hat{\psi}_k|^2 \, \mathrm{d}k + \frac{\lambda}{2}\int [D(k_1) + D(k_2) + D(k_3) + D(k)]$$

$$\times T_{123k}\hat{\psi}_1\hat{\psi}_2\hat{\psi}_3^*\hat{\psi}_k^*\delta(k_1 + k_2 - k_3 - k) \, \mathrm{d}k_1 \, \mathrm{d}k_2 \, \mathrm{d}k_3 \, \mathrm{d}k \ . \tag{2.54}$$

After averaging, one has

$$\frac{\mathrm{d}\langle H\rangle}{\mathrm{d}t} = 2\int \omega(k)D(k)n_k \, \mathrm{d}k + \frac{\lambda}{2}\int [D(k_1) + D(k_2) + D(k_3) + D(k)]$$

$$\times T_{123k}\,\mathrm{Re}\,J_{123k}\delta(k_1 + k_2 - k_3 - k) \, \mathrm{d}k_1 \, \mathrm{d}k_2 \, \mathrm{d}k_3 \, \mathrm{d}k \ . \tag{2.55}$$

The right-hand side of Eq. (2.55) can be found if the nonlinearity is weak. In this case, the assumption of Gaussian statistics leads to (recall Eq. (2.21))

$$\mathrm{Re}\,J_{123k} \approx n_1 n_2 [\delta(k_1 - k_3) + \delta(k_1 - k)] \ . \tag{2.56}$$

Simple calculations yield

$$\frac{\mathrm{d}\langle H\rangle}{\mathrm{d}t} = 2\int \widetilde{\omega}(k)D(k)n_k \, \mathrm{d}k \ , \tag{2.57}$$

where

$$\widetilde{\omega}(k) = \omega(k) + 2\lambda\int T_{1k}n(k_1) \, \mathrm{d}k_1$$

is the renormalized frequency (see Table 1 for the definition of T_{1k}).

In the case $\beta = 0$, $T_{1k} = 1$ and

$$\frac{\mathrm{d}\langle H\rangle}{\mathrm{d}t} = 2\int \omega(k)D(k)n_k \, \mathrm{d}k + 2\lambda N\langle Q\rangle \ . \tag{2.58}$$

In a strongly nonlinear situation, the estimate of the total flux of energy is more complicated. We will show that in the case of wave collapse, the coherent structure can dissipate and carry wave action to the large wave number region without carrying any energy.
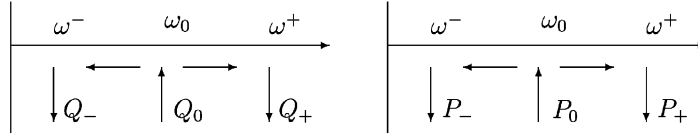
Fig. 2. A system with one source at ω_0 and two sinks at $\omega^\pm$ of wave action and energy; the directions of the fluxes are indicated by the arrows.

In the stationary state, wave action and total energy are conserved as waves interact with each other: $\langle Q \rangle = 0$, $\mathrm{d}\langle H \rangle / \mathrm{d}t = 0$. Going back to the case of weak nonlinearity, we write the balance equations as

$$\int D(k) n_k \, \mathrm{d}k = 0, \quad \int \omega(k) D(k) n_k \, \mathrm{d}k = 0 \ . \tag{2.59}$$

In this particular case, the renormalization of the frequency does not influence the balance equations. The total flux of energy can be replaced by the flux of quadratic energy P.

Let us consider the situation shown in Fig. 2. The balance equations (2.59) can be rewritten as

$$Q_0 = Q^+ + Q^-, \quad P_0 = P^+ + P^- \ , \tag{2.60}$$

where Q_0 and P_0 are the input of wave action and energy in the area of instability $\omega \approx \omega_0$, Q^+ and P^+ are the sinks of wave action and energy in the high frequency region $\omega \approx \omega^+$, Q^- and P^- are the sinks in the low-frequency region $\omega \approx \omega^-$.

Roughly speaking,

$$P_0 \approx \omega_0 Q_0, \quad P^+ \approx \omega^+ Q^+, \quad P^- \approx \omega^- Q^- \ , \tag{2.61}$$

so that

$$Q_0 = Q^+ + Q^-, \quad \omega_0 Q_0 \approx \omega^+ Q^+ + \omega^- Q^- \ . \tag{2.62}$$

Hence

$$\frac{Q^+}{Q^-} \approx \frac{\omega_0 - \omega^-}{\omega^+ - \omega_0}, \quad \frac{P^+}{P^-} \approx \frac{\omega^+}{\omega^-} \frac{\omega_0 - \omega^-}{\omega^+ - \omega_0} \ . \tag{2.63}$$

For $\omega^- \approx \omega_0 \ll \omega^+$, one has

$$\frac{Q^+}{Q^-} \approx \frac{\omega_0 - \omega^-}{\omega^+}, \quad \frac{P^+}{P^-} \approx \frac{\omega_0 - \omega^-}{\omega^-} \ . \tag{2.64}$$

In other words, if $\omega_0 \ll \omega^+$, most of the wave action is absorbed at low frequencies. The amounts of energy absorbed in both ranges have the same order of magnitude. If, in addition, $\omega^- \ll \omega_0$, $P^+ \gg P^-$ and most of the energy is absorbed at high frequencies. These two cases of equilibrium are summarized in Fig. 3.

These conclusions are valid only under the hypothesis of approximate Gaussianity of wave turbulence.

3. What is the difference between a soliton and a quasisoliton?

Section 2 provided an overview of the theory of weak turbulence. As said in the introduction, wave turbulence is often influenced by coherent structures. In this section, we introduce two types of
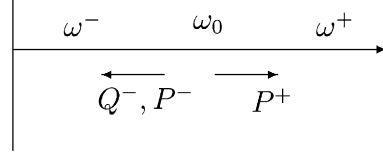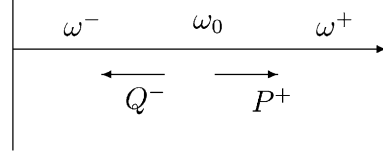
Case 1. $\omega^- \approx \omega_0 \ll \omega^+$, $Q^+ \ll Q^-$, $P^+ \sim P^-$.

Case 2. $\omega^- \ll \omega_0 \ll \omega^+$, $Q^+ \ll Q^-$, $P^+ \gg P^-$.

Fig. 3. Two special cases of equilibrium. The directions of the fluxes are indicated by the arrows.

coherent structures: solitons[4] and quasisolitons [97]. Formally, solitons and quasisolitons are defined as solutions to Eq. (2.5) of the form

$$\hat{\psi}_k(t) = e^{i(\Omega - kV)t}\hat{\phi}_k \ . \tag{3.1}$$

Here Ω and V are constants. In the physical space

$$\psi(x,t) = e^{i\Omega t}\xi(x - Vt) \ , \tag{3.2}$$

where $\xi(\cdot)$ is the inverse Fourier transform of $\hat{\phi}_k$ and V is the soliton or quasisoliton velocity. Thus the amplitude $|\psi(x,t)| = |\xi(x - Vt)|$ propagates without change of form. The quantity $\hat{\phi}_k$ satisfies the integral equation

$$\hat{\phi}_k = -\frac{\lambda}{\Omega - kV + \omega(k)} \int T_{123k}\hat{\phi}_1\hat{\phi}_2\hat{\phi}_3^*\delta(k_1 + k_2 - k_3 - k)\,dk_1\,dk_2\,dk_3 \ . \tag{3.3}$$

Let us introduce the functionals

$$\mathbf{T}(k) = \lambda \int T_{123k}\hat{\phi}_1\hat{\phi}_2\hat{\phi}_3^*\delta(k_1 + k_2 - k_3 - k)\,dk_1\,dk_2\,dk_3 \tag{3.4}$$

and

$$\mathbf{F} = -\Omega + kV - \omega(k) = -\Omega + kV - |k|^\alpha \ . \tag{3.5}$$

The quantity $\hat{\phi}_k$ now takes the form

$$\hat{\phi}_k = \frac{\mathbf{T}(k)}{\mathbf{F}} \ . \tag{3.6}$$

---

[4] In the literature, the word 'soliton' is sometimes used to describe solitary waves with special properties, such as preserving their shapes when they collide with each other. In this review, the word 'soliton' is regarded as being synonymous with solitary wave.
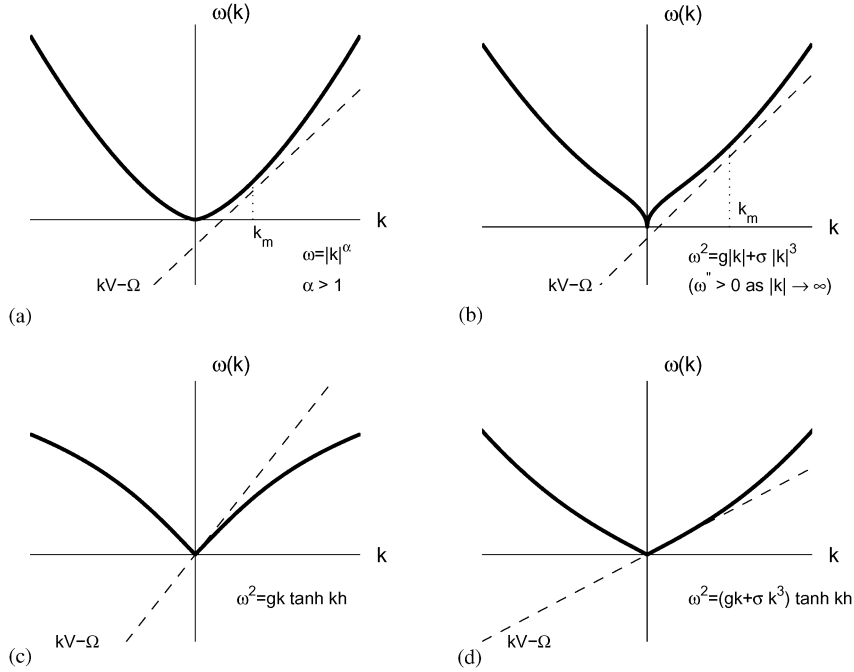
Fig. 4. Four examples of typical 'solitonic' situations. (a) The dispersion relation is $\omega = |k|^\alpha$, with $\alpha > 1$. The constant Ω is positive and the functional $\mathbf{F}$ is negative for all $k \in \mathbb{R}$. The case $\alpha = 2$ corresponds to the dispersion relation for the NLS equation. (b) The dispersion relation is $\omega^2 = g|k| + \sigma|k|^3$, with g the acceleration due to gravity and σ the coefficient of surface tension. The constant Ω is positive but small. This case corresponds to steady envelope solitons for capillary-gravity waves. (c) The dispersion relation is $\omega^2 = gk \tanh kh$. This is the dispersion relation for gravity waves on the surface of a fluid layer of finite depth h. This case corresponds to solitons for gravity waves in shallow water. Their speed V is greater than $\sqrt{gh}$. The constant Ω is equal to zero. (d) The dispersion relation is $\omega^2 = (gk + \sigma k^3) \tanh kh$, with $\sigma > gh^2/3$. This case corresponds to capillary-gravity waves on very shallow water. The soliton speed V is less than $\sqrt{gh}$. The constant Ω is equal to zero.

The key feature in the expression for $\hat{\phi}_k$ is the presence of the denominator $\Omega - kV + \omega(k)$. If this denominator has no zeros on the axis $k \in \mathbb{R}$, then solitons may exist. They may also exist if $\mathbf{T}(0) = 0$ and the denominator has only one zero at $k = 0$. In this case, $\Omega = 0$ and solitons may exist if zeros of the numerator and the denominator in (3.6) cancel each other. The 'classical' soliton in the Korteweg-de Vries equation belongs to this case. The solitons in the MMT model will be discussed in Section 4. Four typical 'solitonic' situations are shown in Fig. 4. The quantity $\hat{\phi}_k$ is sharply localized near the wave number k_m. The case shown in Fig. 4(b) has been widely studied in recent years. It occurs when the phase velocity $\omega(k)/k$ exhibits a local minimum at a nonzero wave number, which results in a gap in the spectrum $\omega(k)$. Depending on the community, this case is called differently: capillary-gravity waves with damped oscillations in the water wave community (see for example [84,24]), ice waves with decaying oscillations in the ice community (see for example [69]), Cherenkov radiation in the theoretical physics community (see for example [97]). The existence of a minimum phase velocity is analogous to the existence of the Landau critical velocity for the phonon-roton energy spectrum in a superfluid helium (see for example [73]).
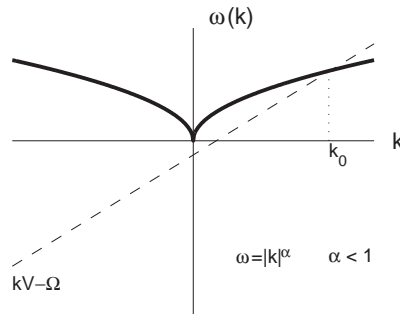
Fig. 5. Example of a typical situation where 'true' solitons cannot exist. The dispersion relation is $\omega = |k|^{\alpha}$, with $\alpha < 1$.

The next figure, Fig. 5, demonstrates a typical case where 'true' solitons cannot exist for any type of nonlinearity. In this case $\mathbf{F} = -\Omega + kV - |k|^{\alpha}$ always has at least one zero. Suppose that $\mathbf{F}(k)$ has one zero at $k = k_0$. There are no localized solitons in this case. However one can hope to be able to construct a nonlocal solution to Eq. (3.3), consisting of the localized soliton and of one or two oscillating tails. In this case, one can talk about 'quasisolitons'. This special case will be discussed in detail in Section 5.

Let us consider the situation presented in Fig. 6(a). In this case, a 'true' soliton is impossible. Nevertheless, Eq. (3.3) has a solution consisting of the localized soliton, propagating in the right direction, and of an oscillating tail $\epsilon e^{ik_0 x}$ (with $\epsilon \ll 1$) propagating with group velocity $\omega'(k_0)$ towards the left. If the straight line $-\Omega + kV = \omega$ is almost tangent to the dispersion curve $\omega(k)$, the solution is the well-known 'envelope soliton' on the surface of a deep water layer. Another possibility is illustrated in Fig. 6(b). This is the dispersion relation for gravity-capillary waves in deep water. It was shown in Fig. 4 that true solitons are possible in this case. However quasisolitons are also possible. They have two oscillating tails, one going to the left with wave number k_0, the other one going to the right with wave number k_r. If the amplitudes of the tails are small, quasisolitons can be treated as 'slowly decaying' real solitons which lose their energy by radiation in order to form the tail. Finally, we mention that the 'classical' soliton of gravity waves on the surface of shallow water turns into a quasisoliton in the presence of moderate surface tension. This situation is illustrated in Fig. 6(c). It has been widely studied in recent years. It results from the interaction between a solitary wave and a periodic mode that have the same phase velocity (see for example [62]).

In a conservative medium, quasisolitons exist for a finite time only, due to radiation. In reality, this time can be much greater than the lifetime resulting from linear damping, and the difference between a soliton and a quasisoliton is minor. A review on weakly nonlocal solitons with an extensive list of references can be found in the book by Boyd [13] and in [25]. In all cases, the adjective "weakly" means that the wave is very much like a classical soliton in that the amplitude of the "far field" oscillations is very small in comparison to the maximum amplitude of the soliton. Boyd's definitions are as follows. A classical solitary wave is a steadily-translating, finite amplitude disturbance of permanent shape and form which is spatially localized. A weakly nonlocal solitary wave is a coherent structure which approximately satisfies the classical definition of a solitary wave. The adjective "nonlocal" means that the wave asymptotes to a small amplitude oscillation as $|x - Vt|$ increases (rather than asymptotes to zero). Depending on the size of the asymptotic oscillations (exponentially small or algebraically small), such weakly nonlocal solitary waves are sometimes called nanopterons
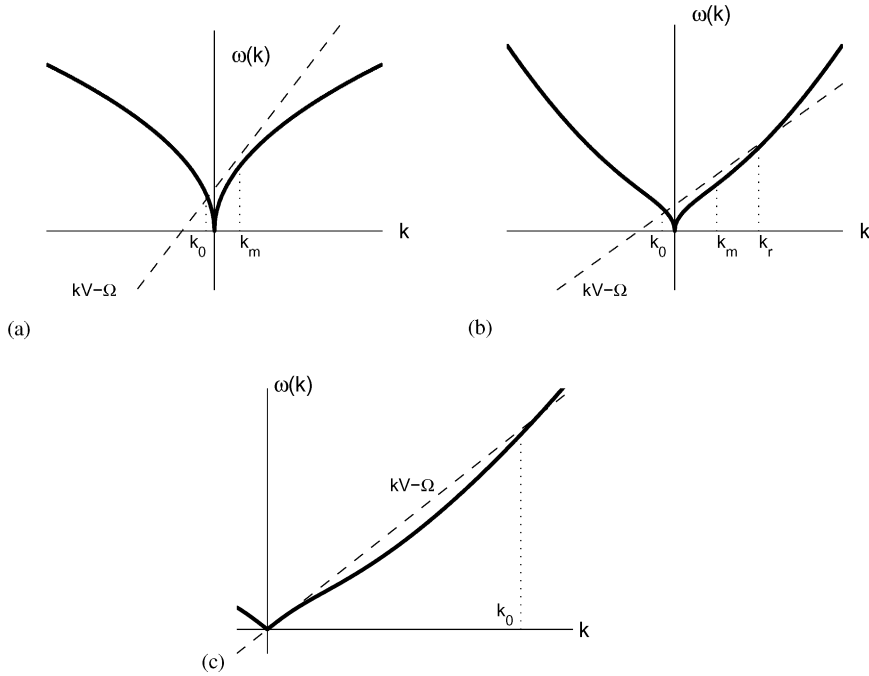
Fig. 6. Occurrence of quasisolitons. In the three examples, the straight line always crosses the curve $\omega = \omega(k)$. Therefore the denominator $\Omega - kV + \omega(k)$ in Eq. (3.3) has one or several zeros. (a) The dispersion relation is $\omega = |k|^\alpha$, with $\alpha < 1$ (for example $\alpha = \frac{1}{2}$). The constant Ω is negative and the velocity V is positive. (b) The dispersion relation is $\omega^2 = g|k| + \sigma|k|^3$. Again the constant Ω is negative and the velocity V is positive. This example corresponds to capillary-gravity waves, with g the acceleration due to gravity and σ the coefficient of surface tension. (c) The dispersion relation is $\omega^2 = (gk + \sigma k^3)\tanh kh$, with $\sigma < gh^2/3$. The constant Ω is equal to zero. This case corresponds to capillary-gravity waves on the surface of a fluid layer of finite depth h with moderate surface tension.

or micropterons. His definition of a *radiatively decaying soliton* is what we call a quasisoliton. It is a nonlinear solution which satisfies all the requirements of a classical soliton including spatial localization except that the structure decays very slowly with time through the radiation of energy to large $|x|$.

4. Solitons and collapses in the focusing MMT model

It was shown in [96] that 'true' solitons can only exist in the focusing MMT model ($\lambda = -1$). The structure of solitons depends critically on α. As said in Section 3, for $\alpha > 1$, solitons exist for any value of the velocity V. However, for $\alpha < 1$, solitons can only have zero velocity. They are solutions to Eq. (2.5) of the form

$$\hat{\psi}_k(t) = e^{i\Omega t}\hat{\phi}_k \ , \tag{4.1}$$

where Ω is a positive constant. In the physical space,

$$\psi(x, t) = e^{i\Omega t}\xi(x) \ , \tag{4.2}$$

where $\xi(x)$ is the inverse Fourier transform of $\hat{\phi}_k$. The amplitude $\hat{\phi}_k$ satisfies the integral equation

$$(\Omega + |k|^\alpha)\hat{\phi}_k = \int |k_1 k_2 k_3 k|^{\beta/4} \hat{\phi}_1 \hat{\phi}_2 \hat{\phi}_3^* \, \delta(k_1 + k_2 - k_3 - k)\, dk_1\, dk_2\, dk_3 \ . \tag{4.3}$$

The free parameter Ω can be eliminated by the scaling

$$\hat{\phi}_k = \Omega^{-\beta/2\alpha + 1/2 - 1/\alpha} \chi(K), \quad K = \Omega^{-1/\alpha} k \ , \tag{4.4}$$

where $\chi(K)$ satisfies the equation

$$(1 + |K|^\alpha)\chi(K) = \int |K_1 K_2 K_3 K|^{\beta/4} \chi_1 \chi_2 \chi_3^* \delta(K_1 + K_2 - K_3 - K)\, dK_1\, dK_2\, dK_3 \ . \tag{4.5}$$

The total wave action in the soliton is

$$N = \int |\hat{\phi}_k|^2 \, dk = \Omega^{-\beta/\alpha + 1 - 1/\alpha} N_0 \ , \tag{4.6}$$

where

$$N_0 = \int |\chi|^2 \, dK. \tag{4.7}$$

The stability question can be answered by computing $\partial N/\partial \Omega$. As is well-known (see for example [83] or [56]), a soliton is stable if $\partial N/\partial \Omega > 0$. In our case,

$$\frac{\partial N}{\partial \Omega} = -\left(\frac{\beta - \alpha + 1}{\alpha}\right) \frac{N}{\Omega} \ . \tag{4.8}$$

The soliton is stable if $\beta < \alpha - 1$, otherwise the soliton is unstable. For $\alpha = \frac{1}{2}$, the condition of soliton instability reads

$$\beta > -\tfrac{1}{2} \ . \tag{4.9}$$

This condition is satisfied in all the cases considered in this review paper.

The soliton instability is an indication that the typical coherent structure in the case of negative nonlinearity is a collapsing singularity. Typically, the formation of such singularities is described by self-similar solutions to the initial equations. Eq. (2.5) has the following family of self-similar solutions:

$$\hat{\psi}_k(t) = (t_0 - t)^{p+i\varepsilon} \chi(K), \quad K = k(t_0 - t)^{1/\alpha}, \quad p = \frac{\beta - \alpha + 2}{2\alpha} \ , \tag{4.10}$$

where ε is an unknown real constant. The constant ε is in fact an eigenvalue of the following nonlinear boundary value problem for $\chi(K)$:

$$i(p + i\varepsilon)\chi + \frac{i}{\alpha} K\chi' + |K|^\alpha \chi$$

$$- \int |K_1 K_2 K_3 K|^{\beta/4} \chi_1 \chi_2 \chi_3^* \, \delta(K_1 + K_2 - K_3 - K)\, dK_1\, dK_2\, dK_3 = 0 \ . \tag{4.11}$$

The boundary conditions will be given below.

Solution (4.10) should stay finite when $t \to t_0$. This requirement imposes the following asymptotic behavior on $\chi(K)$:

$$|\chi(K)| \to \text{const.} \times K^{-\beta/2 + \alpha/2 - 1}, \quad K \to 0 \ . \tag{4.12}$$

At time $t = t_0$, solution (4.10) turns to the power-like function

$$|\hat{\psi}_k| \rightarrow \text{const.} \times k^{-v}, \quad v = \alpha p = \frac{\beta - \alpha + 2}{2} \ . \tag{4.13}$$

In reality, the self-similar solution is realized in physical space in a finite domain of order L. Hence solution (4.13) should be cut off at $k \approx 1/L$. In Fourier space, solution (4.13) represents the formation of a powerlike "tail" (4.13). The wave action concentrated in this tail must be finite. Therefore the integral

$$\int_0^\infty |\hat{\psi}_k|^2 \, \mathrm{d}k \tag{4.14}$$

should converge as $k \rightarrow \infty$. It leads to the condition on parameters

$$\beta > \alpha - 1 \ , \tag{4.15}$$

which coincides with the condition for soliton instability.

Plugging (4.10) into the Hamiltonian in Fourier space (2.8) gives

$$H = \int \omega(k)|\hat{\psi}_k|^2 \, \mathrm{d}k - \frac{1}{2} \int T_{123k}\hat{\psi}_1\hat{\psi}_2\hat{\psi}_3^*\hat{\psi}_k^* \delta(k_1 + k_2 - k_3 - k) \, \mathrm{d}k_1 \, \mathrm{d}k_2 \, \mathrm{d}k_3 \, \mathrm{d}k$$

$$= (t_0 - t)^{\beta/\alpha - 2 + 1/\alpha} H_0 \ , \tag{4.16}$$

where

$$H_0 = \int |K|^\alpha |\chi|^2 \, \mathrm{d}K - \frac{1}{2} \int |K_1 K_2 K_3 K|^{\beta/4} \chi_1 \chi_2 \chi_3^* \chi^* \, \delta(K_1 + K_2 - K_3 - K) \, \mathrm{d}K_1 \, \mathrm{d}K_2 \, \mathrm{d}K_3 \, \mathrm{d}K \ .$$

If $\alpha - 1 < \beta < 2\alpha - 1$, then $H \rightarrow \infty$ as $t \rightarrow t_0$, unless

$$H_0 = 0 \ . \tag{4.17}$$

Identity (4.17) holds on the whole interval $\alpha - 1 < \beta < 2\alpha - 1$. Solutions of Eq. (4.11) must be continuous in β. The same holds for H. Hence H_0 must be equal to zero at the ends of the interval, in particular when $\beta = 2\alpha - 1$. Condition (4.17) imposes implicitly a constraint on the constant ε. In fact, it can be realized only at one specific value of ε, which is an eigenvalue of the boundary problem (4.11) with the boundary conditions

$$|\chi(K)| \rightarrow \text{const.} \times K^{-\beta/2 + \alpha/2 - 1}, \ K \rightarrow 0 \quad \text{and} \quad |\chi(K)| \rightarrow 0, \ |K| \rightarrow \infty \ .$$

Note that there is a typo in the limit as $|K| \rightarrow \infty$ in [96]. In the case $\beta > 2\alpha - 1$, $H \rightarrow 0$ as $t \rightarrow t_0$. There is no limitation on the value of H_0. If $v < 1$ in Eq. (4.13), i.e. $\alpha - 1 < \beta < \alpha$, a collapse is the formation of an integrable singularity in physical space. If $v > 1$, i.e. $\beta > \alpha$, the singularity is the formation of a discontinuity of the function $\psi(x)$ or its derivatives.

The formation of singularities leads to the formation in Fourier space of a powerlike spectrum

$$n_k = \langle |\hat{\psi}_k|^2 \rangle \approx |k|^{-2v} = |k|^{-\beta + \alpha - 2} \ . \tag{4.18}$$

Estimate (4.18) can be obtained from simple considerations. Assuming that in the Hamiltonian H (4.16) the quadratic term (linear part) and the quartic term (nonlinear part) are of the same order of magnitude leads precisely to estimate (4.18)! At large wave numbers (or large frequencies), the

spectrum (4.18) decays faster than the Kolmogorov spectrum. The case $\alpha = \frac{1}{2}$, $\beta = 0$ is marginal ($\beta = 2\alpha - 1$). In this case one obtains

$$n_k \approx |k|^{-3/2} = \omega^{-3} , \tag{4.19}$$

while the KZ spectrum gives $n_k \approx |k|^{-1}$. The quadratic energy

$$E = \int e(k,t)\,\mathrm{d}k \approx \int \frac{1}{\omega}\,\mathrm{d}\omega$$

diverges logarithmically as $\omega \to \infty$. There is no contradiction since the total energy in any collapsing structure is zero.

By analogy with deep water gravity waves, let us study the case $\alpha = \frac{1}{2}$, $\beta = 3$ in more detail. Spectrum (4.18)

$$n_k \approx |k|^{-9/2} = \omega^{-9} \tag{4.20}$$

can be called Phillips spectrum by analogy to the well-known "ω^{-5} spectrum" for deep water waves [72]. The KZ spectrum is $n_k \approx |k|^{-3}$. For both of these spectra, the quadratic part of the total energy converges as $\omega \to \infty$.

The shape of the free surface is given by Eq. (B.3), that is [5]

$$\eta_k = \frac{|k|^{1/4}}{\sqrt{2}} (\hat{\psi}_k + \hat{\psi}^*_{-k}) . \tag{4.21}$$

Since $\langle |\hat{\psi}_k| \rangle^2 \approx |k|^{-9/2}$, we have $\langle |\eta_k| \rangle^2 \approx |k|^{-4}$, which implies discontinuity of the first spatial derivative in agreement with Phillips initial assumption. The spectral density of the free-surface elevation $e(k,t) = \omega(k)n(k,t)$ behaves like $\langle |\eta_k|^2 \rangle$, so that one has $e(k) \approx |k|^{-4}$. This result holds in the one-dimensional case as well as in the two-dimensional case. Note that the Phillips spectrum $\mathbf{E}(\omega) \approx \omega^{-5}$ is realized only in the two-dimensional case. In the one-dimensional case,

$$\mathbf{E}(\omega)\,\mathrm{d}\omega = e(k)\frac{\mathrm{d}k}{\mathrm{d}\omega}\,\mathrm{d}\omega$$

and $\mathbf{E}(\omega) \approx \omega^{-7}$. This is the limiting spectrum of one-dimensional swell. At the same time, the WT KZ spectrum $\mathbf{E}(\omega)$ behaves like ω^{-4} in any dimension, and $\langle |\eta_k| \rangle^2 \approx |k|^{-5/2}$.

In this section, we have shown that the formation of singularities in the focusing case leads to spectra steeper that KZ spectra. In the next section, we describe the influence of coherent structures in the defocusing case.

5. Quasisolitons in the defocusing MMT model

It was shown in [96] that *quasisolitons* are important structures in the defocusing MMT model ($\lambda = 1$). For quasisolitons the denominator in (3.3) is allowed to have a zero at $k = k_0$ and $\hat{\phi}_k$ is assumed to be a function which is sharply localized near the wave number $k = k_m$. Let the width of $\hat{\phi}_k$ near $k = k_m$ be q.

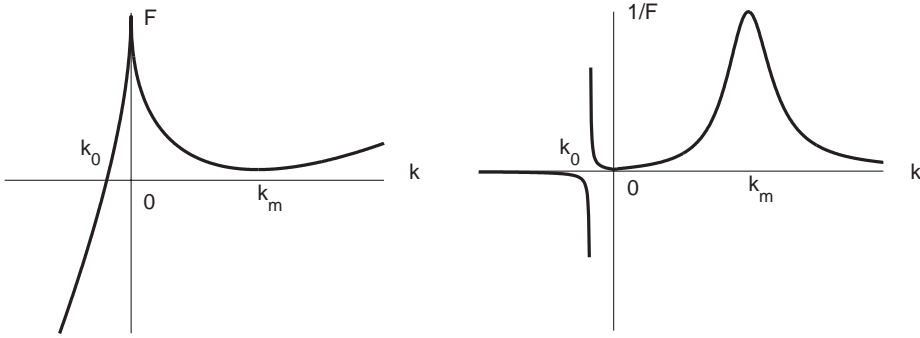[5] See comment in the footnote just before Eq. (2.13).

Fig. 7. Qualitative behavior of the function $\mathbf{F}$ and of its inverse $1/\mathbf{F}$. The expression of $\mathbf{F}$ is given by Eq. (5.5).

Recalling expression (3.4) for $\mathbf{T}(k)$, we might expect that

$$\mathbf{T}(k_0) \approx e^{-C|k_m - k_0|/q}\mathbf{T}(k_m) \ , \tag{5.1}$$

where C is a constant. In other words, $\hat{\phi}_k$ has a pole at $k = k_0$ but the residue at this pole is exponentially small. It means that solution (3.2) is not exactly localized and goes to a very small-amplitude monochromatic wave with wave number $k = k_0$ as $x \to -\infty$.

In reality, quasisolitons are localized. They radiate quasimonochromatic waves with wave number k_0 in the backward direction. If $q/k_m \ll 1$, this radiation is a very slow process. The velocity of the quasisoliton V is obtained from the equation

$$\left.\frac{\partial \mathbf{F}}{\partial k}\right|_{k=k_m} = 0 \ . \tag{5.2}$$

This implies

$$V = \alpha k_m^{\alpha-1} \ . \tag{5.3}$$

For quasisolitons which are narrow in Fourier space, Ω can be present in the form

$$\Omega = (\alpha - 1)k_m^{\alpha}\left(1 + \frac{1}{2}\alpha\left(\frac{q}{k_m}\right)^2\right) \ , \tag{5.4}$$

with $q/k_m \ll 1$. Then

$$\mathbf{F} = k_m^{\alpha} - |k|^{\alpha} + \alpha k_m^{\alpha-1}(k - k_m) + \tfrac{1}{2}\alpha(1 - \alpha)k_m^{\alpha-2}q^2 \ . \tag{5.5}$$

Note that if $\alpha < 1$, $\mathbf{F}$ has a zero at $k = k_0 < 0$ for any k_m. Hence, $1/\mathbf{F}$ always has a pole on the negative real axis, and soliton (3.3) cannot be a real soliton. But if $q \ll k_m$, $1/\mathbf{F}$ has a sharp maximum at $k \approx k_m$. The qualitative behavior of the function $\mathbf{F}$ and of its inverse $1/\mathbf{F}$ are shown in Fig. 7. Introducing $\kappa = |k - k_m|$, one has approximately

$$\mathbf{F} \approx \tfrac{1}{2}\alpha(1 - \alpha)k_m^{\alpha-2}(\kappa^2 + q^2) \ , \tag{5.6}$$

and one gets for the width of the maximum of $1/\mathbf{F}$

$$\kappa \approx q \ . \tag{5.7}$$

If $\kappa \ll |k_0|$, one can construct a quasisoliton which is supported in Fourier space near k_m. In the general case, $|k_0| \approx k_m$. If $\alpha = \frac{1}{2}$ and $q = 0$, one can easily find

$$k_0 = -(\sqrt{2} - 1)^2 k_m . \tag{5.8}$$

The quasisoliton moves to the right direction with the velocity $V(k_m)$ and radiates backward monochromatic waves of wave number k_0. The shape of the quasisoliton can be found explicitly in the limit $q \to 0$. Now $\kappa \ll k_m$ and one has approximately

$$\mathbf{T}(k) \approx k_m^\beta \int \hat{\phi}_1 \hat{\phi}_2 \hat{\phi}_3^* \delta(\kappa_1 + \kappa_2 - \kappa_3 - \kappa) \, \mathrm{d}\kappa_1 \, \mathrm{d}\kappa_2 \, \mathrm{d}\kappa_3 . \tag{5.9}$$

Taking into account Eq. (5.6), one can rewrite Eq. (3.3) as

$$\frac{1}{2} \alpha(1 - \alpha) k_m^{\alpha-2} (\kappa^2 + q^2) \hat{\phi}_\kappa = k_m^\beta \int \hat{\phi}_1 \hat{\phi}_2 \hat{\phi}_3^* \delta(\kappa_1 + \kappa_2 - \kappa_3 - \kappa) \, \mathrm{d}\kappa_1 \, \mathrm{d}\kappa_2 \, \mathrm{d}\kappa_3 . \tag{5.10}$$

Using the inverse Fourier transform, one can transform (5.10) into the stationary NLS equation

$$\frac{1}{2} \alpha(1 - \alpha) k_m^{\alpha-2} \left(-\frac{\partial^2 \phi}{\partial x^2} + q^2 \phi \right) = k_m^\beta |\phi|^2 \phi , \tag{5.11}$$

which has the soliton solution

$$\phi(x) = \sqrt{\frac{\alpha(1 - \alpha)}{k_m^{\beta-\alpha+2}}} \frac{q}{\cosh qx} . \tag{5.12}$$

It gives the following approximate quasisoliton solution to Eq. (2.1) with $\lambda = 1$:

$$\psi(x, t) = \phi(x - Vt) \mathrm{e}^{\mathrm{i}\Omega t} \mathrm{e}^{\mathrm{i}k_m(x - Vt)} ,$$

$$\Omega = -(1 - \alpha) k_m^\alpha - \tfrac{1}{2} \alpha(1 - \alpha) k_m^{\alpha-2} q^2 ,$$

$$V = \alpha k_m^{\alpha-1} . \tag{5.13}$$

Quasisoliton (5.13) is an "envelope soliton". In [96], it was shown that it can be obtained directly from Eq. (2.1), by looking for a solution of the form

$$\psi(x, t) = U(x, t) \mathrm{e}^{-\mathrm{i}(1-\alpha)k_m^\alpha t} \mathrm{e}^{\mathrm{i}k_m(x - Vt)} , \tag{5.14}$$

and using a Taylor expansion. At leading order, U satisfies the nonstationary NLS equation

$$\mathrm{i}\left(\frac{\partial U}{\partial t} + V \frac{\partial U}{\partial x} \right) = \frac{1}{2} \alpha(1 - \alpha) k_m^{\alpha-2} \frac{\partial^2 U}{\partial x^2} + k_m^\beta |U|^2 U , \tag{5.15}$$

which has soliton solutions of the form

$$U(x, t) = \phi(x - Vt) \exp(-\tfrac{1}{2} \mathrm{i}\alpha(1 - \alpha) k_m^{\alpha-2} q^2 t) . \tag{5.16}$$

To find the shape of the quasisoliton more accurately, one should keep more terms in the Taylor expansion. The expansion runs in powers of the parameter q/k_m. Note that one cannot find the lifetime of the quasisoliton. The lifetime grows as $\mathrm{e}^{|k_0|/q}$ and its calculation goes beyond a perturbation expansion.

As a matter of fact, the parameter q/k_m is crucial for quasisolitons. The smaller it is, the closer the quasisoliton is to a "real soliton". The amplitude of a quasisoliton is proportional to q/k_m. Quasisolitons of small amplitude satisfy the integrable NLS equation and are stable. It is not obvious for quasisolitons of finite amplitude. One can guess that at least in the case $\beta > 0$, when collapse is not forbidden, there is a critical value of the amplitude of a quasisoliton. Above that value it is unstable and generates a singularity at a finite time. Our numerical experiments confirm this conjecture for $\beta = 3$.

Quasisolitons move with different velocities and collide. If the amplitudes of the quasisolitons are small and their velocities are close, they obey the NLS equation and their interaction is elastic. One can guess that the same holds for small-amplitude quasisolitons even if their velocities are quite different. This is not obvious for quasisolitons of moderate amplitude. One can conjecture that their interaction is inelastic: they merge and form a quasisoliton of larger amplitude.

6. Brief description of the numerical tools

The direct method employed to perform numerical computations on the model is similar to the method used in [61]. With the aim of observing direct and inverse cascades, the complete equation to be integrated reads

$$\mathrm{i}\,\frac{\partial\hat{\psi}_k}{\partial t} = \omega(k)\hat{\psi}_k + \lambda \int T_{123k}\hat{\psi}_1\hat{\psi}_2\hat{\psi}_3^*\delta(k_1+k_2-k_3-k)\,\mathrm{d}k_1\,\mathrm{d}k_2\,\mathrm{d}k_3 + \mathrm{i}[F(k)+D(k)]\hat{\psi}_k \ . \tag{6.1}$$

Typical expressions for the forcing term F and the damping term D are

$$F(k) = \sum_j f_j\delta(k-k_j) \quad \text{and} \quad D(k) = -v^-|k|^{-d^-} - v^+|k|^{d^+} \ .$$

The forcing term $F(k)$ denotes an instability localized in a narrow spectral band. The damping part $D(k)$ contains a wave action sink at large scales and an energy sink at small scales. The presence of these two sinks is necessary to reach a stationary regime if two different fluxes are assumed to flow in opposite k-directions from the stirred zone. In our experiments, we set $d^- = 8$ and $d^+ = 16$ unless other values are specified. The purpose of using high-order viscosity (also referred to as hyperviscosity), which separates sharply the inertial and dissipative ranges, is to minimize the effects of dissipation at intermediate scales of the simulated spectrum. In connection with Section 2, we introduce the dissipation rates of wave action and quadratic energy for small wave numbers

$$Q^- = 2\int_{k<k_{\mathrm{f}}} v^-|k|^{-d^-}|\hat{\psi}_k|^2\,\mathrm{d}k \ , \tag{6.2}$$

$$P^- = 2\int_{k<k_{\mathrm{f}}} v^-|k|^{-d^-}\omega(k)|\hat{\psi}_k|^2\,\mathrm{d}k \ , \tag{6.3}$$

and for large wave numbers

$$Q^+ = 2\int_{k>k_{\mathrm{f}}} v^+|k|^{d^+}|\hat{\psi}_k|^2\,\mathrm{d}k \ , \tag{6.4}$$

$$P^+ = 2 \int_{k > k_{\mathrm{f}}} v^+ |k|^{d^+} \omega(k) |\hat{\psi}_k|^2 \, \mathrm{d}k \;, \tag{6.5}$$

where k_{f} is the characteristic wave number of forcing.

A pseudospectral code solves Eq. (6.1) in a periodic interval of Fourier modes. We define the discrete direct Fourier transform (FT) as

$$\hat{\psi}(k_n) = \hat{\psi}_n = \mathrm{FT}(\psi_j) = \frac{1}{N_d} \sum_{j=0}^{N_d-1} \psi_j \mathrm{e}^{-\mathrm{i}k_n x_j} \;, \tag{6.6}$$

and the discrete inverse Fourier transform (FT^{-1}) as

$$\psi(x_j) = \psi_j = \mathrm{FT}^{-1}(\hat{\psi}_n) = \sum_{n=-N_d/2+1}^{N_d/2} \hat{\psi}_n \mathrm{e}^{\mathrm{i}k_n x_j} \;, \tag{6.7}$$

where N_d is the number of grid points, $k_n = 2\pi n/L$ is the nth wave number, $x_j = jL/N_d$ is the location of the jth grid point and L is the size of the computational domain $0 < x < L$. We usually choose $L = 2\pi$ so that the k_n's are integers and the spacing in Fourier space is $\Delta k = 1$.

In our experiments, quantities defined as integrals along the spectral interval are computed in their discrete forms without any renormalisation. For instance, we use for wave action the formula

$$N = \sum_{n=-N_d/2+1}^{N_d/2} |\hat{\psi}_n|^2 \;, \tag{6.8}$$

and for the quadratic part of energy

$$E = \sum_{n=-N_d/2+1}^{N_d/2} \omega(k_n) |\hat{\psi}_n|^2 \;. \tag{6.9}$$

The linear frequency term is treated exactly by an integrating factor technique, thus removing it from the timestepping procedure. As emphasized by MMT, the natural stiffness of the problem as well as possible numerical instabilities are thus avoided. Consequently, we do not need to shorten the inertial interval by downshifting the cutoff of ultraviolet absorption (as in [75]). The nonlinear term is calculated through the Fast Fourier Transform by first transforming to real space where a multiplication is computed and then transforming back to spectral space. For the multiplication operation, twice the effective number of grid points are required in order to avoid aliasing errors. A fourth-order Runge–Kutta scheme integrates the conservative model in time, giving a solution to which the diagonal factor $\exp([F(k) + D(k)]\Delta t)$ is applied at each time step Δt. For our purpose, it is not necessary to use symplectic integrators (see for example [5] for cases when symplectic integrators must be used).

A series of numerical simulations of Eq. (6.1) with resolution up to $N_d = 2048$ de-aliased modes has been performed. It is important to check carefully the level of nonlinearity. It was shown for example in [21,74] that for a very weak nonlinearity the modes which can take part in the resonances, the active modes, are very sparse. There is therefore a critical level of nonlinearity below which an energy cascade may not be possible. The effects of discretization of the spectrum on the evolution of weak turbulence of surface gravity waves were investigated by direct numerical simulations in [81].

7. Numerical experiments on weak turbulence and collapses (focusing MMT model)

In this section, numerical computations based on the focusing model ($\lambda = -1$) with $\beta = 0$ are presented. Originally, this case was chosen in order to test the direct cascade of weak turbulence. Forcing is located at large scales and the inertial interval is defined by the right transparency window $k_{\mathrm{f}} \ll |k| \ll k_{\mathrm{d}}$ (where k_{f} and k_{d} are the characteristic wave numbers of forcing and ultraviolet damping, respectively). The forcing and damping used in Eq. (6.1) are

$$F(k) = \begin{cases} 0.2 & \text{if } 6 \leqslant |k| \leqslant 9 \\ 0 & \text{otherwise} \end{cases} \quad \text{and} \quad D(k) = -196.61|k|^{-8} - 2.16 \times 10^{-47}|k|^{16} \ .$$

As displayed in Table 2, the theoretical spectrum which can be realized in this window is

$$n_k \approx |k|^{-1} \ . \tag{7.1}$$

Typically, initial conditions are given by random noise in the spectral space. Simulations are run until a quasi-steady regime is established. By quasi-steady, we mean a regime which is characterized by small fluctuations of the energy and the wave action around some mean value. Then time averaging begins and continues for a length of time which significantly exceeds the characteristic time scale of the slowest harmonic from the inertial range (free of the source and the sink). The time-step of the integration has to provide, at least, accurate enough resolution of the fastest harmonic in the system. It turns out that one has to use an even smaller time-step than defined by the last condition: the presence of fast nonlinear events in the system requires the use of a time-step $\Delta t = 0.005$, which is roughly equal to $2\pi\omega_{\max}^{-1}/40$, where $\omega_{\max}$ is the largest linear frequency in the system. Time averaging with such a small time step leads to a computationally time-consuming procedure despite the one-dimensionality of the problem.

The time-averaged values of the wave action N, quadratic energy E and corresponding fluxes Q^-, Q^+, P^-, P^+ in the stationary state are

$$N = 1, \quad E = 9, \quad Q^- = 0.0098, \quad Q^+ = 0.0478, \quad P^- = 0.014, \quad P^+ = 1.430 \ . \tag{7.2}$$

One sees that $Q^+/Q^- \approx 4.9$ and $P^+/P^- \approx 102$. Sporadic collapsing events developing on top of the WT background have been observed. They send most of wave action to large wave numbers without violation of energy conservation, since in each self-similar collapse structure the amount of total energy is zero. Fig. 8 displays the evolution towards collapse at the point $x = 1.006$ between $t = 4999.980$ and 5000.205. One can conjecture that collapses are described by self-similar solutions (see Section 4). For such solutions $H \equiv 0$. It means that the collapse can carry wave action to high frequencies, *without carrying any energy*! Since the Hamiltonian is the difference of quadratic and quartic terms and both of them go to infinity, it becomes possible to explain the apparent contradictions of the dissipation rates.

The hypothesis related to the prevailing role of collapses at $\lambda = -1$ is corroborated by the following facts:

- Intermittency in dissipation rates of quadratic energy and wave action for $\lambda = -1$ is much higher than for $\lambda = 1$ in the region of large wave numbers. This intermittency can be explained by outbursts of dissipation when wave collapses occur.
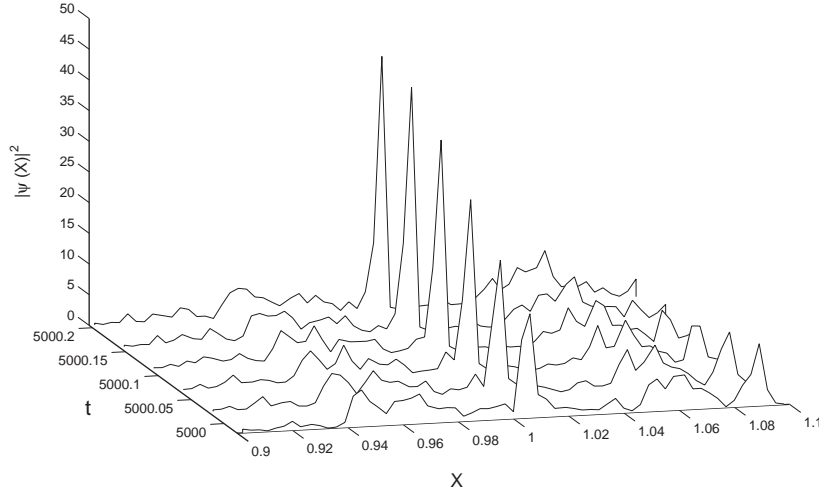
Fig. 8. Focusing MMT model ($\lambda = -1$) with $\alpha = \frac{1}{2}$, $\beta = 0$. Evolution towards collapse at $x \approx 1$ between $t = 4999.980$ and 5000.205. The period corresponding to the fastest frequency in the system is roughly 0.2.

- The analysis of time Fourier transforms of separate harmonics (e.g. $k = 200$) shows the presence of two components, as shown in Fig. 9. The peak at $\omega \approx 13$ corresponds to a linear wave with a moderate nonlinear shift of frequency. This right peak is the "weak turbulence" component of the wave field. Another component is roughly symmetrical with respect to the reflection $\omega \to -\omega$, with maximum at $\omega = 0$. This is certainly a strongly nonlinear component which could be associated with wave collapses.

Another experiment is performed by taking the isolated initial condition

$$\psi(x, 0) = \psi_0 e^{-(x-\pi)^2/2\sigma^2}, \quad \sigma \in \mathbb{R} . \tag{7.3}$$

Fig. 10 shows the early stages of the conservative evolution of the system. A sufficiently large initial condition collapses into a sharp spike. This experiment could serve as an evidence of the finite-time singularity formation for the case $\lambda = -1$.

Fig. 11 provides a plot of the Kolmogorov spectrum calculated by putting $P = P^+ = 1.430$ and $a = 0.376$ in Eq. (2.48). The spectrum provides a higher level of turbulence than the observed one.

The high-frequency asymptotics is fairly close to the one predicted by WT theory. One can explain this fact as follows. In this case, the turbulence is the coexistence of collapsing events and weak turbulence. Collapses carry most of wave action to high frequencies. But their contribution to the high-frequency part of the spectrum is weak, because they produce Phillips-type spectra that decay very fast as $|k| \to \infty$. Recall that this spectrum is given by Eq. (4.19) and is equal to $n_k \approx |k|^{-3/2}$. Hence as $|k| \to \infty$, only the WT component survives. Even $P \approx 10^{-2} P^+$ is enough to provide an observable tail in the WT Kolmogorov spectrum. Cai et al. [20], who performed similar numerical experiments both in the case of free waves and the case of driven-damped waves, claim that they observed the Phillips-type spectrum for free waves evolving from smooth initial data (see their Fig. 15 showing a collapsing wave front in Fourier space, with $\alpha = \frac{1}{2}$ and $\beta = 0$).
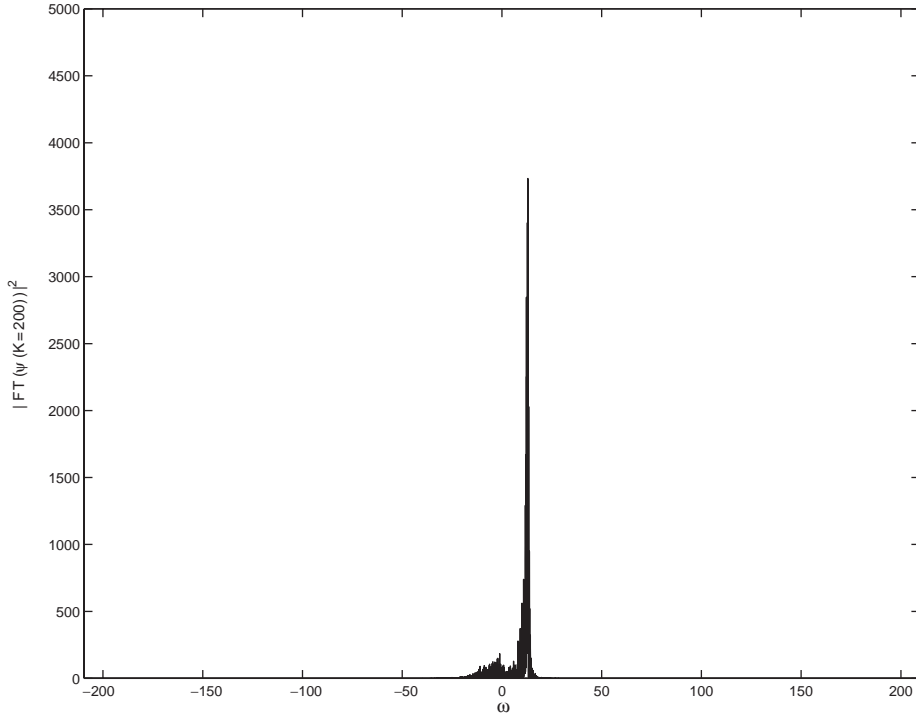
Fig. 9. Focusing MMT model ($\lambda = -1$) with $\alpha = \frac{1}{2}$, $\beta = 0$. Square amplitude of the time Fourier transform for the mode $k = 200$ vs. frequency (the time resolution is 0.015). There are two peaks: one at $\omega \approx 13$ (linear wave with moderate nonlinear frequency shift) and one at $\omega \approx 0$ (strong nonlinear component associated with wave collapses).
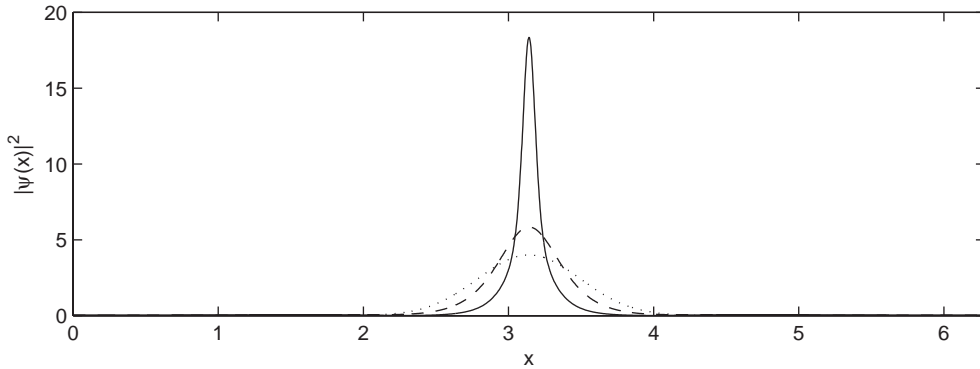

Fig. 10. Focusing MMT model ($\lambda = -1$) with $\alpha = \frac{1}{2}$, $\beta = 0$. Evolution towards a collapsing peak of the isolated solution (7.3) for the initial amplitude $\psi_0 = 2$ and $\sigma = 0.5$: dotted line $t = 0$, dashed line $t = 0.55$, solid line $t = 1.1$.

8. Supercritical wave turbulence and self-organized criticality in the focusing MMT model

In this section, we continue to discuss one-dimensional wave turbulence in the framework of the focusing ($\lambda = -1$) MMT model (2.1), in the case $\beta/2 > \alpha$, that is $\beta > 1$ if $\alpha = \frac{1}{2}$. The reason for
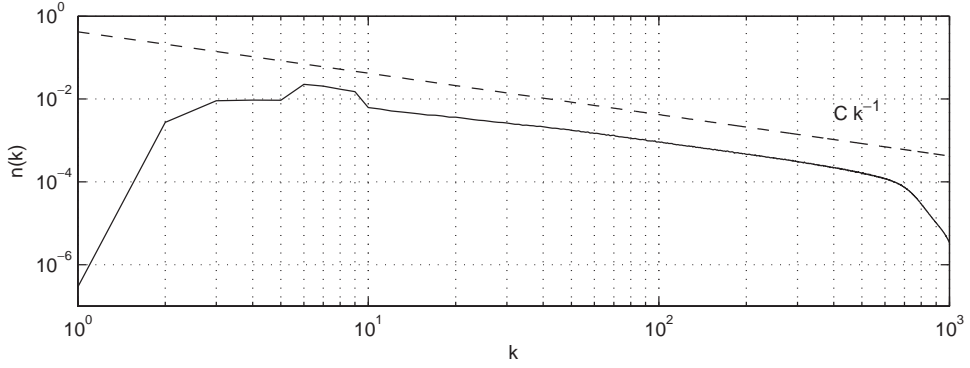
Fig. 11. Focusing MMT model ($\lambda = -1$) with $\alpha = \frac{1}{2}$, $\beta = 0$. Computed spectrum and weak-turbulence spectrum vs. wave number. The weak-turbulence spectrum (straight line) is given by $n(k) = aP^{1/3}|k|^{-1}$, with $aP^{1/3} \approx 0.42$ (see Eq. (2.48)).

choosing $\beta/2 > \alpha$ will be explained below: a short-wave instability develops. The equation

$$i \frac{\partial \hat{\psi}_k}{\partial t} = \omega(k)\hat{\psi}_k - \int T_{123k}\hat{\psi}_1\hat{\psi}_2\hat{\psi}_3^* \delta(k_1 + k_2 - k_3 - k)\, \mathrm{d}k_1\, \mathrm{d}k_2\, \mathrm{d}k_3 \tag{8.1}$$

has an exact solution describing nonlinear monochromatic waves with wave number $k_0 > 0$ and linear frequency $\omega_0 = \omega(k_0)$:

$$\hat{\psi}_k(t) = A\delta(k - k_0)\mathrm{e}^{-\mathrm{i}(\omega_0 - T_0|A|^2)t} \ , \tag{8.2}$$

where T_0 is defined in Table 1. One can study the stability of this solution, assuming that the perturbation $\delta\hat{\psi}_k$ of $\hat{\psi}_k$ satisfies the linearized equation

$$i \frac{\partial \delta\hat{\psi}_k}{\partial t} = \lambda_k \delta\hat{\psi}_k - R_{kk_0}|A|^2 \delta\hat{\psi}_{2k_0-k}^* \ . \tag{8.3}$$

Here

$$\lambda_k = \omega_k - \omega_0 + (T_0 - 2T_{k0})|A|^2$$

and R_{kk_0} was defined in Table 1. Assuming that $\delta\hat{\psi}_k$ and $\delta\hat{\psi}_{2k_0-k}^*$ are proportional to $\mathrm{e}^{\mathrm{i}\Lambda t}$, one finds after simple calculations:

$$\Lambda = \tfrac{1}{2}(\lambda_{2k_0-k} - \lambda_k) \pm \sqrt{\tfrac{1}{4}(\lambda_k + \lambda_{2k_0-k})^2 - R_{kk_0}^2|A|^4} \ . \tag{8.4}$$

Note that

$$\lambda_k + \lambda_{2k_0-k} = \omega_k + \omega_{2k_0-k} - 2\omega_0 + 2(T_0 - T_{k0} - T_{2k_0-k,k_0})|A|^2 \ . \tag{8.5}$$

Let us consider modulational instabilities. Let $k \to k_0$ and denote $k - k_0$ by δk. In this limit

$$\lambda_k + \lambda_{2k_0-k} \approx \omega_0''(\delta k)^2 - 2T_0|A|^2$$

or

$$\sqrt{\tfrac{1}{4}(\lambda_k + \lambda_{2k_0-k})^2 - R_{kk_0}^2|A|^4} \approx \sqrt{-T_0\omega_0''(\delta k)^2|A|^2 + \tfrac{1}{4}\omega_0''^2(\delta k)^4} \ . \tag{8.6}$$

Formula (8.6) describes modulational instability if $\omega'' > 0$. In our case, $\omega'' < 0$ and modulational instability does not occur. However, it does not mean that the nonlinear monochromatic wave is always stable. Instability occurs in a neighborhood of the point where

$$\lambda_k + \lambda_{2k_0-k} = 0 \ .$$

In the present report,

$$\omega_k = |k|^\alpha, \quad T_{123k} = |k_1 k_2 k_3 k|^{\beta/4} \ .$$

Assuming $k \gg k_0$, one can write

$$\lambda_k + \lambda_{2k_0-k} \approx 2k^\alpha - 4k^{\beta/2} k_0^{\beta/2} |A|^2 \ . \tag{8.7}$$

If $\beta/2 > \alpha$, $\lambda_k + \lambda_{2k_0-k}$ always has a zero at

$$k = k_{\text{unstable}} = \left(\frac{1}{2k_0^{\beta/2}|A|^2} \right)^{1/(\beta/2-\alpha)} \ . \tag{8.8}$$

If $|A|^2 \to 0$, $k_{\text{unstable}} \to \infty$. Apparently perturbations with wave number close to k_{unstable} are unstable and grow exponentially.

   To understand the nature of this instability one should mention that in the presence of a monochromatic wave of amplitude A, the dispersion relation for waves of small amplitude is modified as follows:

$$\omega_k \to \tilde{\omega}_k = \omega_k - 2T_{k0}|A|^2 = k^\alpha - 2k^{\beta/2} k_0^{\beta/2} |A|^2 \ . \tag{8.9}$$

For $\beta/2 > \alpha$, $\tilde{\omega}_k$ changes sign and becomes negative at large wave numbers. This short-wave instability corresponds in fact to the excitation of waves of negative energy. Usually, instabilities of this type are not suppressed by nonlinear terms. Moreover, the nonlinear terms could enhance instability, leading to singularity formation. This explosive singularity can take place over an interval of finite length rather than at one spatial point. We will call such a singularity a 'broad collapse'.

   It would be interesting to prove the existence of the broad collapse analytically. In this paper we describe numerical results showing this phenomenon. We take $\beta=3$. Eq. (6.1) was solved numerically in the domain $[0, 2\pi]$ in real space using fast Fourier transforms algorithms for the spatial integration and a split-step technique for the integration in time. The spatial resolution was 2048 modes and the time step was $\omega_{\text{max}}^{-1}/50$, where ω_{max} is the largest linear frequency in the system. The parameters of the forcing and damping terms in Eq. (6.1) were chosen as follows:

$$F(k) = \begin{cases} 0.1 & \text{if } 30 < |k| < 42, \\ 0 & \text{otherwise} \end{cases} \quad \text{and } D(k) = \begin{cases} -0.01(4 - |k|)^{-2} & \text{if } |k| < 4 \ , \\ -0.001(|k| - 824)^2 & \text{if } |k| > 824 \ . \end{cases}$$

The numerical integration of the equation started from low-level random noise initial conditions. It was found that the system of waves did not reach a stationary state, but exhibited a complicated quasiperiodic behavior. The total wave action $N(t)$ shows strong nonlinear relaxation oscillations. Its maximum and minimum differ by one order of magnitude, as shown in Fig. 12(a). The level of nonlinearity and the rate of energy damping are both quasiperiodic functions of time, consisting of a sequence of sporadic outbursts that occur roughly when $N(t)$ reaches its maximum (see Figs. 12(b) and (c)). Fig. 13 presents plots of $|\psi|^2$ as a function of x at successive times close to the occurrence
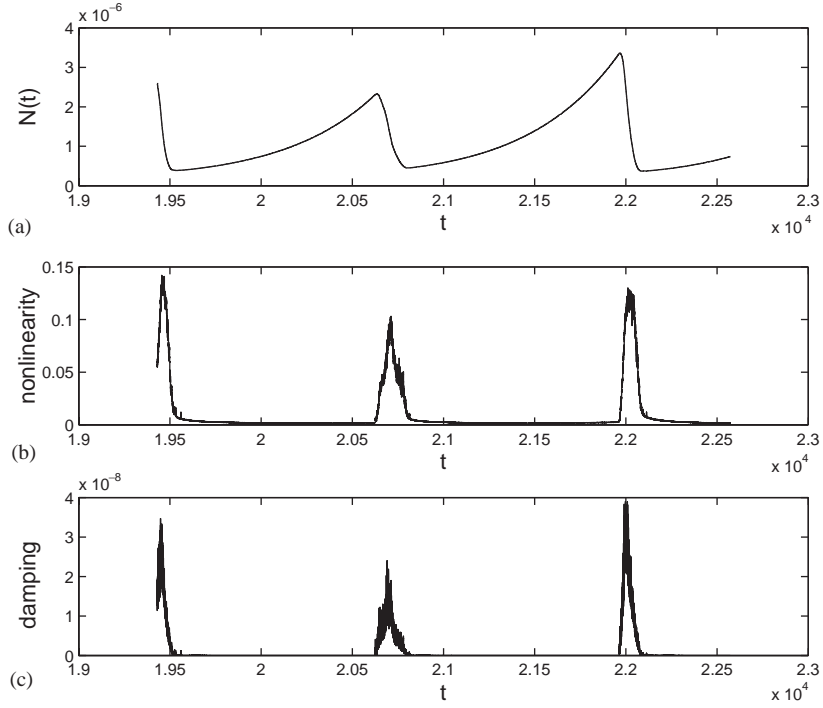
Fig. 12. Focusing MMT model ($\lambda = -1$) with $\alpha = \frac{1}{2}$, $\beta = 3$. (a) Total wave action vs. time. (b) Level of nonlinearity vs. time. (c) Rate of energy damping vs. time. The time unit is roughly five times the period of the fastest harmonic.

of the first maximum of $N(t)$. Before the maximum the wave field consists of modes concentrated in the interval of unstable modes $30 < |k| < 40$. This estimate is obtained by looking at the wavelength of the oscillations in Fig. 13(a) for example. Wave amplitudes grow almost exponentially, as shown in Fig. 14. When the total wave action reaches a certain critical level (approximately 2 or 3×10^{-6}), the short wave instability explodes (see Fig. 13(e)). The oscillations have become much shorter. The development of the instability leads to the formation of a 'broad collapse', which plays the role of a black hole, sucking energy from the rest of space. This is possible because wave interactions at $\beta = 3$ are very nonlocal in space. Very soon, the system is cooled up to a level that is one order of magnitude less than critical. Then the short waves making up the black hole disappear due to linear damping. After that the scenario repeats itself. A zoom of the region of broad collapse is shown in Fig. 15.

One should also note that wave field absorption is performed, contrary to the case of collapsing turbulence, in *noncoherent events* of spatially localized bursts of the instability developing randomly in space and quasiperiodically in time. It makes sense to call such turbulence 'supercritical' since the mechanism of wave field absorption is related to the fact that some critical amplitude of the wave field is exceeded. It would be interesting to find a physical system properly described by the model discussed above. It could be a Hamiltonian where $H_{NL} > 0$, while $E < 0$. In this case, ω_k would be negative (the linear waves would have negative energy).
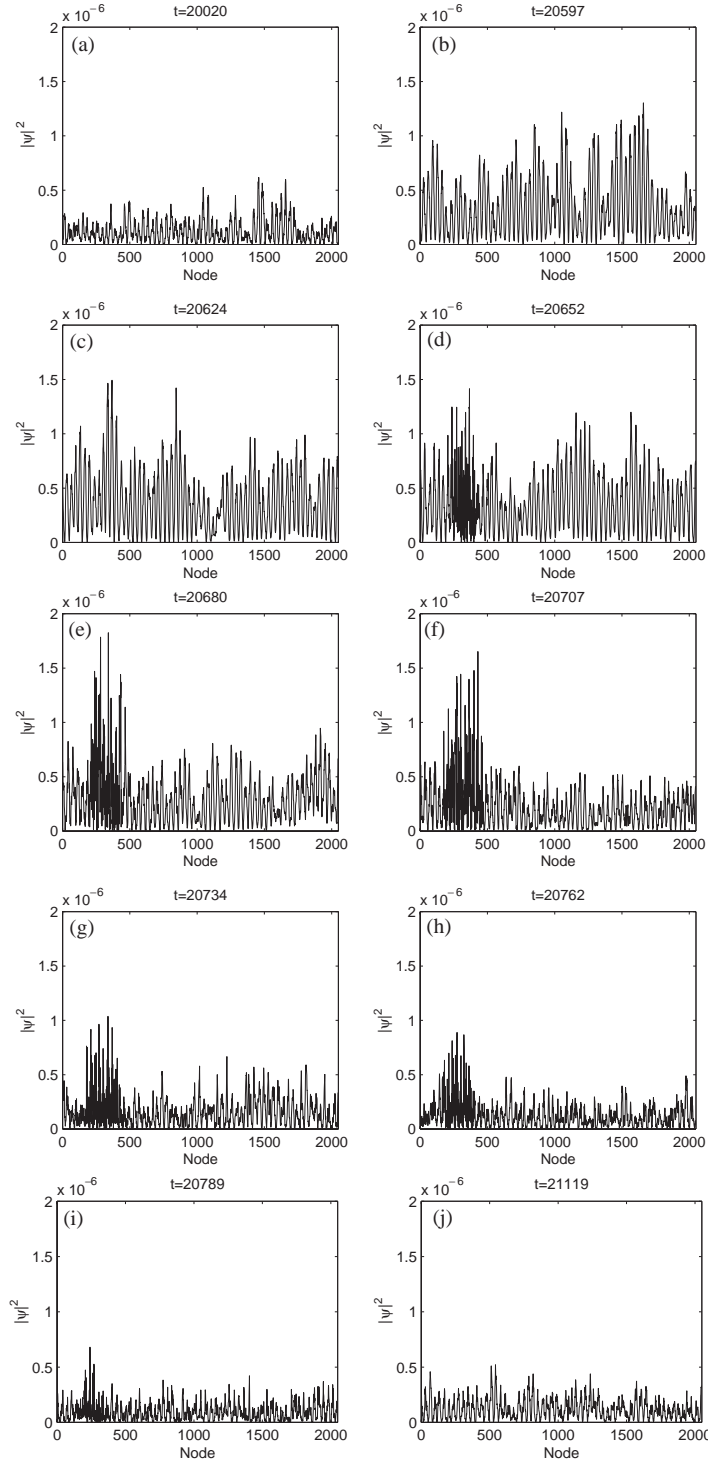
Fig. 13. Focusing MMT model ($\lambda = -1$) with $\alpha = \frac{1}{2}$, $\beta = 3$. Plots of $|\psi(x)|^2$ vs. x at successive times close to the occurrence of the first maximum of $N(t)$. The time unit is roughly five times the period of the fastest harmonic. The actual value of $x \in [0, 2\pi]$ is $x = \text{Node} \times (2\pi/N_d)$.
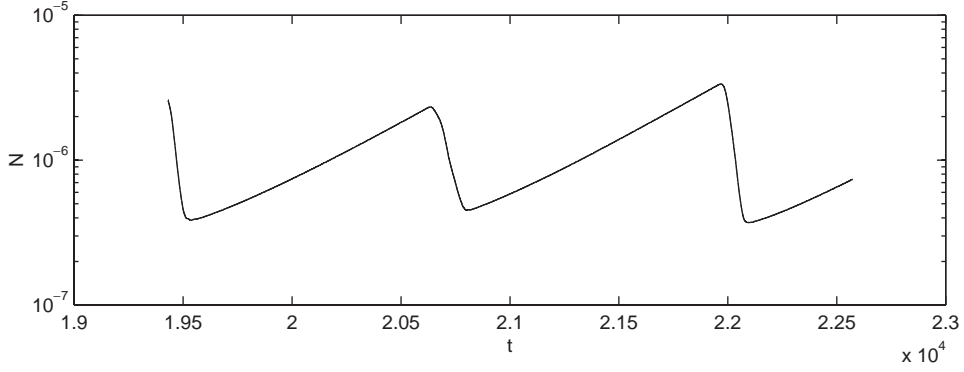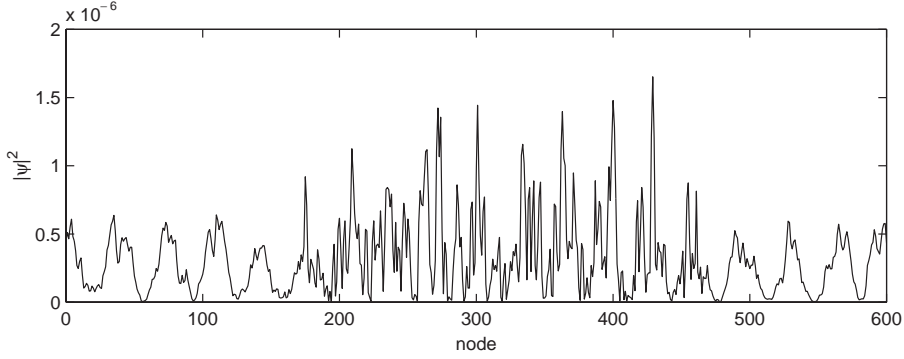
Fig. 14. Same as Fig. 12(a) in semi-log plot.

Fig. 15. Blow-up of Fig. 13(f). Time $t = 20707$. The horizontal axis is in fact x: $x = \text{node} \times (2\pi/N_d)$.

9. Numerical experiments on turbulence in the defocusing MMT model

In this section, numerical computations based on the defocusing model ($\lambda = 1$) with $\beta = 0$ are presented. Again, forcing is located at large scales and the inertial interval is defined by the right transparency window $k_f \ll |k| \ll k_d$ (where k_f and k_d are the characteristic wave numbers of forcing and ultraviolet damping, respectively). The forcing and damping used in Eq. (6.1) are

$$F(k) = \begin{cases} 0.2 & \text{if } 6 \leqslant |k| \leqslant 9, \\ 0 & \text{otherwise} \end{cases} \quad \text{and} \quad D(k) = -196.61|k|^{-8} - 5.39 \times 10^{-48}|k|^{16} \ .$$

While the weak turbulence theory makes no difference between the focusing and the defocusing cases, the numerical results show major differences. For example let us consider the dissipation rates of wave action and quadratic energy. The time-averaged values of the wave action N, quadratic energy E and corresponding fluxes in the stationary state (6.2)–(6.5) are

$$N = 3, \quad E = 19, \quad Q^- = 0.1957, \quad Q^+ = 0.0090, \quad P^- = 0.276, \quad P^+ = 0.258 \ . \tag{9.1}$$
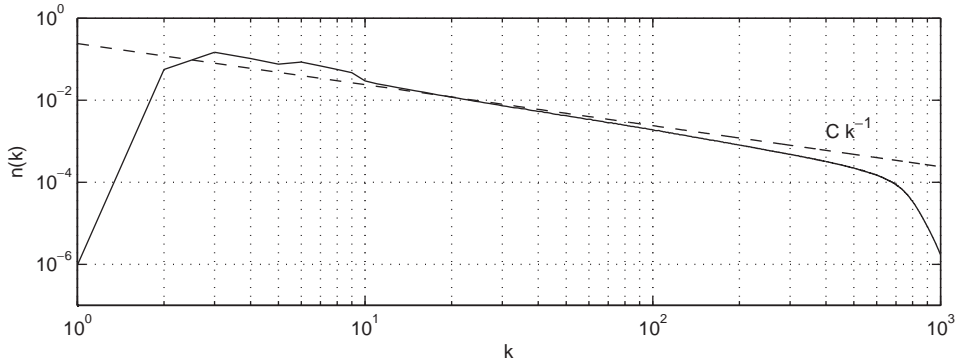
Fig. 16. Defocusing MMT model ($\lambda = 1$) with $\alpha = \frac{1}{2}$, $\beta = 0$. Computed spectrum and weak-turbulence spectrum vs. wave number. The weak-turbulence spectrum (straight line) is given by $n(k) = aP^{1/3}|k|^{-1}$, with $aP^{1/3} \approx 0.24$ (see Eq. (2.48)).
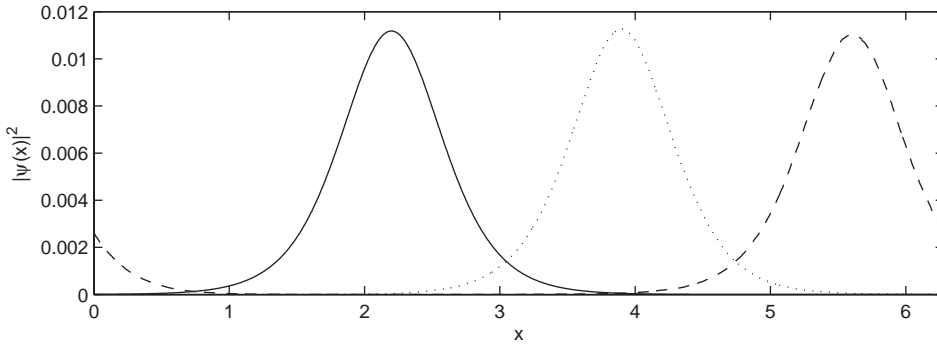

Fig. 17. Defocusing MMT model ($\lambda = 1$) with $\alpha = \frac{1}{2}$, $\beta = 0$. Plot of $|\psi(x)|^2$ vs. x, showing the evolution of the envelope of a small amplitude quasisoliton ($q/k_m = 0.1$). Solid line $t = 0$, dotted line $t = 1250$, dashed line $t = 2500$.

One can see that the case $\lambda = 1$ quantitatively fits WT theory. Indeed, in this case $Q^+/Q^- \approx 0.046 \ll 1$ and $P^+/P^- \approx 0.94$.

The Kolmogorov spectrum calculated by putting $P = P^+ = 0.258$ and $a = 0.376$ in Eq. (2.48) is shown in Fig. 16. The spectrum provides a higher level of turbulence than the observed one, but not as much as in the focusing case. The observed spectrum almost coincides with the weak turbulence one at low frequencies and then decays faster at higher wave numbers. It should stressed out again that at $\lambda = 1$ the picture of turbulence matches the WT prediction both quantitatively and qualitatively. Meanwhile, the spectrum at high wave numbers is steeper. We conjecture that it is somehow connected with quasisolitons (see next Section).[6] As an illustration, Fig. 17 shows the

---

[6] Majda et al. [61] introduced a new spectrum, which is now called the MMT spectrum, to explain the observed spectrum. At large wave numbers, the slope of the spectrum follows closely the MMT spectrum. The MMT spectrum was revisited in Section 10 of [96].

conservative evolution of the initial quasisoliton (5.13) with parameter $q/k_m = 0.1$, which is small enough to justify the Taylor expansion used in its derivation. As expected, we observe that the solution propagates and persists over a relatively long time.

10. Numerical experiments on quasisolitons and quasisolitonic turbulence (defocusing MMT model)

In the positive (defocusing) MMT model for $\alpha < 1$, quasisolitons do exist for any value of β. One property of quasisolitons is completely universal. Quasisolitons of small amplitude obey the nonlinear Schrödinger equation. They are stable and collide completely elastically. However the stability and the interaction of large amplitude quasisolitons still are open questions which can hardly be solved analytically. In this section, an attempt to solve these problems by numerical simulations is made. In the same way, conditions for the generation of quasisolitons and their role in wave turbulence can also be handled by massive numerical simulations. Results of such simulations are presented.

Fig. 18 shows the initial and final stages of collision of two quasisolitons in the case $\alpha = \frac{1}{2}$, $\beta = 0$. From now on in this section, the case $\alpha = \frac{1}{2}$, $\beta = 3$ is considered. We would like to stress once more that the MMT model with these parameters values can be considered as a heuristic model for the description of gravity surface waves in deep water.

In all experiments, damping was included in the equations. The numerical simulation of Eq. (6.1) was performed on a grid of 2048 points in the real space domain of length 2π.

The parameters of damping in the "hyperviscosity" were chosen as follows:

$$D(k) = \begin{cases} -0.05(4 - k)^8 & \text{if } 0 < k < 4 , \\ -0.1(k - 824)^2 & \text{if } 824 < k < 1024 , \\ 0 & \text{otherwise} . \end{cases}$$

Aliasing effects were not of concern due to the run-time control of the fastness of the spectrum decay toward large wave numbers. As in Section 8, the time-step of integration was equal to $\omega_{\max}^{-1}/50$ where $\omega_{\max}$ is the largest linear frequency in the system. Such a small value was chosen due to the fact that the time dependence of the individual Fourier harmonics corresponding to intermediate range wave numbers showed the presence of processes of time scale smaller than $\omega_{\max}^{-1}$. This observation was an initial indication of the significant role of nonlinearity in the problem under consideration.

Fig. 19 shows the propagation of a quasisoliton of relatively large amplitude ($q/k_m = 0.3$). The profile $\eta(x)$ is given by Eq. (2.13). One can see that the quasisoliton is unstable. The development of the instability leads first to the loss of symmetry of the envelope profile, then to the formation of singularity in finite time. The amplitude of $\eta(x)$ remains finite and continuous at the point of singularity, while its slope becomes discontinuous. The experiments are not accurate enough to conclude whether there is formation of a cusp or of a wedge. A zoom of the singular point is shown in Fig. 20.
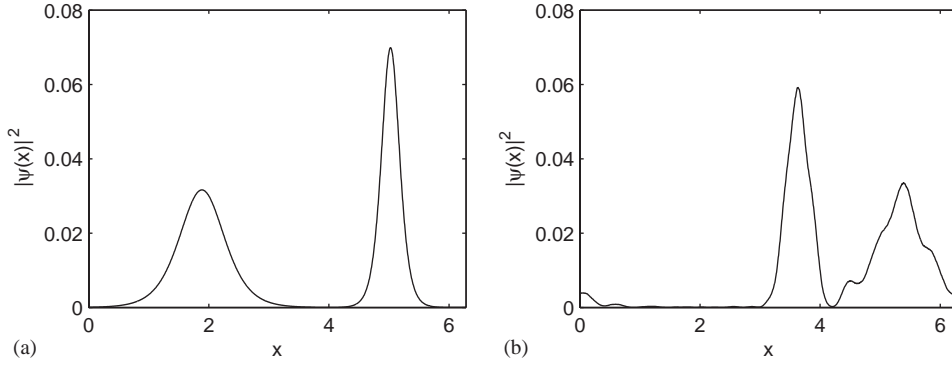
Fig. 18. Defocusing MMT model ($\lambda = 1$) with $\alpha = \frac{1}{2}$, $\beta = 0$. Plot of $|\psi(x)|^2$ vs. x, showing the interaction of the envelopes of two quasisolitons characterized by $q/k_m = 0.2$ and 0.25, respectively: (a) $t = 0$, (b) $t = 100$.
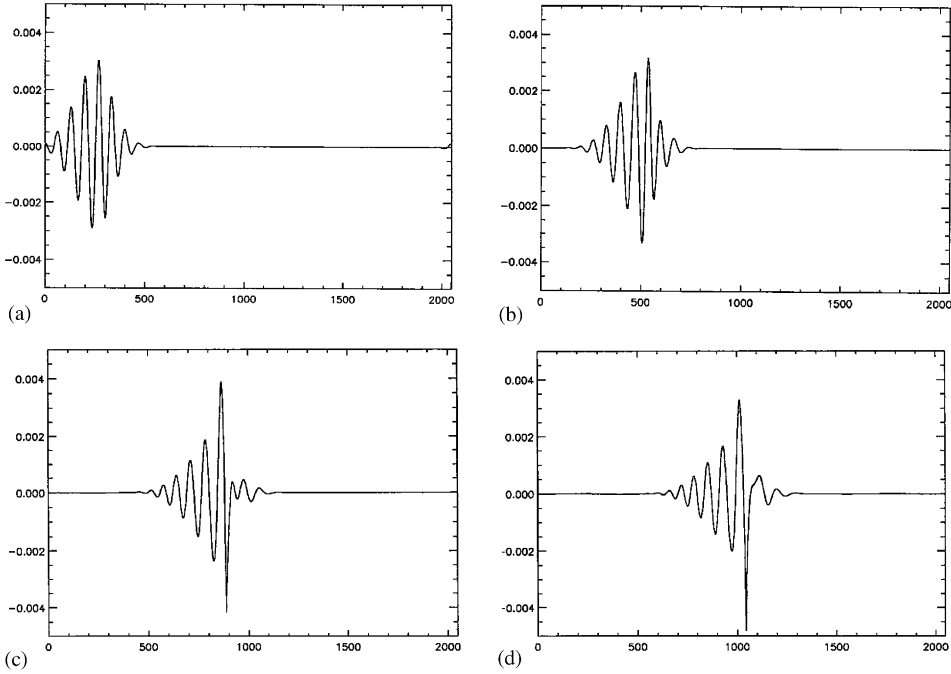

Fig. 19. Defocusing MMT model ($\lambda = 1$) with $\alpha = \frac{1}{2}$, $\beta = 3$. Plot of $\eta(x)$, given by Eq. (2.13), vs. x, showing the propagation of a quasisoliton with $q/k_m = 0.3$: (a) $t = 7.854$, (b) $t = 15.708$, (c) $t = 26.704$, (d) $t = 31.416$. The actual value of $x \in [0, 2\pi]$ is $x = (2\pi/N_d)x_{\text{graph}}$. The time unit is roughly five times the period of the fastest harmonic.

Another experiment was performed to study the development of the modulational instability of a monochromatic wave. The monochromatic wave is chosen as

$$\psi(x) = \psi_0 e^{ik_0 x}, \quad \psi_0 = 10^{-3}, \quad k_0 = 30 . \tag{10.1}$$
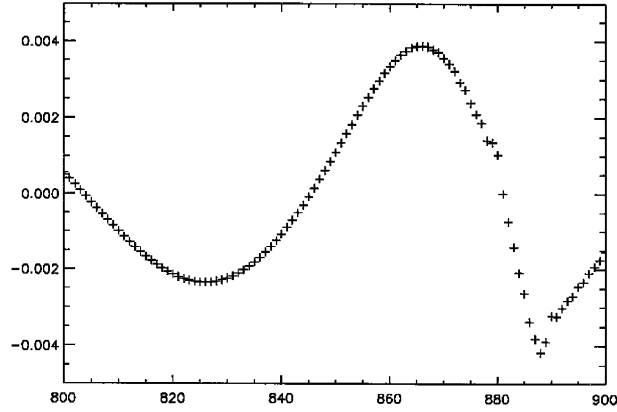
Fig. 20. Blow up of the singular point in Fig. 19(c) ($t = 26.704$).

This choice gives for the unperturbed surface elevation: [7]

$$\eta(x) = a \cos k_0 x = \sqrt{\frac{\omega(k_0)}{2}} (\psi(x) + \psi^*(x)), \quad a = \sqrt{2\omega(k_0)}\psi_0 = 3.31 \times 10^{-3} \ .$$

The dimensionless parameter measuring nonlinearity (surface slope) is $k_0 a \approx 0.1$. This value corresponds to a wave of moderately large amplitude. The wave is then perturbed as follows:

$$\psi(x) = \psi_0 e^{ik_0 x}(1 + 0.1 \cos px), \quad p = 6 \ . \tag{10.2}$$

In Fig. 21, $|\psi(x)|^2$ is plotted against x. Initially, the modulational instability develops exponentially according to linear theory. Then the amplitude of the perturbations reaches the level of the amplitude of the initial wave (Fig. 21(a)). After that, the development of the modulational instability becomes nonlinear. Initially uniform monochromatic waves break into a sequence of quasisolitons of approximately equal amplitude (Figs. 21(b)–(e)). Then these quasisolitons become unstable and the amplitude of one of them overruns the growth of the others (Fig. 21(f)). The growth of this 'champion' soliton eventually turns into collapse, which can be interpreted as the onset of wave breaking (Fig. 21(g)).

In another series of experiments, we included wave forcing. The forcing parameters are defined by

$$F(k) = \begin{cases} 0.001 & \text{if } 30 < k < 42 \ , \\ 0 & \text{otherwise} \ . \end{cases}$$

Eq. (6.1) was integrated numerically over long times for different kinds of initial conditions: low-level random noise and single harmonic excitation ($k = 30$). While the initial stages of computations were quantitatively different, the later stages of the evolution processes were strikingly similar. After a fairly long time, the wave system was separated into several soliton-like moving structures

---

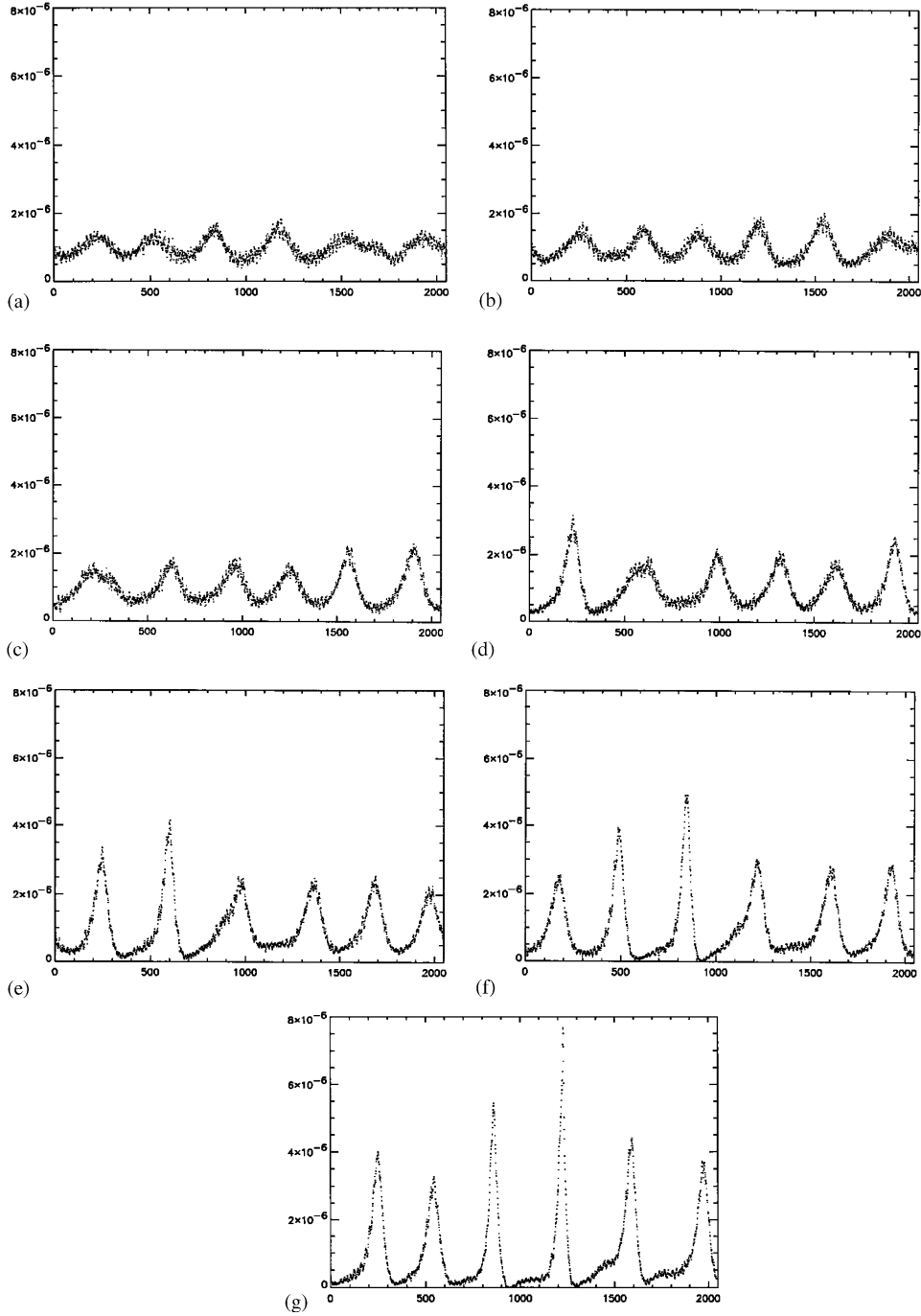[7] See comment in the footnote just before Eq. (2.13).

Fig. 21. Defocusing MMT model ($\lambda = 1$) with $\alpha = \frac{1}{2}$, $\beta = 3$. Plot of $|\psi(x)|^2$ vs. x, showing the development of the modulational instability. The monochromatic wave (10.1) is perturbed by (10.2). (a) $t = 349.502$, (b) $t = 361.283$, (c) $t = 373.064$, (d) $t = 384.845$, (e) $t = 396.626$, (f) $t = 404.480$, (g) $t = 416.261$. The actual value of $x \in [0, 2\pi]$ is $x = (2\pi/N_d)x_{\mathrm{graph}}$. The time unit is roughly five times the period of the fastest harmonic.
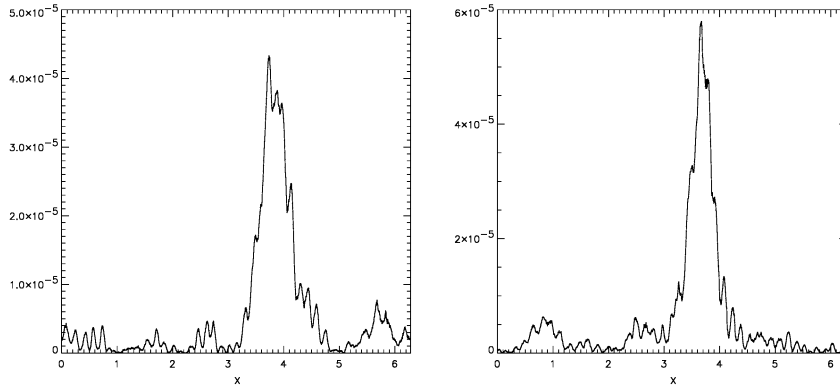
Fig. 22. Defocusing MMT model ($\lambda = 1$) with $\alpha = \frac{1}{2}$, $\beta = 3$. Plot of $|\psi(x)|^2$ vs. x, showing the propagation of a single moving soliton (left: $t = 6915$, right: $t = 10880$). The time unit is roughly five times the period of the fastest harmonic.

and low-amplitude quasi-linear waves. The interactions between the solitons and the waves slowly redistributed the number of waves in a way leading to the growth of initially bigger solitons and the collapse of initially smaller solitons. Finally the system was clearly separated into a state with one moving soliton and quasi-linear waves.

The observed phenomenon can be interpreted similarly to the "droplet" effect observed earlier in nonintegrable NLS equations [99]. The soliton solution turns out to be the statistical attractor for nonlinear nonintegrable wave systems: the long time evolution leads to the condensation of the wave action integral N into the single soliton which minimizes the Hamiltonian H.

Fig. 22 shows snapshots of the final state of the system: the single soliton is moving with constant speed on a background of quasi-linear waves. A quantitative comparison shows that the parameters of the observed structure are close to the parameters of the quasisoliton solution (5.13).

One should emphasize that there is a difference between the situation observed in the present work and former observations of "droplet" effects in nonintegrable NLS equations. The solitons observed in [99] were exact stable solutions to the corresponding NLS equation. The solitary wave solutions observed in the present work are "quasisolitons" which are unstable at least in a certain range of parameters.

In the presence of damping and forcing, initially unstable solitons become stable. These stationary quasisolitons pump energy from the outer space and provide its dissipation. Such quasisolitons realize a permanent transport of wave energy from large to small scales.

The wave turbulence that is dominated by quasisolitons can be called 'quasisolitonic turbulence'. Quasisolitonic turbulence is not weak, because quasisolitons are nonlinear structures.

We performed one more massive series of experiments in order to model quasisolitonic turbulence. In these experiments a forcing term which mimics the forcing of surface gravity waves by wind was included:

$$F(k) = \begin{cases} 0 & \text{if } k < 30, \\ 10^{-5}(k-30)^{3/2} & \text{if } 30 < k < 900 \end{cases} \quad \text{and} \quad D(k) = -\frac{1}{2}\,k_{\max}^{-7/2}k^4 \quad \text{if } k > 900 \ .$$
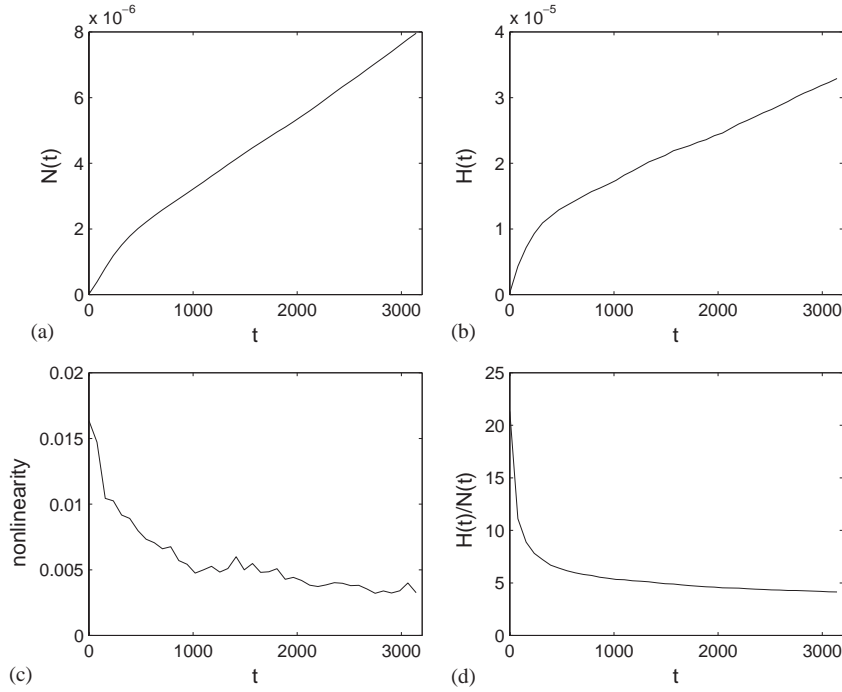
Fig. 23. Defocusing MMT model ($\lambda = 1$) with $\alpha = \frac{1}{2}$, $\beta = 3$ in the presence of forcing and damping: (a) Wave action $N(t)$, (b) Hamiltonian $H(t)$, (c) Level of nonlinearity vs. time, (d) Ratio $H(t)/N(t)$ vs. time. The time unit is roughly five times the period of the fastest harmonic.

In these experiments we started with noise. After a very short linear stage (approximately 250 times the period of the fastest harmonic), the system reached a nonlinear quasistationary state where both important integrals $N(t)$ and $H(t)$ grow almost linearly (Fig. 23). Both the ratio H_{NL}/E, shown in Fig. 23(c), and the average frequency $\langle \omega \rangle = H/N$, shown in Fig. 23(d), slowly decrease. This behavior is qualitatively similar to the weak-turbulence regime [76], but both regions are quantitatively different. For instance, the downshift in the present case is slower.

The distributions of $|\psi(x)|^2$ (Fig. 24) and $\eta(x)$ (Fig. 25) are typically quasisolitonic. Waves are concentrated in chaotic oscillating groups. The main part of wave energy is concentrated in one quasisoliton of slowly growing amplitude. Fig. 26 presents plots of

$$\Gamma(x,t) \approx |\psi_{xx}|^2 \tag{10.3}$$

at various times. The function $\Gamma(x,t)$ can be treated as the spatial distribution of energy damping. One can see that this damping is extremely intermittent both in space and in time. It is clear that the damping is created by collapses which can be compared with wave breaking events. Fig. 27 presents squared moduli of Fourier spectra averaged over some periods of time. In spite of averaging, spectra are very rough. It is interesting that not only downwind waves are present. There is also a component of upwind waves. Their average wave action is less than the wave action of downwind waves by one order of magnitude. Apparently upwind waves appear due to four-wave interactions. Spectra of both components are powerlike, but the exponents are different. At the early stage of the process,
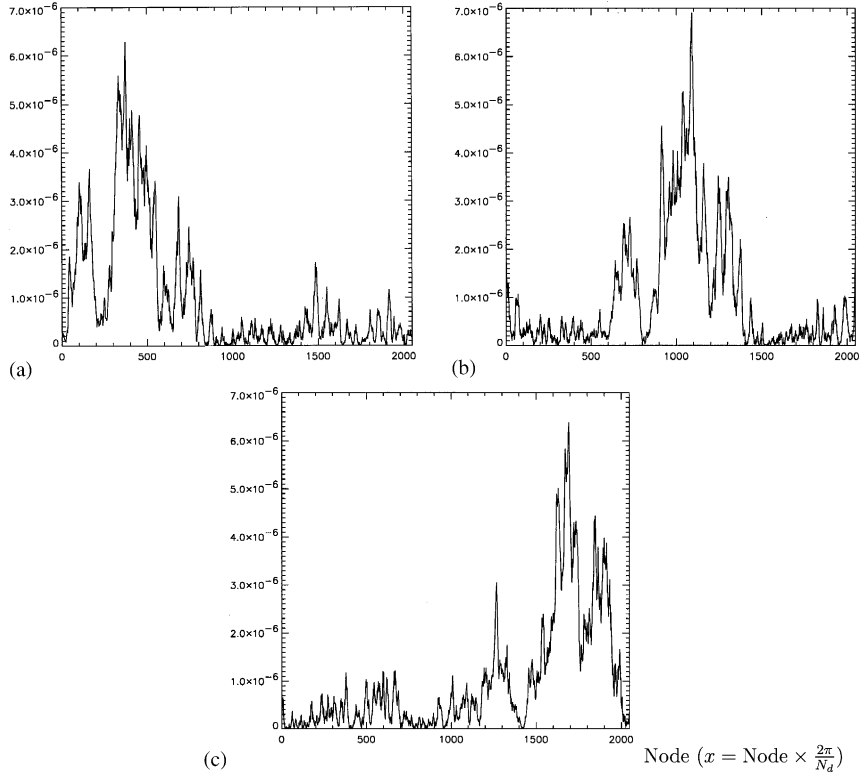
Fig. 24. Defocusing MMT model ($\lambda = 1$) with $\alpha = \frac{1}{2}$, $\beta = 3$ in the presence of forcing and damping. Plot of $|\psi(x)|^2$ vs. x. (a) $t = 2358.16$, (b) $t = 2373.87$, (c) $t = 2389.57$. The actual value of $x \in [0, 2\pi]$ is $x = (2\pi/N_d)x_{\text{graph}}$. The time unit is roughly five times the period of the fastest harmonic.

the downwind component of spectra is well described by the Phillips' formula

$$\langle |\hat{\psi}|^2 \rangle \approx |k|^{-9/2} \ . \tag{10.4}$$

In the process of wave development, the spectrum becomes flatter. At large times, it is well-described by the weak-turbulence Kolmogorov spectrum

$$\langle |\hat{\psi}|^2 \rangle \approx |k|^{-3} \ . \tag{10.5}$$

The upwind component of the spectrum fits the Kolmogorov asymptotics from the beginning.

In spite of the fact that the average level of nonlinearity is relatively small, local nonlinearity could be very high. Analysing Fig. 25, one sees that the steepness of the wave of maximum amplitude is $ka \approx 0.6$. This wave can be interpreted as a 'freak' or a 'rogue' wave.

The results can be interpreted as follows. Initially, the quasisolitonic scenario is dominant. Then a component which is essentially weakly turbulent appears and the energy flux to large wave numbers gets separated into two different channels—a weakly turbulent one and a strongly turbulent one. Since the weakly turbulent Kolmogorov spectrum decays much more slowly than the Phillips spectrum, it becomes dominant at large wave numbers in the late stage of the process.
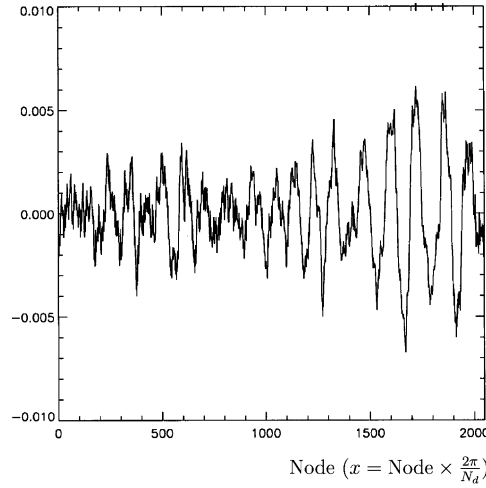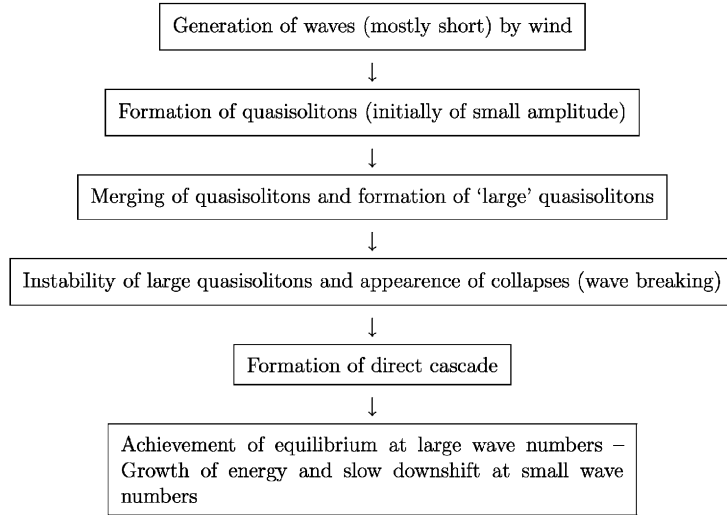
Fig. 25. Defocusing MMT model ($\lambda = 1$) with $\alpha = \frac{1}{2}$, $\beta = 3$ in the presence of forcing and damping. Plot of $\eta(x)$ vs. x, at time $t = 2389.57$.

One can present the following scenario of this quasisolitonic turbulence:

Generation of waves (mostly short) by wind
$\downarrow$
| Formation of quasisolitons (initially of small amplitude) |
$\downarrow$
| Merging of quasisolitons and formation of 'large' quasisolitons |
$\downarrow$
| Instability of large quasisolitons and appearence of collapses (wave breaking) |
$\downarrow$
| Formation of direct cascade |
$\downarrow$
| Achievement of equilibrium at large wave numbers – Growth of energy and slow downshift at small wave numbers |

In the calculations which have been presented, no damping was introduced at small wave numbers. If such a damping was included, it would easily stop the downshift and the inverse cascade. In this case the system would reach some true stationary state (mature sea in the terminology of Phillips).

In general, a lot of details of the scenario of quasisolitonic turbulence that has been presented above look similar to those of the initial scenario for the development of a wind-driven sea offered by Phillips in 1958 [71]. However, in Section 13, we show that there are major differences between the MMT model for $\alpha = \frac{1}{2}$, $\beta = 3$ and one-dimensional turbulence of gravity waves.
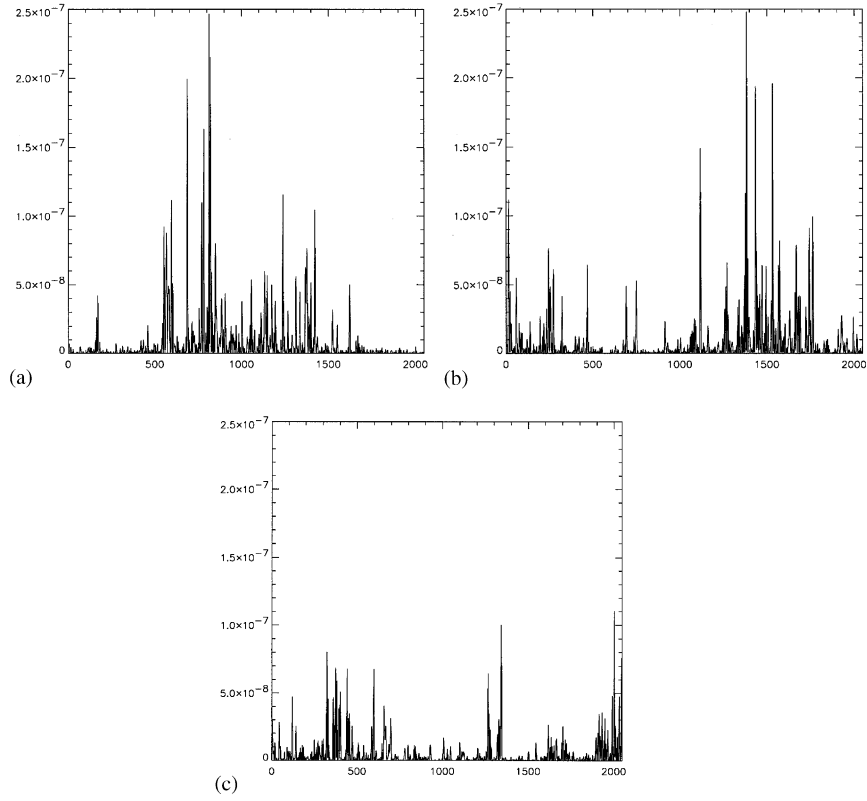
Fig. 26. Defocusing MMT model ($\lambda = 1$) with $\alpha = \frac{1}{2}$, $\beta = 3$ in the presence of forcing and damping. Evidence of intermittency. Plot of $\Gamma(x)$ vs. x. $\Gamma(x)$ is defined by (10.3). (a) $t = 2358.16$, (b) $t = 2373.87$, (c) $t = 2389.57$. The actual value of $x \in [0, 2\pi]$ is $x = (2\pi/N_d)x_{\text{graph}}$. The time unit is roughly five times the period of the fastest harmonic.
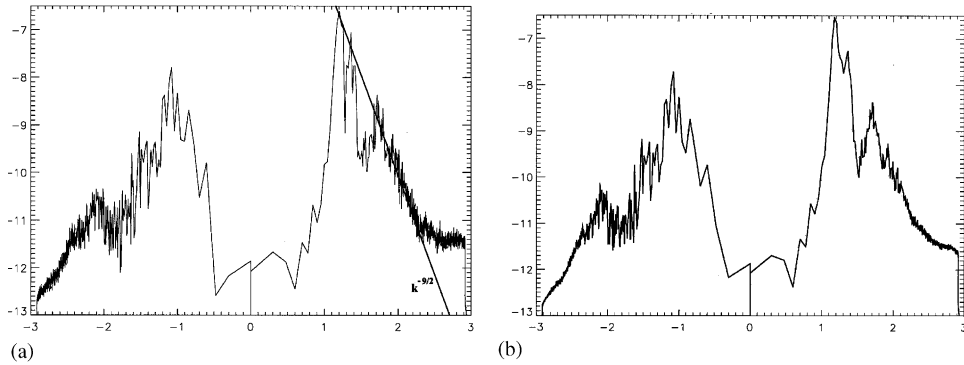
Fig. 27. Defocusing MMT model ($\lambda = 1$) with $\alpha = \frac{1}{2}$, $\beta = 3$ in the presence of forcing and damping. Squared modulus of Fourier spectra averaged over some periods of time: (a) $t = 2358 - 2395$, (b) $t = 2356 - 2749$. The upwind component of the spectrum fits the Kolmogorov asymptotics in $|k|^{-3}$ from the beginning. The downwind component of the spectrum fits first the Phillips spectrum in $|k|^{-9/2}$ (a), and then the Kolmogorov asymptotics in $|k|^{-3}$ (b).

One should stress that real turbulence is essentially two-dimensional and mostly weak. However in many cases real spectra are narrow in angle. In this case, they describe a certain mixture of both scenarios (weak turbulence and quasisolitonic turbulence).

11. Generalization of the MMT model to two types of waves

In [23], a system of one-dimensional equations describing media with two types of interacting waves was introduced. This system can be viewed as an alternative to the MMT model. The predicted Kolmogorov solutions are the same in both models. The main difference between both models is that coherent structures such as wave collapses and quasisolitons cannot develop in the alternative model. As shown previously these coherent structures can influence the weakly turbulent regime. It is shown here that in the absence of coherent structures weak turbulence spectra can be clearly observed numerically. Systems in which two types of waves interact are commonly found. Examples are the interaction of electrons with photons, the interaction of electromagnetic waves with Langmuir waves [98,60], or the interaction of ion-acoustic waves with Langmuir waves [6].

We consider the system of equations proposed in [23]

$$
\mathrm{i}\,\frac{\partial a_k}{\partial t} = \omega_k a_k + \int T_{123k} a_1 b_2 b_3^* \delta(k_1 + k_2 - k_3 - k)\,\mathrm{d}k_1\,\mathrm{d}k_2\,\mathrm{d}k_3\ ,
$$

$$
\mathrm{i}\,\frac{\partial b_k}{\partial t} = s\omega_k b_k + \int T_{123k} b_1 a_2 a_3^* \delta(k_1 + k_2 - k_3 - k)\,\mathrm{d}k_1\,\mathrm{d}k_2\,\mathrm{d}k_3\ , \tag{11.1}
$$

where a_k, b_k denote the Fourier components of two types of interacting wave fields. Like the MMT model, this model is determined by the linear dispersion relation $\omega_k = |k|^\alpha$ and the interaction coefficient $T_{123k} = |k_1 k_2 k_3 k|^{\beta/4}$. Thus ω_k, $s\omega_k$ and T_{123k} are homogeneous functions of their arguments. The three parameters s, α and β are real with the restriction s, $\alpha > 0$. If we set $\alpha = 2$ and $\beta = 0$, Eqs. (11.1) correspond to coupled nonlinear Schrödinger equations.

The system possesses two important conserved quantities, the positive definite Hamiltonian H, which we split into its linear part E and its nonlinear part H_{NL},

$$
H = E + H_{\mathrm{NL}}
$$

$$
= \int \omega_k(|a_k|^2 + s|b_k|^2)\,\mathrm{d}k + \int T_{123k} a_1 b_2 b_3^* a_k^* \delta(k_1 + k_2 - k_3 - k)\,\mathrm{d}k_1\,\mathrm{d}k_2\,\mathrm{d}k_3\,\mathrm{d}k\ ,
$$

and the total wave action

$$
N = \int (|a_k|^2 + |b_k|^2)\,\mathrm{d}k\ .
$$

Note that both individual wave actions $\int |a_k|^2\,\mathrm{d}k$ and $\int |b_k|^2\,\mathrm{d}k$ are conserved in the system.

System (11.1) describes four-wave resonant interactions satisfying

$$
k_1 + k_2 = k_3 + k, \quad \omega_1 + s\omega_2 = s\omega_3 + \omega_k\ . \tag{11.2}
$$

As said already in Section 2, when $s = 1$ conditions (11.2) have nontrivial solutions only if $\alpha < 1$. The case $s = 1$ and $\alpha = \frac{1}{2}$, which mimics gravity waves in deep water, was reviewed earlier. Here

accounting for $s \neq 1$ allows the resonance conditions (11.2) to be satisfied for any α. If $\alpha = 2$, system (11.2) can be solved explicitly:

$$k_3 = k_1 - \frac{2(k_1 - sk_2)}{1 + s}, \quad k = k_2 + \frac{2(k_1 - sk_2)}{1 + s} . \tag{11.3}$$

It is clear that system (11.3) with $s = 1$ gives the trivial solution $k_3 = k_2$, $k = k_1$. As a general rule, for a given α, nontrivial families of resonant quartets obeying system (11.2) can be found for all values of $s \neq 1$.

In the framework of weak turbulence theory, we are interested in the evolution of the two-point correlation functions

$$\langle a_k a_{k'}^* \rangle = n_k^a \delta(k - k') \quad \text{and} \quad \langle b_k b_{k'}^* \rangle = n_k^b \delta(k - k') ,$$

where $\langle \cdot \rangle$ represents ensemble averaging. Under the assumptions of random phases and quasi-gaussianity, it is possible to write the following system of kinetic equations for n_k^a and n_k^b:

$$\frac{\partial n_k^a}{\partial t} = 2\pi \int T_{123k}^2 U_{123k}^{ab} \delta(\omega_1 + s\omega_2 - s\omega_3 - \omega_k) \delta(k_1 + k_2 - k_3 - k) \, \mathrm{d}k_1 \, \mathrm{d}k_2 \, \mathrm{d}k_3 , \tag{11.4}$$

$$\frac{\partial n_k^b}{\partial t} = 2\pi \int T_{123k}^2 U_{123k}^{ba} \delta(s\omega_1 + \omega_2 - \omega_3 - s\omega_k) \delta(k_1 + k_2 - k_3 - k) \, \mathrm{d}k_1 \, \mathrm{d}k_2 \, \mathrm{d}k_3 \tag{11.5}$$

with

$$U_{123k}^{ab} = n_1^a n_2^b n_3^b + n_1^a n_2^b n_k^a - n_1^a n_3^b n_k^a - n_2^b n_3^b n_k^a .$$

The stationary power-law solutions to Eqs. (11.4) and (11.5) can be found explicitly. To do so, let us examine Eq. (11.4) only since the problem is similar for Eq. (11.5) by permuting n_k^a and n_k^b as well as ω_k and $s\omega_k$. Looking for solutions of the form $n_k^a \approx \omega_k^{-\gamma}$, $n_k^b \approx (s\omega_k)^{-\gamma}$ and applying Zakharov's conformal transformations, the kinetic equation (11.4) becomes

$$\frac{\partial \mathbf{N}^a(\omega)}{\partial t} \propto \omega^{-y-1} I_{s\alpha\beta\gamma}^a \tag{11.6}$$

with $\mathbf{N}^a(\omega) \, \mathrm{d}\omega = n^a(k(\omega)) \, \mathrm{d}k$ and

$$I_{s\alpha\beta\gamma}^a = \int_\Delta \frac{2\pi}{\alpha^4 s^{2\gamma}} (\xi_1 \xi_2 \xi_3)^{\beta/2\alpha + 1/\alpha - 1 - \gamma} [1 + (s\xi_3)^\gamma - (s\xi_2)^\gamma - \xi_1^\gamma] \delta(1 + s\xi_3 - s\xi_2 - \xi_1)$$

$$\times \delta(1 + \xi_3^{1/\alpha} - \xi_2^{1/\alpha} - \xi_1^{1/\alpha}) [1 + (s\xi_3)^y - (s\xi_2)^y - \xi_1^y] \, \mathrm{d}\xi_1 \, \mathrm{d}\xi_2 \, \mathrm{d}\xi_3 \tag{11.7}$$

with

$$\Delta = \{0 < \xi_1 < 1, 0 < s\xi_2 < 1, \xi_1 + s\xi_2 > 1\} \quad \text{and} \quad y = 3\gamma + 1 - \frac{2\beta + 3}{\alpha} .$$

The nondimensionalized integral $I_{s\alpha\beta\gamma}^a$ results from the change of variables $\omega_j \to \omega\xi_j$ ($j = 1, 2, 3$).

Thermodynamic equilibrium solutions ($\gamma = 0, 1$) given by

$$n_k^{a,b} = \text{const} \quad \text{and} \quad n_k^{a,b} \approx \omega_k^{-1} \tag{11.8}$$

are obvious. In addition, there exist Kolmogorov-type solutions ($y = 0, 1$)

$$n_k^{a,b} \approx \omega_k^{-2\beta/3\alpha - 1/\alpha + 1/3} \quad \text{and} \quad n_k^{a,b} \approx \omega_k^{-2\beta/3\alpha - 1/\alpha} , \tag{11.9}$$

which correspond to a finite flux of wave action Q and energy P, respectively. We point out that Eqs. (11.8) and (11.9) are also steady solutions to Eq. (11.5) and they are identical to those derived

from the MMT model [61]. The fact that the kinetic equation depends on the parameter s implies that the fluxes and the Kolmogorov constants also depend on s (see below). However there is no s-dependence on the Kolmogorov exponents because of the property of scale invariance. As found in Section 2, the criterion for appearance of the Kolmogorov spectra (11.9) is

$$\beta < -\tfrac{3}{2} \quad \text{or} \quad \beta > 2\alpha - \tfrac{3}{2} . \tag{11.10}$$

This means physically that a flux of wave action towards large scales (inverse cascade with $Q < 0$) and a flux of energy towards small scales (direct cascade with $P > 0$) should occur in the system. The full expressions of solutions (11.9) can be obtained from dimensional analysis yielding

$$n_k^a = c_1^a Q_a^{1/3} \omega_k^{-2\beta/3\alpha - 1/\alpha + 1/3}, \quad n_k^b = c_1^b Q_b^{1/3} (s\omega_k)^{-2\beta/3\alpha - 1/\alpha + 1/3} \tag{11.11}$$

and

$$n_k^a = c_2^a P_a^{1/3} \omega_k^{-2\beta/3\alpha - 1/\alpha}, \quad n_k^b = c_2^b P_b^{1/3} (s\omega_k)^{-2\beta/3\alpha - 1/\alpha} , \tag{11.12}$$

where

$$c_1^{a,b} = \left(-\left. \frac{\partial I_{s\alpha\beta\gamma}^{a,b}}{\partial y} \right|_{y=0} \right)^{-1/3}, \quad c_2^{a,b} = \left(\left. \frac{\partial I_{s\alpha\beta\gamma}^{a,b}}{\partial y} \right|_{y=1} \right)^{-1/3} \tag{11.13}$$

denote the dimensionless Kolmogorov constants. These can be computed directly by using integral (11.7) and its analogue for $\partial \mathbf{N}^b(\omega)/\partial t$.

In the numerical computations, we fix $\alpha = \tfrac{3}{2} > 1$ in order to prevent the emergence of coherent structures such as wave collapses and quasisolitons revealed in the original MMT model. Our goal is to check the validity of the Kolmogorov spectra which are relevant in several real wave media. The study is restricted to solutions (11.12) associated with the direct cascade.

The numerical scheme is exactly the same as the one described in Section 6. To generate weakly turbulent regimes, source terms of the form

$$\mathrm{i} \begin{pmatrix} f_k^a \\ f_k^b \end{pmatrix} \mathrm{e}^{\mathrm{i}\theta_k} - \mathrm{i} \left[\begin{pmatrix} v_-^a \\ v_-^b \end{pmatrix} (k - k_d^-)^2 + \begin{pmatrix} v_+^a \\ v_+^b \end{pmatrix} (k - k_d^+)^2 \right] \begin{pmatrix} a_k \\ b_k \end{pmatrix} \tag{11.14}$$

were added to both right-hand sides of Eqs. (11.1). The first term in Eq. (11.14) denotes a white-noise forcing where $0 \leqslant \theta_k < 2\pi$ is a uniformly distributed random number varying in time. The term in square brackets consists of a wave action sink at large scales and an energy sink at small scales. The random feature of the forcing makes it uncorrelated in time with the wave field. Consequently it is easier to control the input energy with a random forcing than with a deterministic forcing. For the results presented below, the forcing region is located at small wave numbers, i.e.

$$f_k^{a,b} = \begin{cases} 6,3 & \text{if } 8 \leqslant |k| \leqslant 12 , \\ 0 & \text{otherwise} . \end{cases}$$

Parameters of the sinks are

$$v_-^{a,b} = \begin{cases} 16,0.8 & \text{if } |k| \leqslant k_d^- \ (k_d^- = 5) , \\ 0 & \text{otherwise} \end{cases}$$
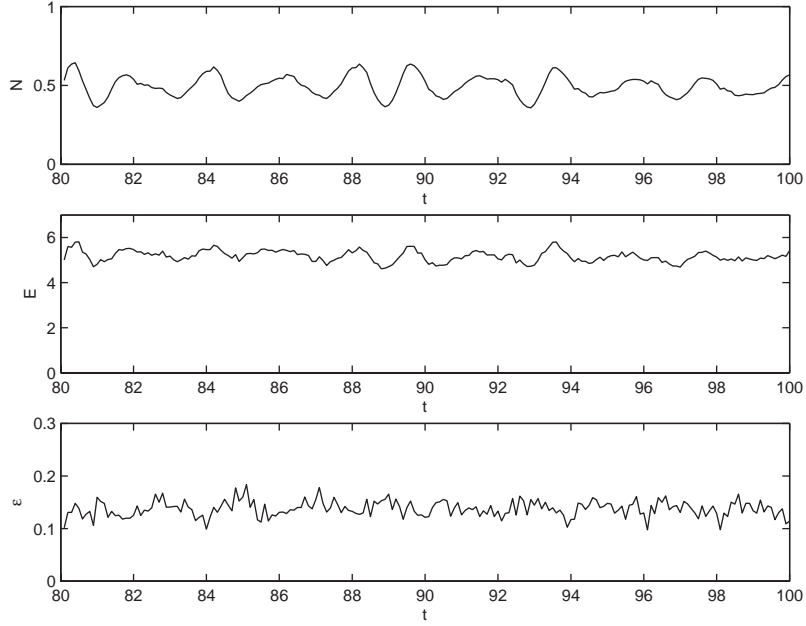
Fig. 28. Model with two types of interacting waves. The parameter values are $s = \frac{1}{10}$, $\alpha = \frac{3}{2}, \beta = 2$. Evolution of wave action N, quadratic energy E and ϵ vs. time in the stationary state.

and

$$v_+^{a,b} = \begin{cases} 10^{-2}, 7 \times 10^{-4} & \text{if } |k| \geqslant k_d^+ \ (k_d^+ = 550) , \\ 0 & \text{otherwise} . \end{cases}$$

Using this kind of selective dissipation ensures large enough inertial ranges at intermediate scales where solutions can develop under the negligible influence of damping. According to criterion (11.10), we focused on $\beta = 2$ and $s = \frac{1}{10}$ as a typical case for testing weak turbulence predictions. Simulations are run from low-level initial data until a quasi-steady state is reached and then averaging is performed over a sufficiently long time to compute the spectra. The time step, set equal to $\Delta t = 2 \times 10^{-5}$, has to resolve accurately the fastest harmonics $\tau \approx 1/\omega_{\max}$ of the medium or at least those from the inertial range. Time integration with such a small time step leads to a computationally time-consuming procedure despite the one-dimensionality of the problem. This explains why we chose $\alpha = \frac{3}{2}$ rather than a greater integer value (e.g. $\alpha = 2$) as well as $s = \frac{1}{10}$ rather than a value $s > 1$. Otherwise the constraint on Δt would have been more severe. There is a priori no special requirement in the choice of the value of s, except $s \neq 1$.

Fig. 28 shows the temporal evolution of the wave action N, the quadratic energy E and the average nonlinearity over the window $80 \leqslant t \leqslant 100$. At this stage, the stationary regime is clearly established since the wave action and the quadratic energy fluctuate around some mean values $N \approx 0.5$ and $E \approx 5.3$. Typically, the time interval for both the whole computation and the time averaging must exceed significantly the largest linear period. As said in previous sections, the average level of nonlinearity ϵ (2.3) provides a relatively good estimate of the level of nonlinearity once the system
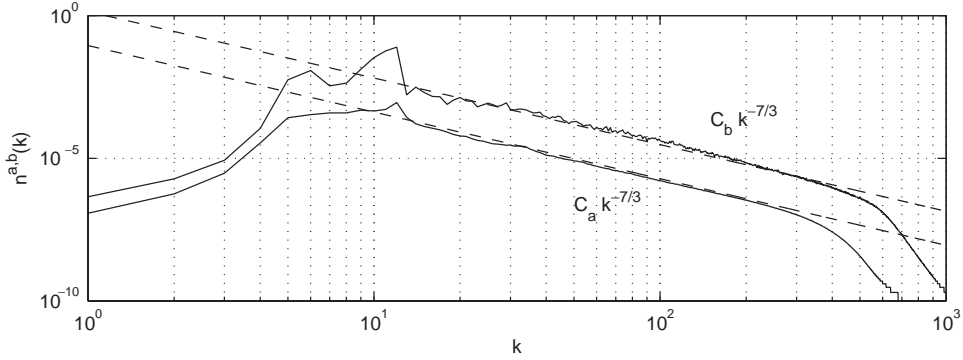
Fig. 29. Model with two types of interacting waves. The parameter values are $s = \frac{1}{10}, \alpha = \frac{3}{2}, \beta = 2$. Computed spectra ($n_k^a$ for the lower one and n_k^b for the upper one) and predicted Kolmogorov spectra $C_{a,b}k^{-7/3}$ with $C_a = c_2^a P_a^{1/3}$ and $C_b = c_2^b P_b^{1/3} s^{-14/9}$ (dashed lines).

reaches the steady state. The average nonlinearity fluctuates around some mean value $\epsilon \approx 0.14$, which indicates that the condition of weak nonlinearity holds in our experiments. However it should be emphasized that ϵ could not be imposed too small (by decreasing the forcing) otherwise the different modes would not be excited enough to generate an effective flux of energy. This problem is particularly important in numerics due to the discretization which restricts the possibilities for four-wave resonances.

Fig. 29 displays the stationary isotropic spectra $n_k^{a,b}$ realized in the present situation. By comparison, we also plotted the predicted Kolmogorov solutions given by Eq. (11.12): For $\alpha = \frac{3}{2}$ and $\beta = 2$, they read

$$n_k^a = c_2^a P_a^{1/3} \omega_k^{-14/9} = c_2^a P_a^{1/3} |k|^{-7/3} \tag{11.15}$$

and

$$n_k^b = c_2^b P_b^{1/3} (s\omega_k)^{-14/9} = c_2^b P_b^{1/3} s^{-14/9} |k|^{-7/3}, \quad s = \frac{1}{10} , \tag{11.16}$$

where $c_2^a = 0.094$ and $c_2^b = 0.047$ are numerically calculated from Eq. (11.13). The mean fluxes of energy $P_{a,b}$ in Eqs. (11.15) and (11.16) can be expressed as

$$P_a = 2 \int_{k > k_d^+} v_+^a (k - k_d^+)^2 \omega_k n_k^a \, dk \quad \text{and} \quad P_b = 2 \int_{k > k_d^+} v_+^b (k - k_d^+)^2 s\omega_k n_k^b \, dk ,$$

with k_d^+ the cutoff of ultraviolet dissipation. Then it is straightforward to get their values $P_a = 0.86$ and $P_b = 0.56$ from simulations. It can be observed in Fig. 29 that for both wave fields the spectra are well approximated by the Kolmogorov power-laws over a wide range of scales (say $20 < |k| < 300$). Here the agreement between theory and numerics is found with respect to both the slope and the level of the spectra.

12. Generalization of the MMT model to $1 \rightarrow 3$ interacting waves

This section reviews numerical results on a modified MMT model, which includes 'one-to-three' wave interactions not conserving wave action. In these interactions, one wave is split into three. In the reverse process, three waves are combined into one. With properly chosen parameters, this model behaves according to WT theory [101].

In Fourier space the model is

$$\mathrm{i}\,\frac{\partial \hat{\psi}_k}{\partial t} = \omega(k)\hat{\psi}_k + \lambda \int T_{123k}\hat{\psi}_1\hat{\psi}_2\hat{\psi}_3^*\delta(k_1 + k_2 - k_3 - k)\,\mathrm{d}k_1\,\mathrm{d}k_2\,\mathrm{d}k_3$$

$$+ \lambda g \int T_{123k}(\hat{\psi}_1\hat{\psi}_2\hat{\psi}_3\delta(k_1 + k_2 + k_3 - k)$$

$$+ 3\hat{\psi}_1\hat{\psi}_2^*\hat{\psi}_3^*\delta(k_1 - k_2 - k_3 - k))\,\mathrm{d}k_1\,\mathrm{d}k_2\,\mathrm{d}k_3 \ . \tag{12.1}$$

Here $\omega(k) = |k|^\alpha$, $T_{123k} = |k_1 k_2 k_3 k_4|^{\beta/4}$, $\alpha > 1$. If $g = 0$, this model becomes the MMT model.

Model (12.1) can be written as

$$\mathrm{i}\,\frac{\partial \hat{\psi}_k}{\partial t} = \frac{\delta H}{\delta \hat{\psi}_k^*} \tag{12.2}$$

with

$$H = E + H_{\mathrm{NL}}$$

$$= \int \omega(k)|\hat{\psi}_k|^2\,\mathrm{d}k + \frac{1}{2}\,\lambda \int T_{123k}\hat{\psi}_1\hat{\psi}_2\hat{\psi}_3^*\hat{\psi}_k^*\delta(k_1 + k_2 - k_3 - k)\,\mathrm{d}k_1\,\mathrm{d}k_2\,\mathrm{d}k_3\,\mathrm{d}k$$

$$+ \lambda g \int T_{123k}(\hat{\psi}_1^*\hat{\psi}_2^*\hat{\psi}_3\hat{\psi}_k^* + \hat{\psi}_1\hat{\psi}_2\hat{\psi}_3^*\hat{\psi}_k)\delta(k_1 + k_2 - k_3 + k)\,\mathrm{d}k_1\,\mathrm{d}k_2\,\mathrm{d}k_3\,\mathrm{d}k \ ,$$

where E is the part of the Hamiltonian corresponding to the linearization of (12.1).

Eq. (12.1) describes four-wave resonant interactions satisfying

$$k_1 + k_2 = k_3 + k, \quad \omega_1 + \omega_2 = \omega_3 + \omega \ . \tag{12.3}$$

It also describes resonant conditions corresponding to 'one-to-three' wave decay (and the reverse process of gluing three waves into one):

$$k_1 + k_2 + k_3 = k, \quad \omega_1 + \omega_2 + \omega_3 = \omega \ . \tag{12.4}$$

In the case $\alpha > 1$, Eq. (12.3) only has the trivial solution $k_3 = k_1, k = k_2$ (or $k_3 = k_2, k = k_1$), while solutions to Eq. (12.4) describe a two-dimensional manifold in the space (k_1, k_2, k_3, k). If $\lambda = 1$ and g is small, the Hamiltonian is positive definite. This makes it possible to get rid off any type of coherent structures.

Introduce the two-point correlation function

$$\langle \hat{\psi}(k, t)\hat{\psi}^*(k', t) \rangle = n(k, t)\delta(k - k') \ ,$$
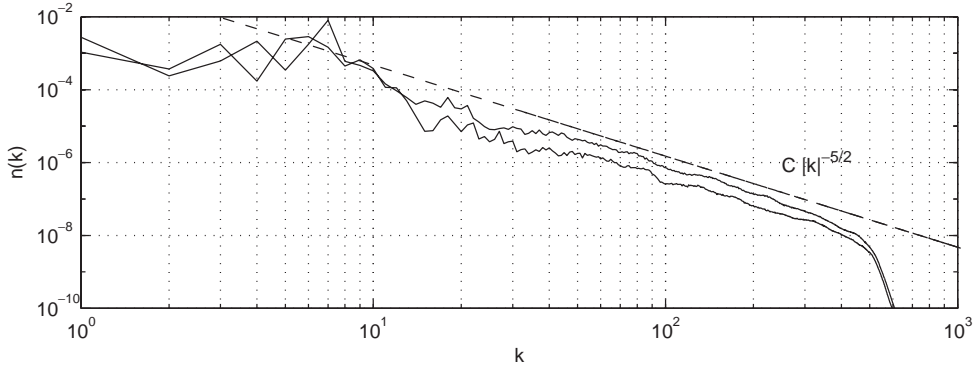
Fig. 30. Model with one-to-three wave interactions. The parameter values are $\alpha = \frac{3}{2}$, $\beta = \frac{9}{4}$, $g = 0.15$. Computed spectra for positive and negative k and predicted Kolmogorov spectrum $0.15|k|^{-5/2}$ (dashed line).

where $\langle \cdot \rangle$ represents ensemble averaging. Under the same assumptions as in Section 2, it is possible to derive the kinetic equation

$$
\begin{aligned}
\frac{\partial n_k}{\partial t} = &\, 4\pi g^2 \int T_{123k}^2 (n_1 n_2 n_3 - n_1 n_2 n_k - n_1 n_3 n_k - n_2 n_3 n_k) \\
&\times \delta(\omega - \omega_1 - \omega_2 - \omega_3)\delta(k - k_1 - k_2 - k_3)\, \mathrm{d}k_1\, \mathrm{d}k_2\, \mathrm{d}k_3 \\
&+ 12\pi g^2 \int T_{123k}^2 (n_1 n_2 n_3 + n_1 n_2 n_k + n_1 n_3 n_k - n_2 n_3 n_k) \\
&\times \delta(\omega_1 - \omega_2 - \omega_3 - \omega)\delta(k_1 - k_2 - k_3 - k)\, \mathrm{d}k_1\, \mathrm{d}k_2\, \mathrm{d}k_3 \;.
\end{aligned}
\tag{12.5}
$$

Kolmogorov-type stationary solutions to the kinetic equation are found to be

$$
n_k = a P^{1/3} k^{-2\beta/3 - 1} \;,
\tag{12.6}
$$

where a is the dimensionless Kolmogorov constant and P is the energy flux.

Eq. (12.1) was integrated numerically in [101]. The parameters values are $\alpha = \frac{3}{2}, \beta = \frac{9}{4}$. The parameter g varies from 0 to 0.2. The number of modes is 2048. The forcing and damping are as follows:

$$
F(k) = \begin{cases} 0.005 & \text{if } 5 \leqslant |k| \leqslant 10, \\ 0 & \text{otherwise} \end{cases} \quad \text{and} \quad D(k) = \begin{cases} 400(k/512 - 0.5)^2 & \text{if } |k| \geqslant 512\,, \\ 0 & \text{otherwise}\,. \end{cases}
$$

The spectrum is shown in Fig. 30. In the range $30 < k < 300$, the spectra are well approximated by the predicted Kolmogorov spectra with exponent $\frac{5}{2}$.

13. One-dimensional wave turbulence on the surface of a deep layer of fluid

The turbulence of gravity waves on the surface of a deep layer of fluid is an extremely interesting subject to study, because of the variety of its practical applications, including the theory of wind-driven ocean waves and the theory of freak waves. Of course, the full three-dimensional

water-wave equations are a subject of major interest, but the simpler two-dimensional equations are interesting too.[8] It is well-known from observations that the spectrum of wind-driven ocean waves near the leading frequency is narrow in angle. Thus the one-dimensional approach makes sense.

However, one-dimensional surface wave turbulence is a sophisticated problem, which is quite different from the MMT model with $\alpha = \frac{1}{2}$, $\beta = 3$. In order to explain the difference, we will introduce the standard canonical variables η and ψ. Here $\eta = \eta(x, t)$ is the elevation of the free surface, and $\psi = \psi(x, t)$ is the velocity potential on the free surface. As shown in Appendix B, the equations describing the fluid motion are

$$\frac{\partial \eta}{\partial t} = \frac{\delta H}{\delta \psi}, \quad \frac{\partial \psi}{\partial t} = -\frac{\delta H}{\delta \eta} \ . \tag{13.1}$$

It was recalled in Appendix B that, after suitable transformations, Eqs. (13.1) can be transformed into

$$\frac{\partial b_k}{\partial t} + \mathrm{i} \frac{\delta H}{\delta b_k^*} = 0 \ , \tag{13.2}$$

where b_k is a normal variable introduced in order to eliminate the cubic terms on the resonant manifold corresponding to four-wave interactions, and

$$H = H_0 + H_{\text{int}} \ , \tag{13.3}$$

with

$$H_0 = \int \omega_k b_k^* b_k \, \mathrm{d}k, \quad \omega_k = \sqrt{g|k|} \ ,$$

$$H_{\text{int}} = \frac{1}{4} \int T_{123k}^{WW} b_1 b_2 b_3^* b_k^* \delta(k_1 + k_2 - k_3 - k) \, \mathrm{d}k_1 \, \mathrm{d}k_2 \, \mathrm{d}k_3 \, \mathrm{d}k \ .$$

The coupling coefficient T_{123k}^{WW} is a complicated homogeneous function of k_1, k_2, k_3 and k:

$$T^{WW}(\xi k_1, \xi k_2, \xi k_3, \xi k) = \xi^3 T^{WW}(k_1, k_2, k_3, k), \quad \xi > 0 \ . \tag{13.4}$$

This function is strictly defined only on the resonant manifold

$$k_1 + k_2 = k_3 + k, \quad \omega_1 + \omega_2 = \omega_3 + \omega \ . \tag{13.5}$$

Outside of manifold (13.5), T_{123k}^{WW} can be changed by a proper canonical transformation. As we mentioned before, in nontrivial solutions to these equations, the sign of one of the wave numbers is opposite to the others. For instance, we can choose

$$k_1 > 0, \ k_2 < 0, \ k_3 > 0, \ k > 0.$$

In this sector,

$$T_{123k}^{WW} = -\frac{1}{4\pi^2} \, \omega_1 (\omega_1 \omega_2 \omega_3 \omega)^2 [-3\omega_2 \omega_3 \omega + \omega_2 (\omega_1 + \omega_2)^2 - \omega_3 (\omega_1 - \omega_3)^2$$

$$- \omega(\omega_1 - \omega)^2] \ . \tag{13.6}$$

---

[8] To remain consistent with the terminology used in this report, a solution depending upon only one horizontal space variable, x, is called a one-dimensional solution, even though it is truly a two-dimensional solution, the second direction being the vertical direction. Similarly, a solution depending upon two horizontal space variables, x and y, is called a two-dimensional solution, even though it is truly a three-dimensional solution to the water-wave equations.

On the resonant manifold (13.5),

$$\omega_1 = A(1 + \xi + \xi^2), \quad \omega_2 = A\xi, \quad \omega_3 = A(1 + \xi), \quad \omega = A\xi(1 + \xi) . \tag{13.7}$$

By plugging parametrization (13.7) into (13.6), we get

$$T_{123k}^{WW} = -\frac{1}{4\pi^2} \omega_1(\omega_1\omega_2\omega_3\omega)^2 A^3 \xi(1 + \xi)[-3\xi(1 + \xi) + (1 + \xi)^3 - \xi^3 - 1] \equiv 0 . \tag{13.8}$$

In other words, four-wave resonant interactions vanish in one-dimensional geometry. This miraculous fact makes things more complicated, but so much more interesting. The KZ spectra $n_k \approx |k|^{-3}, |k|^{-17/6}$ (see Eqs. (B.8) and (B.9) with $d = 1$) do not exist anymore. However quasisolitons survive. Moreover, due to the absence of four-wave weak turbulence, quasisolitons predominate, and the turbulence becomes "pure quasisolitonic." This fact justifies up to a certain degree the use of the MMT model. This model predicts KZ spectra (this is an artifact), but describes properly quasisolitons. Thus we believe that the quasisolitonic scenario of turbulence outlined in Section 10 is still valid. All these facts make the study of quasisolitons, their stability and the rules of merging in the framework of the realistic model (13.2) very urgent.

This question can be tackled by direct numerical simulation of the primitive dynamic equations. It seems natural to solve numerically the Zakharov equation (13.2). However the complexity of the coupling coefficient T_{123k}^{WW} does not allow the use of the most efficient spectral codes. It is more economical to solve directly Eqs. (13.1). Several groups have tried to solve Eqs. (13.1) on the computer. They achieved some success [68,47,33,93] but found that the whole business is tricky, and the computations easily become unstable. In our opinion, this can be explained by an inappropriate choice of the basic variables. In fact, there is no reason to believe that η and ψ are the 'best' possible canonical variables that can be used for the description of gravity waves on the free surface of an incompressible fluid. It looks promising that a proper canonical transformation into some new variables could improve the situation dramatically and make the numerical computations much more efficient. Further developments of this issue are beyond the framework of this article.

Since it was found that four-wave resonances are not important in the 1D turbulence of gravity waves, one can ask the following question about five-wave resonance processes. Do they also cancel? The answer can be found in the articles of Dyachenko et al. [31] and Lvov [57]. Craig and Worfolk [22] also obtained independently the same answer.

The answer is far from being trivial. The five-wave interactions are governed by the resonant conditions

$$k_1 + k_2 + k_3 = k_p + k_q, \quad \omega_1 + \omega_2 + \omega_3 = \omega_p + \omega_q . \tag{13.9}$$

In (13.9), all the frequencies ω_i are positive, but the wavenumbers k_i can have different signs. The coupling coefficient $T_{123,\,pq}^{WW}$ depends on these signs as well as on relations between the absolute values of the wavenumbers k_i. All together, there are nine different 'sectors' where $T_{123,\,pq}^{WW}$ is defined. In two of them, it is zero; in the other seven, the coefficient $T_{123,\,pq}^{WW}$ is given by astonishingly compact expressions. All the results are presented in Table 3.

Table 3
Values for $T_{123,pq}^{WW}$ for five-wave interactions on the resonant manifold

$$k_1 + k_2 + k_3 = k_p + k_q, \quad \omega_1 + \omega_2 + \omega_3 = \omega_p + \omega_q, \quad \omega_k = \sqrt{g|k|}.$$

Parametrization	$T_{123,pq}^{WW}(g^{9/2}\pi^{3/2})$
(i) All wave numbers are positive	
$\omega_1 = c(a^2 - b^2 + 1 - 2a)$	$2(\omega_1\omega_2\omega_3)^{5/2}(\omega_p\omega_q)^{3/2}/\max(\omega_1^2,\omega_2^2,\omega_3^2)$
$\omega_2 = c(a^2 - b^2 + 1 + 2a)$	
$\omega_3 = 4c$	
$\omega_p = c(a^2 - b^2 + 3 - 2b)$	
$\omega_q = c(a^2 - b^2 + 3 + 2b)$	
$c > 0, 0 < a, b < 1, |a \pm b| < 1$	
(ii) Positive p and q, and one of k_1, k_2, k_3 negative, choose $k_1 > k_2$	
$\omega_1 = c(a + ab + b)$	$\omega_1^{3/2}\omega_2^{11/2}\omega_3^{1/2}\omega_p^{1/2}\omega_q^{1/2}$
$\omega_2 = c(ab - 1)$	if $\omega_1 > \omega_p, \omega_q > \omega_3 > \omega_2$
$\omega_3 = c \quad (k_3 < 0)$	
$\omega_p = c(a+1)b$	$\omega_1^{3/2}\omega_2^{3/2}\omega_3^{5/2}\omega_p^{1/2}\omega_q^{1/2}(2\omega_2^2 - \omega_3^2)$
$\omega_q = c(b+1)a$	if $\omega_1 > \omega_p, \omega_q > \omega_2 > \omega_3$
$a, b > 0, ab > 1$	
(iii) Positive p and q, and two of k_1, k_2, k_3 negative	zero
(iv) p and q have different signs, k_1, k_2, k_3 positive	zero
(v) p and q have different signs, and one of k_1, k_2, k_3 negative, choose $k_1 > k_2$	
$\omega_p = \omega_1 + (\omega_2^2 + \omega_2\omega_3)/(\omega_1 + \omega_2 + \omega_3)$	$-\omega_1^{1/2}\omega_2^{1/2}\omega_3^{11/2}\omega_p^{3/2}\omega_q^{1/2}$
$\omega_q = (\omega_1 + \omega_3)(\omega_2 + \omega_3)/(\omega_1 + \omega_2 + \omega_3)$	if $\omega_1 > \omega_2 > \omega_3, \quad \omega_p > \omega_q$
$k_1 = \omega_1^2/g$	
$k_2 = \omega_2^2/g$	$\omega_1^{1/2}\omega_2^{5/2}\omega_3^{3/2}\omega_p^{3/2}\omega_q^{1/2}(\omega_2^2 - 2\omega_3^2)$
$k_3 = -\omega_3^2/g$	if $\omega_1 > \omega_3 > \omega_2, \quad \omega_p > \omega_q$
$k_p = -\omega_p^2/g$	
$k_q = \omega_q^2/g$	$\omega_1^{1/2}\omega_2^{1/2}\omega_3^{3/2}\omega_p^{3/2}\omega_q^{1/2}(\omega_1^4 + \omega_2^4 - 2\omega_1^2\omega_3^2 - 2\omega_2^2\omega_3^2 + \omega_3^4)$
	if $\omega_3 > \omega_1 > \omega_2, \omega_p > \omega_q$
	$-2\omega_1^{5/2}\omega_2^{5/2}\omega_3^{3/2}\omega_p^{3/2}\omega_q^{1/2}$
	if $\omega_3 > \omega_1 > \omega_2, \quad \omega_q > \omega_p$

Let us study the simplest case—all the wavenumbers are positive. In this case,

$$T_{123,pq}^{WW} = \frac{2}{g^{1/2}\pi^{3/2}}\sqrt{\frac{\omega_1\omega_2\omega_3}{\omega_p\omega_q}}\frac{k_1k_2k_3k_pk_q}{\max(k_1,k_2,k_3)} \tag{13.10}$$

and one can write the kinetic equation

$$\frac{\partial n_k}{\partial t} = \pi \int |T_{123k}^{WW}|^2 f_{123k}\, dk_1\, dk_2\, dk_3$$

$$+ \frac{\pi}{3}\int |T_{123,k5}^{WW}|^2 f_{123,k5}\, dk_1\, dk_2\, dk_3\, dk_5 - \frac{\pi}{2}\int |T_{k23,45}^{WW}|^2 f_{k23,45}\, dk_2\, dk_3 dk_4\, dk_5, \tag{13.11}$$

where

$$f_{123k} = \delta(k_1 + k_2 - k_3 - k)\delta(\omega_1 + \omega_2 - \omega_3 - \omega)\{n_1 n_2(n_k + n_3) - n_k n_3(n_1 + n_2)\} \ ,$$

$$f_{123,45} = \delta(k_1 + k_2 + k_3 - k_4 - k_5)\delta(\omega_1 + \omega_2 + \omega_3 - \omega_4 - \omega_5)$$

$$\times \{n_1 n_2 n_3(n_4 + n_5) - n_4 n_5(n_1 n_2 + n_1 n_3 + n_2 n_3)\} \ .$$

The wave action $N = \int n_k \, dk$ is no longer a constant of motion. However Eq. (13.11) still has two integrals, the momentum M and the energy E:

$$M = \int k n_k \, dk, \quad E = \int \omega_k n_k \, dk \ .$$

Thus the stationary equation

$$\frac{\partial n_k}{\partial t} = 0$$

has two KZ solutions, describing direct and inverse cascades. The inverse cascade is the cascade of energy. It is described by the following Kolmogorov solution to (13.11):

$$n_k = aP^{1/4}|k|^{-25/8} \ , \tag{13.12}$$

where P is the energy flux towards small wave numbers. The corresponding energy spectrum is

$$\mathbf{E}(\omega) = aP^{1/4}\omega^{-17/4} \ .$$

The direct cascade is the cascade of momentum:

$$n_k \approx |k|^{-13/4}, \quad \mathbf{E}(\omega) \approx \omega^{-9/2} \ .$$

But, even though there are KZ spectra corresponding to five-wave resonant interactions, the wave turbulence is dominated by quasisolitons.

14. What is beyond weak turbulence?

As said above, massive numerical computations are needed in order to better understand one-dimensional wave turbulence. Existing numerical approaches must be revisited. Such an attempt was recently made by Zakharov et al. [93]. Their new method, which is briefly described below, is able to capture strongly nonlinear effects in gravity waves, including wave breaking and the formation of freak waves. In the near future, it should allow a systematic study of the appearance of freak waves from a "smooth sea."

First the fluid domain

$$(x, z) \in \mathbb{R} \times [-\infty, \eta]$$

is transformed through a conformal mapping into the lower half-plane

$$(u, v) \in \mathbb{R} \times [-\infty, 0] \ .$$

The profile of the free surface $\eta(x, t)$ can then be written in the parametric form

$$z = z(u, t), \quad x = x(u, t) = u + \tilde{x}(u, t) \ .$$

Here $\tilde{x}(u,t)$ and $z(u,t)$ are related through the Hilbert transform:

$$z = \hat{H}\tilde{x}, \quad \tilde{x} = -\hat{H}z, \quad \hat{H}^2 = -1 \quad \text{and} \quad \hat{H}(f(u)) = \text{PV}\left(\frac{1}{\pi}\int_{-\infty}^{\infty}\frac{f(u')\,du'}{u'-u}\right) ,$$

where PV stands for principal value. Through the conformal mapping, $\phi(x,z,t)$ and $\psi(x,t)$ are transformed into $\phi(u,v,t)$ and $\psi(u,t)$. It was shown in [30] (see also [7,32,92]) that $z(u,t)$ and $\psi(u,t)$ satisfy the following system of equations:

$$z_t = (z_u\hat{H} - x_u)\frac{\hat{H}\psi_u}{J} , \tag{14.1}$$

$$\psi_t = -\frac{\psi_u^2 + \hat{H}\psi_u^2}{2J} + \hat{H}\left(\frac{\hat{H}\psi_u}{J}\right)\psi_u + \frac{\hat{H}\psi_u}{J}\hat{H}\psi_u - gz . \tag{14.2}$$

Here J is the Jacobian of the mapping:

$$J = x_u^2 + z_u^2 = 1 + 2\tilde{x}_u + \tilde{x}_u^2 + z_u^2 . \tag{14.3}$$

Eqs. (14.1) and (14.2) can be written in complex form. The functions $Z = x + iz$ and $\Phi = \psi + i\hat{H}\psi$ are analytic in the lower half-plane. They satisfy the equations

$$Z_t = iUZ_u , \tag{14.4}$$

$$\Phi_t = iU\Phi_u - B + ig(Z - u) . \tag{14.5}$$

Here U is a complex transport velocity:

$$U = \hat{P}\left(\frac{-\hat{H}\psi_u}{|Z_u|^2}\right) \tag{14.6}$$

and

$$B = \hat{P}\left(\frac{|\Phi_u|^2}{|Z_u|^2}\right) . \tag{14.7}$$

In (14.6) and (14.7), $\hat{P}$ is the projection operator generating a function which is analytic in the lower half-plane: $\hat{P}(f) = \frac{1}{2}(1 + i\hat{H})f$.

It turns out that Eqs. (14.4) and (14.5) can be simplified by a change of variables. Indeed, let us replace the functions $Z(u,t)$ and $\Phi(u,t)$ by the following functions $R(u,t)$ and $V(u,t)$:

$$R = \frac{1}{Z_u}, \quad \Phi_u = -iVZ_u . \tag{14.8}$$

Note that V is just $i\partial\Phi/\partial Z$, i.e. the complex velocity. Let $w = u + iv$. Since $Z(w,t)$ is a conformal mapping, its derivative exists in the lower half-plane and does not have zeroes in it. Thus the function $R(w,t)$ is analytic in the lower half-plane and has the following boundary condition:

$$R(w,t) \to 1, \quad |w| \to \infty, \ \text{Im}(w) \leqslant 0 .$$

It is obvious that the boundary condition for V is

$$V(w,t) \to 0, \quad |w| \to \infty, \quad \text{Im}(w) \leqslant 0 .$$

For these analytic functions, the system of equations (14.4) and (14.5) takes an elegant form:

$$R_t = \mathrm{i}(UR' - U'R) \ , \tag{14.9}$$

$$V_t = \mathrm{i}(UV' - RB') + g(R - 1) \tag{14.10}$$

with

$$B = \hat{P}'(V\bar{V}), \quad U = \hat{P}(V\bar{R} + \bar{V}R) \ .$$

Eqs. (14.9) and (14.10) are exact, and completely equivalent to the "traditional" system of equations for water waves (see Appendix B). But system (14.9)–(14.10) is much more convenient for analytical and numerical studies than the "traditional" system as well as the Hamiltonian system (B.1). Indeed, one cannot express the Hamiltonian H explicitly in terms of the "natural" variables ψ and η. At best one can give H as an infinite series in powers of η. As a result, the equations in the "natural" variables are presented by the infinite series as well. This is a big obstacle for numerical simulations. On the contrary, the new equations of motion (14.9)–(14.10) are just polynomial (cubic) in terms of the new variables R and V. This property makes it possible to implement the fast Fourier transform more efficiently in order to solve the new exact equations. Incidently, it is interesting to point out that this new formulation recently allowed Iooss et al. [45,46] to provide the first existence proof of standing waves.

Let us mention that the three equivalent systems of equations which describe the free-surface dynamics in conformal variables, (14.1)–(14.2), (14.4)–(14.5), (14.9)–(14.10), are not partial differential equations. They are "Hilbert-differential" equations including, together with derivatives with respect to u,

$$f \rightarrow \frac{\partial f}{\partial u} \ , \tag{14.11}$$

the operation of the Hilbert transform

$$f \rightarrow \hat{H}f \ . \tag{14.12}$$

From an analytical point of view, these two operations are completely different. But from a numerical point of view, both operations are similar. Indeed, in terms of the Fourier transform, operation (14.11) means

$$f_k \rightarrow \mathrm{i}k f_k \ ,$$

while operation (14.12) means

$$f_k \rightarrow \mathrm{i}\, \mathrm{sign}(k) f_k \ .$$

From a computational point of view, these two operations are of the same level of difficulty. It should be mentioned here that the Hilbert transform "corresponds" to the contour (or surface) integration in surface integral methods. Of course, the Hilbert transform is much easier to implement numerically.

Zakharov et al. [93] developed an algorithm for the numerical integration of Eqs. (14.9)–(14.10). They were able to compute very steep waves and the formation of singularities. In another numerical experiment, they were able to follow the development of the modulational instability and the formation of freak waves. Their method looks promising. The nonlinear evolution of the modulational instability for a Stokes wave of moderate amplitude ($ka = 0.15$) was studied numerically. The

results of the computations show the formation of groups of extreme breaking waves that are quite consistent with the scenario of 'quasisolitonic turbulence' described in Section 10.

15. Conclusion

One-dimensional wave turbulence is a rather special type of turbulence. On one hand, it is a type of turbulence that seems to be relatively easy for numerical simulations. For this reason one may think that one-dimensional wave turbulence is a natural field test to examine the applicability of the theory of weak turbulence. This is true up to a certain point. Some specifically designed models of 1D wave turbulence, free of any coherent structure, really display an impressive confirmation of this theory. However, "typical" models of one-dimensional turbulence, including the MMT model, describe wave turbulence in which the weak turbulence coexists with coherent structures: solitons, quasisolitons or wave collapses of different types. In the most interesting case—turbulence of gravity waves on deep water—the quasisolitonic turbulence is a mechanism that predominates.

We would like to stress that 1D wave turbulence is still a hot subject, far from being exhausted. In the future, new massive numerical experiments will make it possible to answer the most fundamental questions that appear in the theory of wave turbulence.

In the cases where weak turbulence is not "contaminated" by the coherent structures (Sections 11 and 12), one can perform more detailed comparisons with predictions of weak turbulent theory. To do this, one has to develop numerical algorithms for the solution to one-dimensional kinetic equations (2.30), (11.4)–(11.5), (12.5). Plunging deeply into this subject, one can study numerically such interesting questions as the behavior of higher cumulants, the intermittency, space-time correlation spectra, etc. The opposite cases, where coherent structures predominate, look even more attractive. It is particularly interesting to study in detail the one-dimensional turbulence of gravity waves on deep or shallow water. In these cases the weak turbulence is mostly suppressed by the quasisolitonic turbulence that leads to the formation of "freak" waves, and occasionally to wave breaking. Needless to say how this subject is important from both theoretical and practical points of view.

Appendix A. Fractional derivative

In order to define the fractional derivative, it is easier to define first the fractional integral. The fractional integral of $\psi(x)$ of order $v > 0$ can be defined by

$$D^{-v}\psi(x) = \frac{1}{\Gamma(v)} \int_0^x (x - \xi)^{v-1} \psi(\xi)\, d\xi \;, \tag{A.1}$$

where $\Gamma(v)$ is the Gamma function.

The fractional derivative of $\psi(x)$ of order $\alpha > 0$ (if it exists) can be defined in terms of the fractional integral $D^{-\nu}\psi(x)$ as

$$D^{\alpha}\psi(x) = \frac{\mathrm{d}}{\mathrm{d}x^m}[D^{-(m-\alpha)}\psi(x)] , \qquad\qquad (A.2)$$

where m is an integer $\geqslant \lceil\alpha\rceil$. The notation $\lceil x\rceil$ denotes the ceiling function.

If one chooses the lower limit of integration to be $-\infty$ instead of 0, one can reproduce the familiar properties of Fourier-transformed integrals and derivatives:

$$\mathrm{FT}\{D^{\alpha}\psi(x)\} = (\mathrm{i}k)^{\alpha}\hat{\psi}(k) .$$

Appendix B. Water waves in deep water

Since a comparison is made between the results obtained from the model equation (2.1) and deep-water gravity waves, it is appropriate to summarize some of the essential results on gravity waves. For an extension to capillary-gravity waves on the surface of a finite-depth fluid, see for example [90,91].

Two-dimensional gravity waves on the surface of an infinitely deep layer of water are usually studied by considering the potential flow of a perfect incompressible fluid with free-surface boundary conditions. Let $\phi(x,z,t)$ be the velocity potential, $\eta(x,t)$ the free-surface elevation with respect to the rest level and g the acceleration due to gravity. In the classical surface wave problem, one wants to solve for $\eta(x,t)$ and $\phi(x,z,t)$ the following set of governing equations and boundary conditions:

$$\phi_{xx} + \phi_{zz} = 0 \quad \text{for } (x,z) \in \Omega, \quad \text{with } \Omega = \mathbb{R} \times [-\infty, \eta] ,$$

$$\eta_t + \phi_x\eta_x - \phi_z = 0 \quad \text{at } z = \eta(x,t),$$

$$\phi_t + \tfrac{1}{2}(\phi_x^2 + \phi_z^2) + g\eta = 0 \quad \text{at } z = \eta(x,t) ,$$

$$|\nabla\phi| \to 0 \quad \text{as } z \to -\infty .$$

The kinetic energy K and the potential energy V are defined as

$$K = \int_{-\infty}^{\infty}\int_{-\infty}^{\eta} \tfrac{1}{2}|\nabla\phi|^2 \,\mathrm{d}z\,\mathrm{d}x, \quad V = \int_{-\infty}^{\infty} \tfrac{1}{2}g\eta^2 \,\mathrm{d}x .$$

Let us introduce the velocity potential evaluated on the free surface $\psi(x,t)$. The kinetic energy in the variables ψ and η can in fact be characterized as the minimal energy for all flows that satisfy the condition $\phi(x,z,t) = \psi(x,t)$ on the free surface:

$$K(\psi,\eta) = \mathrm{Min}\left\{ \int \tfrac{1}{2}(\phi_x^2 + \phi_z^2)|\phi(x,z,t) = \psi(x,t) \text{ at } z = \eta(x,t)\right\} .$$

Indeed, the solution to this minimization problem satisfies

$$\nabla^2\phi = 0 \text{ in } \Omega, \quad |\nabla\phi| \to 0 \text{ as } z \to -\infty, \quad \phi(x,z,t) = \psi(x,t) \text{ at } z = \eta(x,t) ,$$

and conversely.

One can show that the surface wave problem is an infinite dimensional Hamiltonian system in the canonically conjugate variables ψ and η

$$\frac{\partial \psi}{\partial t} = -\frac{\delta H}{\delta \eta}, \quad \frac{\partial \eta}{\partial t} = \frac{\delta H}{\delta \psi} \ , \tag{B.1}$$

where $H = K + V$ is the Hamiltonian [89]. The Hamiltonian is equal to the total energy.

In Fourier space, the expression for the Hamiltonian is

$$H = H_0 + H_1 + H_2 + \cdots \ , \tag{B.2}$$

where

$$H_0 = \frac{1}{2} \int (k|\psi_k|^2 + g|\eta_k|^2) \, \mathrm{d}k \ ,$$

$$H_1 = -\frac{1}{4\pi} \int (k_1 k_2 + |k_1||k_2|)\psi_1 \psi_2 \eta_k \delta(k_1 + k_2 + k) \, \mathrm{d}k_1 \, \mathrm{d}k_2 \, \mathrm{d}k$$

$$H_2 = -\frac{1}{(4\pi)^2} \int \left[|k_1| + |k_2| - \tfrac{1}{2}(|k_1 + k_3| + |k_2 + k_3| + |k_1 + k| + |k_2 + k|) \right]$$

$$\times |k_1||k_2|\psi_1 \psi_2 \eta_3 \eta_k \delta(k_1 + k_2 + k_3 + k) \, \mathrm{d}k_1 \, \mathrm{d}k_2 \, \mathrm{d}k_3 \, \mathrm{d}k \ .$$

One can introduce the normal variables

$$\eta_k = \frac{1}{\sqrt{2}} \left(\frac{|k|}{g} \right)^{1/4} (a_k + a_{-k}^*), \quad \psi_k = \frac{\mathrm{i}}{\sqrt{2}} \left(\frac{g}{|k|} \right)^{1/4} (a_k - a_{-k}^*) \ . \tag{B.3}$$

Using the normal variables, Eq. (B.1) becomes

$$\frac{\partial a_k}{\partial t} + \mathrm{i} \frac{\delta H}{\delta a_k^*} = 0 \ . \tag{B.4}$$

In order to obtain a MMT-type model, one has to perform a canonical transformation which eliminates the cubic terms in the Hamiltonian. This is a cumbersome transformation, which is described in detail in the article [55]. In the new variable, say b_k, the equation still has the canonical form

$$\frac{\partial b_k}{\partial t} + \mathrm{i} \frac{\delta H}{\delta b_k^*} = 0 \ , \tag{B.5}$$

where

$$H = H_0 + H_{\mathrm{int}} \tag{B.6}$$

with

$$H_0 = \int \omega_k |b_k|^2 \, \mathrm{d}k, \quad \omega_k = \sqrt{g|k|} \ ,$$

$$H_{\mathrm{int}} = \frac{1}{4} \int T_{123k}^{WW} b_1 b_2 b_3^* b_k^* \delta(k_1 + k_2 - k_3 - k) \, \mathrm{d}k_1 \, \mathrm{d}k_2 \, \mathrm{d}k_3 \, \mathrm{d}k \ ,$$

The coupling coefficient T_{123k}^{WW} is a complicated homogeneous function of k_1, k_2, k_3 and k:

$$T^{WW}(\xi k_1, \xi k_2, \xi k_3, \xi k) = \xi^3 T^{WW}(k_1, k_2, k_3, k), \quad \xi > 0 \ . \tag{B.7}$$

The full expression for the interaction coefficient T^{WW}_{123k} can be found for example in [55] (see also the earlier work by Zakharov [89]). Hamiltonian (B.6) ought to be compared with Hamiltonian (2.8) corresponding to the MMT model.

A statistical description of nonlinear waves leads to the kinetic equation for two-dimensional water waves. However, as explained in Section 13, there is a problem with two-dimensional water waves on the surface of deep water: four-wave resonant interactions vanish. The kinetic equations for three-dimensional water waves is given for example by Eq. (8.12) in [91]. Steady solutions of the kinetic wave equation can be found in the form of powerlike Kolmogorov solutions:

$$n(k) = a_1 P^{1/3} |k|^{-2-d} \; , \tag{B.8}$$

$$n(k) = a_2 Q^{1/3} |k|^{-11/6-d} \; , \tag{B.9}$$

where d is the spatial dimension ($d = 2$ for three-dimensional waves). The first one corresponds to a constant flux of energy P to the region of small scales (direct cascade of energy). The second one describes the inverse cascade of wave action to large scales, and Q is the flux of wave action. In both cases, a_1 and a_2 are dimensionless "Kolmogorov's constants." They depend on the detailed structure of T^{WW}_{123k} and are represented by some three-dimensional integrals.

References

[1] A.M. Balk, On the Kolmogorov–Zakharov spectra of weak turbulence, Physica D 139 (2000) 137–157. ∗
[2] A.M. Balk, V.E. Zakharov, S.V. Nazarenko, Nonlocal turbulence of drift waves, Sov. Phys. JETP 71 (1990) 249–260.
[3] A.M. Balk, S.V. Nazarenko, V.E. Zakharov, On the nonlocal turbulence of drift type waves, Phys. Lett. A 146 (1990) 217–221.
[4] A.M. Balk, S.V. Nazarenko, V.E. Zakharov, New invariant for drift turbulence, Phys. Lett. A 152 (1991) 276–280.
[5] G. Benettin, F. Fassò, From Hamiltonian perturbation theory to sympletic integrators and back, Appl. Num. Math. 29 (1999) 73–87.
[6] E.S. Benilov, S.P. Burtsev, To the integrability of the equations describing the Langmuir-wave-ion-acoustic-wave interaction, Phys. Lett. A 98 (1983) 256–258.
[7] T.B. Benjamin, P.J. Olver, Hamiltonian structure, symmetries and conservation laws for water waves, J. Fluid Mech. 125 (1982) 137–185.
[8] D.J. Benney, P.G. Saffman, Nonlinear interactions of random waves in a dispersive medium, Proc. R. Soc. Lond. A 289 (1966) 301–320.
[9] D.J. Benney, A.C. Newell, Random wave closures, Stud. Appl. Math. 48 (1969) 29–53.
[10] K.M. Berger, P.A. Milewski, Simulation of wave interactions and turbulence in one-dimensional water waves, SIAM J. Appl. Math. 63 (2003) 1121–1140.
[11] L. Biven, S.V. Nazarenko, A.C. Newell, Weak turbulence and intermittency, Physica D 152–153 (2001) 520–550.
[12] L. Biven, S.V. Nazarenko, A.C. Newell, Breakdown of wave turbulence and the onset of intermittency, Phys. Lett. A 280 (2001) 28–32.
[13] J.P. Boyd, Weakly Nonlocal Solitary Waves and Beyond-all-orders Asymptotics, Kluwer Academic Publishers, Dordrecht, 1998.
[14] M.Yu. Brazhnikov, G.V. Kolmakov, A.A. Levchenko, The turbulence of capillary waves on the surface of liquid hydrogen, JETP 95 (2002) 447–454. ∗ ∗ ∗
[15] M.Yu. Brazhnikov, G.V. Kolmakov, A.A. Levchenko, L.P. Mezhov-Deglin, Capillary turbulence at the surface of liquid hydrogen, JETP Lett. 73 (2001) 398–400.
[16] M.Yu. Brazhnikov, G.V. Kolmakov, A.A. Levchenko, L.P. Mezhov-Deglin, Measurement of the boundary frequency of the inertial interval of capillary wave turbulence at the surface of liquid hydrogen, JETP Lett. 74 (2001) 583–585.

[17] M.Yu. Brazhnikov, G.V. Kolmakov, A.A. Levchenko, L.P. Mezhov-Deglin, Observation of capillary turbulence on the water surface in a wide range of frequencies, Europhys. Lett. 58 (2002) 510–516.

[18] D. Cai, A.J. Majda, D.W. McLaughlin, E.G. Tabak, Spectral bifurcations in dispersive wave turbulence, Proc. Natl. Acad. Sci. 96 (1999) 14216–14221.

[19] D. Cai, D. McLaughlin, Chaotic and turbulent behavior of unstable one-dimensional nonlinear dispersive waves, J. Math. Phys. 41 (2000) 4125–4153.

[20] D. Cai, D. McLaughlin, A. Majda, E. Tabak, Dispersive wave turbulence in one dimension, Physica D 152–153 (2001) 551–572.

[21] C. Connaughton, S. Nazarenko, A. Pushkarev, Discreteness and quasiresonances in weak turbulence of capillary waves, Phys. Rev. E 63 (2001) 046306(4).

[22] W. Craig, P.A. Worfolk, An integrable normal form for water waves in infinite depth, Physica D 84 (1995) 513–531.

[23] F. Dias, P. Guyenne, V.E. Zakharov, Kolmogorov spectra of weak turbulence in media with two types of interacting waves, Phys. Lett. A 291 (2001) 139–145. ∗∗

[24] F. Dias, G. Iooss, Capillary-gravity solitary waves with damped oscillations, Physica D 65 (1993) 399–423. ∗

[25] F. Dias, G. Iooss, Water waves as a spatial dynamical system, Handbook of Mathematical Fluid Dynamics, Vol. 2, Elsevier, Amsterdam, 2003, pp. 443–499.

[26] S. Dyachenko, A.C. Newell, A.N. Pushkarev, V.E. Zakharov, Optical turbulence: weak turbulence, condensates and collapsing filaments in the nonlinear Schrödinger equation, Physica D 57 (1992) 96–160. ∗

[27] A.I. Dyachenko, A.O. Korotkevich, V.E. Zakharov, Decay of the monochromatic capillary wave, JETP Lett. 77 (2003) 477–481.

[28] A.I. Dyachenko, A.O. Korotkevich, V.E. Zakharov, Weak turbulence of gravity waves, JETP Lett. 77 (2003) 546–550. ∗

[29] A.I. Dyachenko, A.O. Korotkevich, V.E. Zakharov, Weak turbulent Kolmogorov spectrum for surface gravity waves, Phys. Rev. Lett. 92 (2004) 134501(4).

[30] A.I. Dyachenko, E.A. Kuznetsov, M.D. Spector, V.E. Zakharov, Analytical description of the free surface dynamics of an ideal fluid (canonical formalism and conformal mapping), Phys. Lett. A 221 (1996) 73–79. ∗∗

[31] A.I. Dyachenko, Y.V. Lvov, V.E. Zakharov, Five-wave interaction on the surface of deep fluid, Physica D 87 (1995) 233–261. ∗∗

[32] A.I. Dyachenko, V.E. Zakharov, Toward an integrable model of deep water waves, Phys. Lett. A 221 (1996) 80–84.

[33] K.B. Dysthe, K. Trulsen, H.E. Krogstad, H. Socquet-Juglard, Evolution of a narrow-band spectrum of random surface gravity waves, J. Fluid Mech. 478 (2003) 1–10.

[34] U. Frisch, Turbulence: The Legacy of A. N. Kolmogorov, Cambridge University Press, Cambridge, 1995.

[35] S. Galtier, S.V. Nazarenko, A.C. Newell, Nonlocal MHD turbulence, Physica D 152–153 (2001) 646–652.

[36] S. Galtier, S. V. Nazarenko, A.C. Newell, A. Pouquet, A weak turbulence theory for incompressible MHD, J. Plasma Phys. 63 (2000) 447–488.

[37] S. Galtier, S.V. Nazarenko, A.C. Newell, A. Pouquet, Anisotropic turbulence of shear-Alfvén waves, Astrophys. J. Lett. 564 (2002) L49–L52.

[38] P. Guyenne, V.E. Zakharov, A.N. Pushkarev, F. Dias, Turbulence d'ondes dans des modèles unidimensionnels, C.R. Acad. Sci. Paris IIb 328 (2000) 757–762.

[39] K. Hasselmann, On the non-linear energy transfer in a gravity-wave spectrum. Part 1. General theory, J. Fluid Mech. 12 (1962) 481–500. ∗∗

[40] K. Hasselmann, On the non-linear energy transfer in a gravity-wave spectrum. Part 2. Conservative theorems; wave-particle analogy; irreversibility, J. Fluid Mech. 15 (1963) 273–281. ∗∗

[41] K. Hasselmann, On the non-linear energy transfer in a gravity-wave spectrum. Part 3. Evaluation of the energy flux and swell-sea interaction for a Neumann spectrum, J. Fluid Mech. 15 (1963) 385–398.

[42] E. Henry, P. Alstrom, M.T. Levinsen, Prevalence of weak turbulence in strongly driven surface ripples, Europhys. Lett. 52 (2000) 27–32. ∗ ∗ ∗

[43] P.A. Hwang, D.W. Wang, E.J. Walsh, W.B. Krabill, R.N. Swift, Airborne measurements of the directional wavenumber spectra of ocean surface waves. Part 1. Spectral slope and dimensionless spectral coefficient, J. Phys. Oceanogr. 30 (2000) 2753–2767.

[44] P.A. Hwang, D.W. Wang, E.J. Walsh, W.B. Krabill, R.N. Swift, Airborne measurements of the directional wavenumber spectra of ocean surface waves. Part 2. Directional distribution, J. Phys. Oceanogr. 30 (2000) 2768–2787.

[45] G. Iooss, P. Plotnikov, J.F. Toland, Standing waves on infinite depth, C.R. Acad. Sci. Paris I 338 (2004) 425–431.

[46] G. Iooss, P. Plotnikov, J.F. Toland, Standing waves on an infinitely deep perfect fluid under gravity, submitted.

[47] P.A.E.M. Janssen, Nonlinear four-wave interactions and freak waves, J. Phys. Oceanogr. 33 (2003) 863–884.

[48] C. Josserand, Y. Pomeau, Nonlinear aspects of the theory of Bose-Einstein condensates, Nonlinearity 14 (2001) R25–R62.

[49] B.B. Kadomtsev, Voprosy teorii plasmy (Problems in Plasma Physics), Vol. 4, Atomizdat, Moscow, 1964.

[50] B.B. Kadomtsev, Plasma Turbulence, Academic Press, New York, 1965.

[51] K.K. Kahma, A study of the growth of the wave spectrum with fetch, J. Phys. Oceanogr. 11 (1981) 1503–1515.

[52] A.V. Kats, V.M. Kontorovich, Drift stationary solutions in the theory of weak turbulence, JETP Lett. 14 (1971) 265–267 Russian original: ZhETF Pis'ma v Redaktsiyu 14 (1971) 392–395.

[53] G.V. Kolmakov, V.L. Pokrovsky, Stability of weak turbulence spectra in superfluid helium, Physica D 86 (1995) 465–469.

[54] A.N. Kolmogorov, The local structure of turbulence in incompressible viscous fluids for very large Reynolds numbers, Dokl. Akad. Nauk. SSSR 30 (1941) 301–305 Reprinted in Proc. R. Soc. Lond. A 434 (1991) 9–13.

[55] V.P. Krasitskii, Canonical transformation in a theory of weakly nonlinear waves with a nondecay dispersion law, Sov. Phys. JETP 71 (1990) 921–927.

[56] E.A. Kuznetsov, A.M. Rubenchik, V.E. Zakharov, Soliton stability in plasmas and hydrodynamics, Phys. Rep. 142 (1986) 103–165.

[57] Y.V. Lvov, Effective five-wave Hamiltonian for surface water waves, Phys. Lett. A 230 (1997) 38–44.

[58] Y.V. Lvov, E.G. Tabak, Hamiltonian formalism and the Garrett-Munk spectrum of internal waves in the ocean, Phys. Rev. Lett. 87 (2001) 168501(4). ∗

[59] Y. Lvov, S. Nazarenko, R. West, Wave turbulence in Bose–Einstein condensates, Physica D 184 (2003) 333–351.

[60] M. Lyutikov, Turbulent four-wave interaction of two types of waves, Phys. Lett. A 265 (2000) 83–90.

[61] A.J. Majda, D.W. McLaughlin, E.G. Tabak, A one-dimensional model for dispersive wave turbulence, J. Nonlinear Sci. 6 (1997) 9–44. ∗ ∗ ∗

[62] H. Michallet, F. Dias, Numerical study of generalized interfacial solitary waves, Phys. Fluids 11 (1999) 1502–1511.

[63] A.B. Mikhailovskii, S.V. Nazarenko, S.V. Novakovskii, A.P. Churicov, O.G. Onishchenko, Kolmogorov weakly turbulent spectra of some types of drift waves in plasmas, Phys. Lett. A 133 (1988) 407–409.

[64] S.L. Musher, A.M. Rubenchik, V.E. Zakharov, Weak Langmuir turbulence, Phys. Rep. 252 (1995) 177–274. ∗

[65] S.V. Nazarenko, Y. Lvov, R. West, Weak turbulence theory for the Gross-Pitaevskii equation, in: C.F. Barenghi, R.J. Donnelly, W.F. Vinen (Eds.), Quantized Vortex Dynamics and Superfluid Turbulence, Lecture Notes in Physics, Vol. 571, Springer, Berlin, 2001, pp. 283–289.

[66] L.W. Nordheim, On the kinetic method in the new statistics and its application in the electron theory of conductivity, Proc. R. Soc. A 119 (1928) 689–698. ∗∗

[67] M. Onorato, A.R. Osborne, M. Serio, S. Bertone, Freak waves in random oceanic sea states, Phys. Rev. Lett. 86 (2001) 5831–5834.

[68] M. Onorato, A.R. Osborne, M. Serio, D. Resio, A. Pushkarev, V.E. Zakharov, C. Brandini, Freely decaying weak turbulence for sea surface gravity waves, Phys. Rev. Lett. 89 (2002) 144501(4). ∗

[69] E. Părău, F. Dias, Nonlinear effects in the response of a floating ice plate to a moving load, J. Fluid Mech. 460 (2002) 281–305.

[70] R. Peierls, Zur kinetischen Theorie der Wärmeleitungen in Kristallen, Ann. Phys. 3 (1929) 1055–1101. ∗∗

[71] O.M. Phillips, The equilibrium range in the spectrum of wind-generated waves, J. Fluid Mech. 4 (1958) 426–434. ∗

[72] O.M. Phillips, The Dynamics of the Upper Ocean, Cambridge University Press, Cambridge, 1977.

[73] Y. Pomeau, S. Rica, Model of superflow with rotons, Phys. Rev. Lett. 71 (1993) 247–250.

[74] A.N. Pushkarev, On the Kolmogorov and frozen turbulence in numerical simulation of capillary waves, Eur. J. Mech. B/Fluids 18 (1999) 345–352.

[75] A.N. Pushkarev, V.E. Zakharov, Turbulence of capillary waves, Phys. Rev. Lett. 76 (1996) 3320–3323. ∗

[76] A. Pushkarev, D. Resio, V. Zakharov, Weak turbulent approach to the wind-generated gravity sea waves, Physica D 184 (2003) 29–63. ∗

[77] A.N. Pushkarev, V.E. Zakharov, Turbulence of capillary waves—theory and numerical simulations, Physica D 135 (2000) 98–116.

[78] S. Sridhar, P. Goldreich, Towards a theory of interstellar turbulence I: weak Alfvén turbulence, Astrophys. J. 432 (1994) 612–621.

[79] E. Schröder, J. S. Andersen, M.T. Levinsen, P. Alstrom, W.I. Goldburg, Relative particle motion in capillary waves, Phys. Rev. Lett. 76 (1996) 4717–4720.

[80] M. Tanaka, Verification of Hasselmann's energy transfer among surface gravity waves by direct numerical simulations of primitive equations, J. Fluid Mech. 444 (2001) 199–221.

[81] M. Tanaka, N. Yokoyama, Effects of discretization of the spectrum in water-wave turbulence, Fluid Dyn. Res. 34 (2004) 199–216.

[82] Y. Toba, Local balance in the air-sea boundary processes. III. On the spectrum of wind waves, J. Oceanogr. Soc. Japan 29 (1973) 209–220.

[83] N.G. Vakhitov, A.A. Kolokolov, Stationary solutions of the wave equation in media with nonlinearity saturation, Radiophys. Quantum Electron. 16 (1973) 1020–1028.

[84] J.-M. Vanden-Broeck, F. Dias, Gravity-capillary solitary waves in water of infinite depth and related free-surface flows, J. Fluid Mech. 240 (1992) 549–557. ∗

[85] J.F. Willemsen, Universal aspects of the Hasselmann nonlinear interaction, Phys. Rev. Lett. 67 (1991) 1964–1967.

[86] J.F. Willemsen, Dynamical time scales generated by a model nonlinear Hamiltonian, Phys. Rev. Lett. 71 (1993) 1172–1175.

[87] W. Wright, R. Budakian, S. Putterman, Diffusing light photography of fully developed isotropic ripple turbulence, Phys. Rev. Lett. 76 (1996) 4528–4531. ∗ ∗ ∗

[88] V.E. Zakharov, Weak turbulent spectrum in plasma without magnetic field, Sov. Phys. JETP 24 (1967) 455–459 Russian original: JETP 51 (1966) 688–696.

[89] V.E. Zakharov, Stability of periodic waves of finite amplitude on a surface of deep fluid, J. Appl. Mech. Tech. Phys. 9 (1968) 190–194.

[90] V.E. Zakharov, Weakly nonlinear waves on the surface of an ideal finite depth fluid, Amer. Math. Soc. Transl. Ser. 2 182 (1998) 167–197.

[91] V.E. Zakharov, Statistical theory of gravity and capillary waves on the surface of a finite-depth fluid, Eur. J. Mech. B/Fluids 18 (1999) 327–344. ∗∗

[92] V.E. Zakharov, A.I. Dyachenko, High-Jacobian approximation in the free surface dynamics of an ideal fluid, Physica D 98 (1996) 652–664.

[93] V.E. Zakharov, A.I. Dyachenko, O.A. Vasilyev, New method for numerical simulation of a nonstationary potential flow of incompressible fluid with a free surface, Eur. J. Mech. B/Fluids 21 (2002) 283–291. ∗

[94] V.E. Zakharov, N.N. Filonenko, Energy spectrum for stochastic oscillations of the surface of a liquid, Sov. Phys. Dokl. 11 (1967) 881–883.

[95] V.E. Zakharov, N.N. Filonenko, Weak turbulence of capillary waves, J. Appl. Mech. Tech. Phys. 4 (1967) 506–515. ∗ ∗ ∗

[96] V.E. Zakharov, P. Guyenne, A.N. Pushkarev, F. Dias, Wave turbulence in one-dimensional models, Physica D 152–153 (2001) 573–619. ∗∗

[97] V.E. Zakharov, E.A. Kuznetsov, Optical solitons and quasisolitons, JETP 86 (1998) 1035–1046. ∗

[98] V.E. Zakharov, V.S. Lvov, G. Falkovich, Kolmogorov Spectra of Turbulence I, Springer, New York, 1992. ∗ ∗ ∗

[99] V.E. Zakharov, A.N. Pushkarev, V.F. Shvets, V.V. Yan'kov, Soliton turbulence, JETP Lett. 48 (1988) 83–87.

[100] V.E. Zakharov, R.Z. Sagdeev, Spectrum of acoustic turbulence, Sov. Phys. Dokl. 15 (1970) 439–441 Russian original: Dokl. Akad. Nauk. SSSR 192 (1970) 297–300.

[101] V.E. Zakharov, O.A. Vasilyev, A.I. Dyachenko, Kolmogorov spectra in one-dimensional weak turbulence, JETP Lett. 73 (2001) 63–65. ∗∗